This dissertation has been 65-9748
microfilmed exactly as received

JEFFRIES, Robert Alan, 1933-
THE KINETICS OF IONIZATION OF STRONGLY SHOCKED HELIUM.

The University of Oklahoma, Ph.D., 1965
Physics, general

University Microfilms, Inc., Ann Arbor, Michigan

Downloaded from SHAREOK. Persistent Handle URL: https://hdl.handle.net/11244/1879

THE UNIVERSITY OF OKLAHOMA

GRADUATE COLLEGE

THE KINETICS OF IONIZATION OF STRONGLY SHOCKED HELIUM

A DISSERTATION

SUBMITTED TO THE GRADUATE FACULTY

in partial fulfillment of the requirements for the

degree of

DOCTOR OF PHILOSOPHY

BY

ROBERT ALAN JEFFRIES

Norman, Oklahoma

1965

THE KINETICS OF IONIZATION OF STRONGLY SHOCKED HELIUM

APPROVED BY

R. G. Fowler

Lyhad Moerme

Stanley E. Babb, Jr.

C. C. Lin

William N. Huff

DISSERTATION COMMITTEE

ACKNOWLEDGMENTS

The author wishes to thank Dr. L. B. Seely, Jr. for suggesting the problem and for his continued interest throughout the course of the research; Professor R. G. Fowler for his critical evaluations and suggestions and his invaluable support; Dr. G. L. Schott for many illuminating discussions; and Mr. R. L. Mowrer for his extremely able technical assistance.

The author also wishes to acknowledge helpful discussions with Dr. J. G. Hirschberg, Professor H. R. Griem, Dr. J. H. Kiefer, Dr. E. D. Loughran and Dr. D. W. Steinhaus.

This research has been supported by the Atomic Energy Commission through both the Advanced Study Program and Graduate Thesis Program of the Los Alamos Scientific Laboratory.

TABLE OF CONTENTS

		Page
LIST OF TABLES		v
LIST OF ILLUSTRATIONS		vi
Chapter		
I.	INTRODUCTION	1
II.	APPARATUS	6
	High-Explosive Shock Tube	6
	Argon Bomb	9
	Smear Camera	10
	Meinel Spectrograph	13
	Electrodeless Discharge	18
	Photographic Material	20
	Microdensitometer	20
III.	EXPERIMENTAL PROCEDURE	23
	Smear Camera Experiments	24
	Spectrograph Experiments	29
	Spectrogram Film Calibration	31
IV.	EXPERIMENTAL RESULTS AND ANALYSIS OF DATA	37
	Qualitative Results	37
	Shock Velocity Data	39
	Time-Resolved Spectra	45
V.	IONIZATION KINETICS	73
VI.	SUMMARY, CONCLUSIONS, AND RECOMMENDATIONS FOR FUTURE EXPERIMENTS	89
APPENDIX	Hydrodynamic Calculations	95

LIST OF TABLES

Table		Page
1.	Measured Average Incident Shock Velocity	40
2.	Measured and Calculated Steady-State Reflected Shock Velocity	44
3.	Relaxation Zone Data	77
4.	Equilibrium Shock Properties	99

LIST OF ILLUSTRATIONS

Figure		Page
1.	High-Explosive Shock Tube	7
2.	Argon Bomb	11
3.	Smear Camera Optical Diagram	12
4.	Meinel Spectrograph	15
5.	Meinel Spectrograph Optical Diagram	17
6.	Correction Curve for Meinel Spectrograph	19
7.	Microdensitometer	22
8.	Arrangement for Smear Camera Experiments	25
9.	Smear Camera Records of Incident Shock	27
10.	Smear Camera Record of Reflected Shock	28
11.	Arrangement for Spectrograph Experiments	30
12.	Time-Resolved Spectrograms	32
13.	Film Calibration Spectrogram	36
14.	Densitometry	46
15.	Observed Line Shape, HeI 3889	49
16.	Observed Line Shape, HeI 4471	50
17.	Observed Line Shape, HeI 5876	51
18.	Stark Broadening of HeI 3889	54
19.	Stark Broadening of HeI 5876	55
20.	Stark Broadening of HeI 4471	56
21.	Relaxation Zone, Comparison of Measurements from Three Spectral Lines	57
22.	Relaxation Zone, P_o = 10 mm	60
23.	Relaxation Zone, P_o = 10 mm - Large Diameter Tube	61

Figure Page

24. Relaxation Zone, P_o = 20 mm 62

25. Relaxation Zone, P_o = 30 mm 63

26. Relaxation Zone, P_o = 30 mm (TNT) 64

27. Arrangement for Absorption Experiment 65

28. Separation of Intensity Peaks vs. Half-Width, HeI 4471 71

29. Ionization Rate Coefficient for Helium 82

30. Three-Body Recombination Rate Coefficient for Helium 88

31. Schematic Distance-Time Plot of the Shocks Generated in the High-Explosive Shock Tube 97

32. State of Relaxation Zone, [He] and T, P_o = 10 mm ... 101

33. State of Relaxation Zone, u_2 and ρ, P_o = 10 mm 102

34. State of Relaxation Zone, [He] and T, P_o = 20 mm ... 103

35. State of Relaxation Zone, u_2 and ρ, P_o = 20 mm 104

36. State of Relaxation Zone, [He] and T, P_o = 30 mm ... 105

37. State of Relaxation Zone, u_2 and ρ, P_o = 30 mm 106

38. State of Relaxation Zone, [He] and T, P_o = 30 mm (TNT) 107

39. State of Relaxation Zone, u_2 and ρ, P_o = 30 mm (TNT) 108

CHAPTER I

INTRODUCTION

This thesis has been submitted to the University of Oklahoma in partial fulfillment of the requirements for the degree of Doctor of Philosophy in Physics. The research was performed at Los Alamos in Group GMX-7 under the Graduate Thesis Program of the Los Alamos Scientific Laboratory. This investigation of the kinetics of ionization of strongly shocked helium followed from the results of an earlier thesis on shocked helium completed by Glenn E. Seay[1] under a similar cooperative agreement and submitted to the University of Oklahoma in 1957.

The problem was selected so as to be of mutual concern to the sponsoring institutions. For many years the Department of Physics at the University of Oklahoma has actively investigated the hydrodynamics and spectra of partially ionized gases generated by spark discharges[2]. Recently this effort has expanded to include the measurement of excitation cross sections[3]. At Los Alamos the properties of gases at high temperature

---

[1] G. E. Seay, "The Visible Radiation from Helium in a Strong Shock Wave," Los Alamos Scientific Laboratory Report, LAMS-2125 (1957).

[2] A complete bibliography may be found in R. G. Fowler, Electrically Energized Shock Tubes (University of Oklahoma Research Institute, Norman, 1963).

[3] R. M. St. John, F. L. Miller, and C. C. Lin, Phys. Rev. 134, A888 (1964).

are of great interest to current laboratory programs, including Project Sherwood (controlled thermonuclear fusion) and Project Rover (nuclear rocket propulsion). Hence an investigation of the kinetic processes which lead to ionization equilibrium in a strongly shocked gas was judged to be of value to both the University of Oklahoma and the Los Alamos Scientific Laboratory.

Seay's earlier research made possible by the unique facilities at Los Alamos resulted in the development and use of a new research tool, the high-explosive shock tube. He found that a tube of stationary gas could be strongly shocked from high explosives to produce a readily observable sample of partially ionized gas at high temperature. Although conventional shock tubes had been previously used for such a purpose[4,5], the development of this device further broadened the range of gases subject to this type of investigation to include helium. Because of its high excitation and ionization potentials, helium must be quite strongly shocked if significant ion densities are to be obtained. However, the nature of the conventional shock tube precludes its use for strongly shocking a gas with high sound speed, so that the required strong shocks can only be generated in a tube driven by high explosive or in an electrically-energized shock tube whose performance is characterized by its complicated flow[6].

---

[4] H. Petschek et al., J. Appl. Phys. 26, 83 (1955).

[5] E. B. Turner, "The Production of Very High Temperatures in the Shock Tube with an Application to the Study of Spectral Line Broadening," University of Michigan Engineering Research Institute Report, OSR TN-56-150 (1956).

[6] Fowler, op. cit.

With this ability to shock helium strongly, Seay, using a medium-dispersion Hilger prism spectrograph, proceeded to verify the existence of kinetic equilibrium with a temperature of about 2 eV and an ion density near 10^{18} cm^{-3} behind a shock reflected from the tube end plate. As a sidelight to these experiments, he noticed that time-resolved spectrograms showed each of the emitted spectral lines to be narrow close behind the shock front but increasing in width with time until they attained a given equilibrium shape some distance behind the shock. However, the line shape as a function of time could not be well resolved due to insufficient photographic exposure and the limited time resolution of the spectrograms.

It was the observation of these transient line shapes which prompted the present research, for it appeared likely that this relaxation zone behind a strong shock in helium could be observed with improved experimental equipment. Such equipment became available at Los Alamos with the installation of an f/3.5 Meinel grating spectrograph coupled with a high-speed rotating mirror. Preliminary experiments demonstrated the ability to make well exposed, time-resolved spectrograms of the emitting gas behind the reflected shock front.

Prior to the time of this research, other investigators had studied a number of chemical reactions as they occurred in shock tubes[7], but it remained to be seen if time-resolved spectrograms of so rapid a reaction as the ionization process could be obtained and analyzed to yield meaningful results. It was felt that by using a standard approach in the

---

[7]For example see A. G. Gaydon and I. R. Hurle, The Shock Tube in High-Temperature Chemical Physics (Reinhold Publishing Corporation, New York, 1963).

field of kinetics, variation of the temperature and concentrations of the reactants and observation of the effects of these changes on the reaction, the kinetic mechanism by which the ionization approached equilibrium could be resolved. However, if such were not the case, empirical relationships which described the process would be of value.

A proper solution of the problem would clearly depend on two basic points: the suitability of spectrographic techniques to determine accurately the state of a luminous gas and a knowledge of the hydrodynamic behavior of the shock tube much more detailed than that required in an investigation of equilibrium conditions. Since the principal origin of line broadening in the shocked helium was the plasma microfields of the electrons and ions, the recent theoretical improvements made by Griem and Baranger in the determination of ion densities from the shape of Stark-broadened helium lines[8] would satisfy the first requirement. On the other hand, the ability to calculate the properties of the shocked gas from fundamental hydrodynamic considerations was questionable. Experiments performed after the completion of Seay's thesis had indicated that, even though the hydrodynamic behavior was in general well predicted by one-dimensional shock theory, under certain conditions perturbations such as boundary layer effects could negate the validity of the relatively simple one-dimensional approach.

This thesis describes both the experiments designed to define the hydrodynamic behavior of the high-explosive shock tube and those specifically intended to reveal the detailed nature of the kinetics of ionization of strongly shocked helium. The results obtained are presented

---

[8] H. R. Griem et al., Phys. Rev. 125, 177 (1962).

and compared with applicable theoretical treatments. Chapter II contains an account of the apparatus employed in the experiments, special attention being given to the Meinel spectrograph. In Chapter III liberal use of photographic reproductions and schematic diagrams has been made in the enumeration of the experimental procedures. The results of the experiments are presented in Chapter IV together with the methods used in the data reduction. Following in Chapter V, the sum of the information on the ionization reaction gained from the hydrodynamic experiments and that acquired from the spectrograms is gathered into a detailed description of the process which is then compared to theoretical predictions. A summary of the research and the conclusions derived therefrom is reserved for the concluding chapter, Chapter VI. In addition, suggestions are made for instrumentation that would increase the versatility of the Meinel spectrograph, and the feasibility of using the high-explosive shock tube in the examination of relaxations in gases other than helium is explored.

CHAPTER II

APPARATUS

High-Explosive Shock Tube

The formation of a shock wave in a shock tube is the result of high pressure gas expanding into a volume of gas at lower pressure[1]. In the conventional shock tube, the regions of different pressure are separated by a diaphragm which when ruptured allows the required expansion. It is the expansion of explosive detonation products that gives rise to a shock wave in the high-explosive shock tube.

A schematic representation of the high-explosive shock tube determined to be optimum in design for this research is given in Fig. 1. It consisted of a Pyrex pipe closed at one end by a Pyrex disk and joined at the other to the high-explosive charge. The charge was a cylindrical booster explosive cemented to a plane wave generator[2] with Eastman 910 adhesive[3]. A thin (<0.005 in.) layer of Furane Adhesive Type X-2[4] was applied to the end of the booster explosive adjacent to the Pyrex pipe in order to insure a vacuum tight surface. This thin layer was achieved

---

[1]The formation of shock waves is completely discussed in standard texts such as R. Courant and K. Friedrichs, Supersonic Flow and Shock Waves (Interscience Publishers, Inc., New York, 1948), Vol. I.

[2]J. H. Cook, Research (London) 1, 474 (1948).

[3]Manufactured by Tennessee Eastman Company, Kingsport, Tenn.

[4]Manufactured by Furane Plastics, Inc., Los Angeles, Calif.

LASL-AEC-OFFICIAL

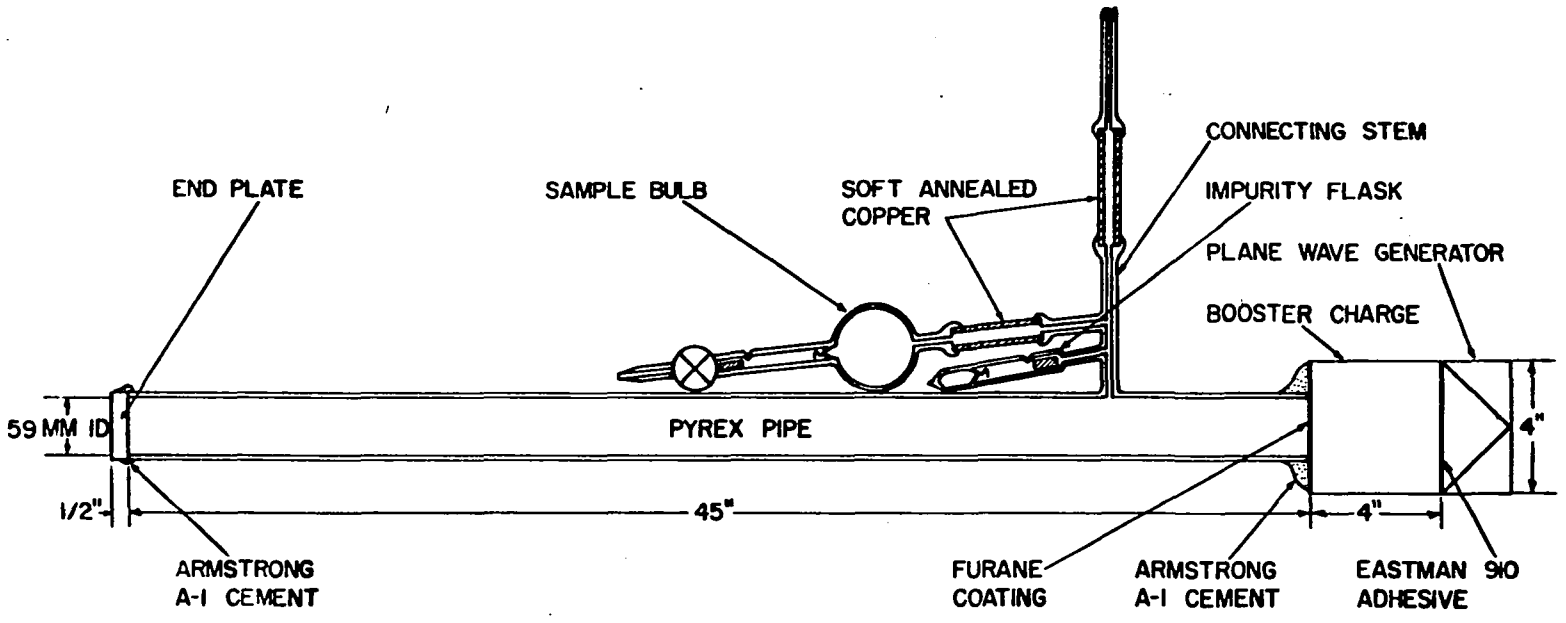

Fig. 1. High-Explosive Shock Tube

by three successive applications of very small amounts of the adhesive using a lintless nylon cloth applicator allowing drying time between coats. The explosive charge and the end plate were cemented to the pipe with Armstrong A-1 cement[5].

Evacuation and filling of the tube were accomplished through a Pyrex stem connected at a small hole in the pipe. The stem was in turn connected to a Pyrex high-vacuum system by a short section of soft annealed copper tubing. The use of the copper tubing was necessitated by the need for a procedure which would allow removal of the tube from the vacuum system without introduction of additional unwanted impurities. There were indications that gases absorbed in the glass were introduced when the tube was removed by heating a constriction in the Pyrex stem with a torch and pulling it away. On the other hand, no impurities were added when the copper tubing was severed and sealed by a cold weld pinch-off device[6]. The stem served the additional purpose of providing a connecting point for other appendages. In all experiments a gas sample bulb was connected to the stem of the tube. Immediately prior to firing this bulb was removed and the gas sample retained for analysis. In a few instances trace amounts of foreign gases, contained in a small glass flask also connected to the stem, were released into the tube by opening a break seal with a magnetic hammer.

The details of the tube assembly, including the choice of the various adhesives, came primarily from the experience of Seay[7]. He found that

---

[5]Manufactured by Armstrong Products Company, Warsaw, Indiana.

[6]Purchased from Kane Engineering Laboratories, Palo Alto, Calif.

[7]Seay, op. cit., p. 6.

this particular combination of materials resulted in a tube that was vacuum tight and generally exhibited excellent planarity of both the incident and reflected shocks. The physical dimensions were resolved to comply with the specific requirements of this research. The diameter of the tube was determined to be small enough to result in an optically-thin gas volume yet large enough to decrease the deleterious effects of boundary layers to an almost unobservable level. The tube was long enough to allow the necessary testing time behind the reflected shock before the arrival of the expanding explosive detonation products at the observation position. There was also the obvious advantage of keeping the overall size of the assembly small to facilitate handling.

The Pyrex high-vacuum system with which the shock tube was evacuated and filled consisted of an oil diffusion pump and forepump, a McLeod gauge, a mercury manometer, an ion gauge, and four liquid-nitrogen cold traps advantageously located. The tube was evacuated to near 10^{-6} mm Hg, baked at about 300°C in regions remote from the high explosive, filled to the desired pressure from a high-pressure tank of helium also connected to the vacuum system, and removed by the pinch-off technique mentioned above.

Argon Bomb

An extremely intense light source was necessary for the calibration of films exposed for very short times. Although commercially available capillary discharge lamps delivered the required intensity, their transient behavior made them less than ideal for this purpose. However, a device in common use at the Los Alamos Scientific Laboratory provided light which was relatively constant at high intensity for a period of

several microseconds. A schematic diagram of the adaptation of this device, the argon bomb, utilized in this research is shown in Fig. 2.

The argon bomb used in the film calibration procedure was essentially a miniature of the high-explosive shock tube. In this case though, since there was no reason to minimize the impurity concentration, the pipe was made of Lucite rather than Pyrex and no vacuum tight surface was applied to the face of the booster charge. Except for the use of Silastic 732[8] to join the Lucite pipe to the booster charge, the adhesives used to assemble the bomb were identical to those employed in the construction of the shock tube. A viewing slit across the Pyrex disk that served as the end plate was defined by black masking tape.

Prior to the initiation of the explosive, the bomb was filled with argon by a flow of gas entering from a high pressure tank through surgical tubing connected to the brass stem and leaving through a small hole located in the pipe near the end plate.

Smear Camera

The velocities and shapes of the shock waves generated in the high-explosive shock tube were observed with a Model 74, f/4, smear (or sweeping-image) camera designed and built by the Optics Group of LASL[9]. An optical diagram for the camera is presented in Fig. 3. The objective lens imaged the object, in this case the shock tube, on the slit. The fraction of the object light that passed through the slit was then reimaged by the camera lens at the film after reflection from the rotating

---

[8]Manufactured by Dow Corning Corporation, Midland, Michigan.

[9]A complete description of a similar camera is given by B. Brixner, J. Soc. Motion Picture Television Engrs. 70, 180 (1961).

LASL-AEC-OFFICIAL

LASL-AEC-OFFICIAL

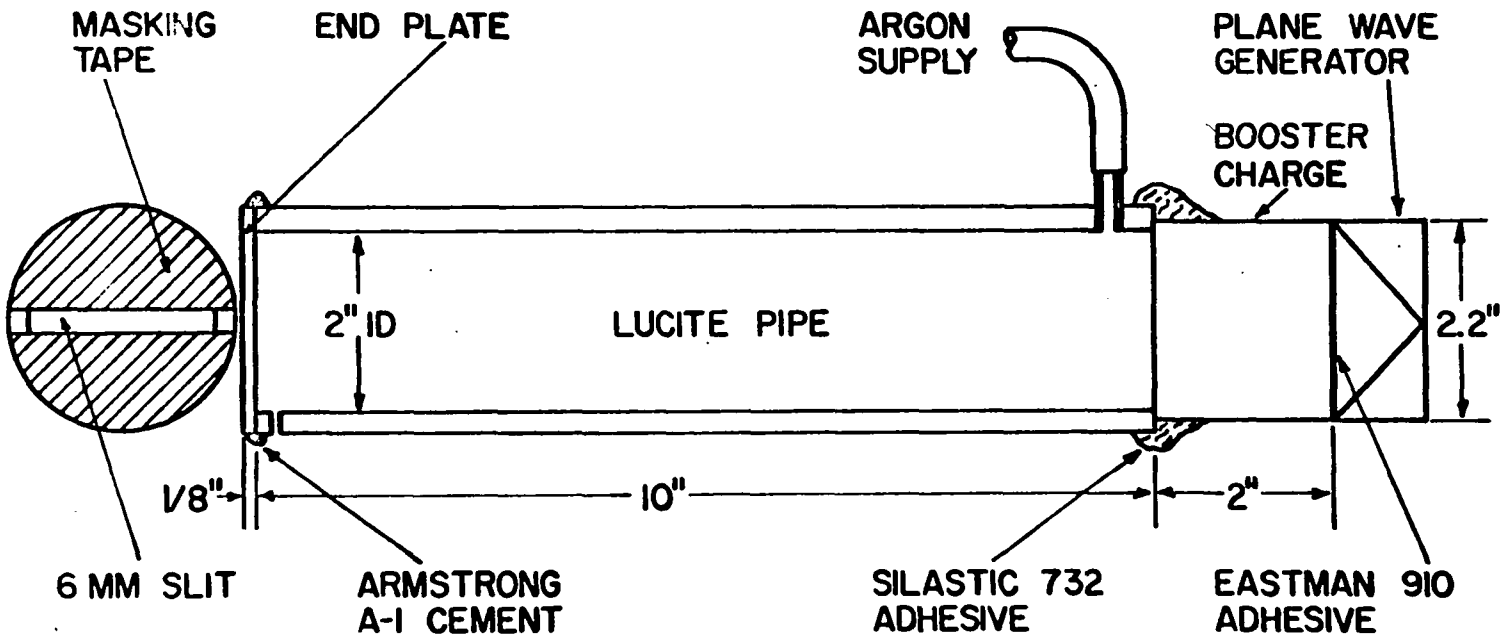

Fig. 2. Argon Bomb

LASL-AEC-OFFICIAL

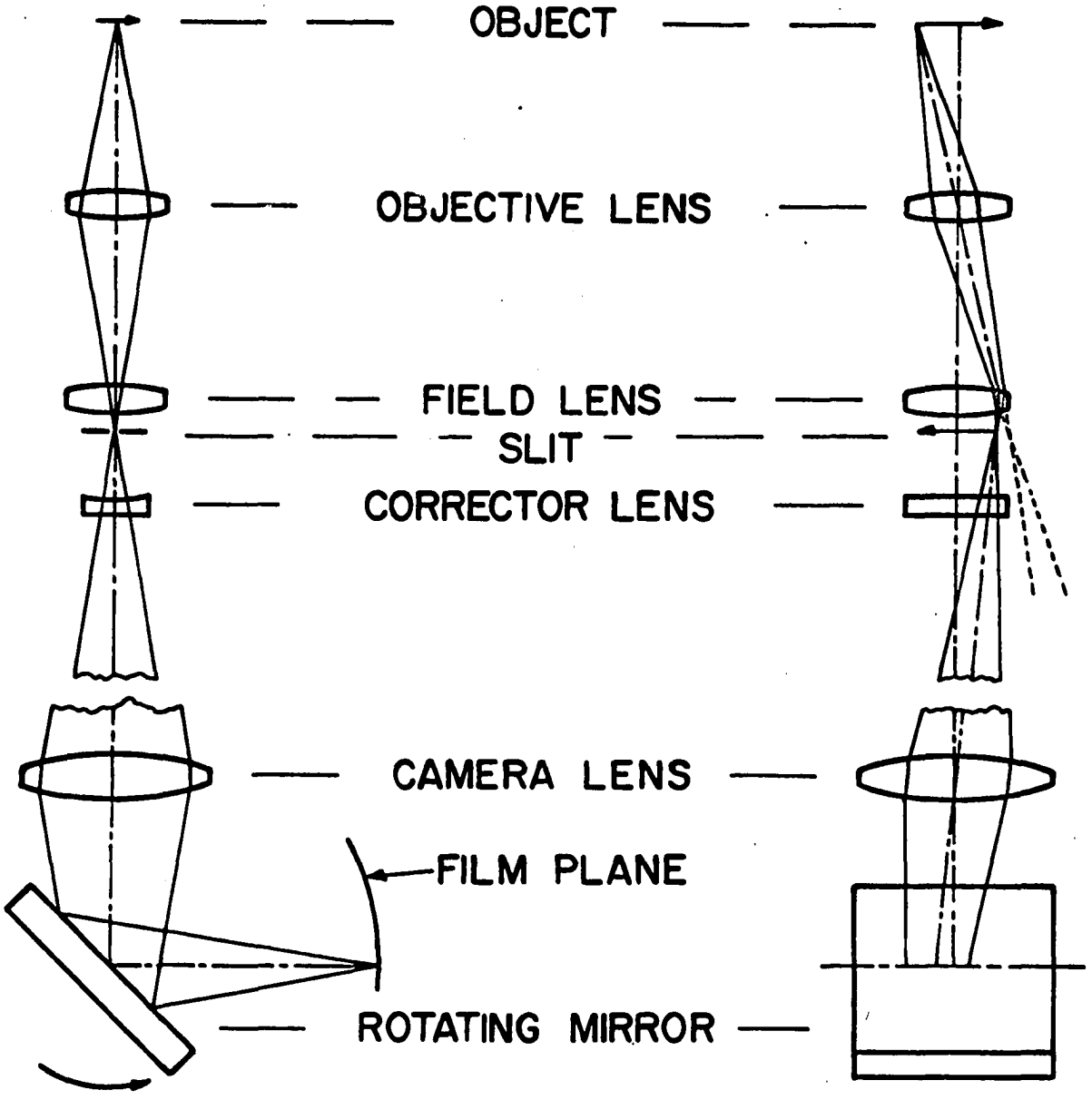

Fig. 3. Smear Camera Optical Diagram

LASL-AEC-OFFICIAL

mirror. Operation of the basic optical system was improved by the corrector lens which compensated for high-speed distortion of the rotating mirror and the field lens which reduced vignetting by the camera lens. The film record that resulted had space and time for its coordinates.

The rotating mirror was driven by an air turbine capable of operation at speeds up to 2000 rps. For these experiments mirror speeds of 200 rps (image speed on the film of 0.459 mm μsec^{-1}) and 400 rps were used for recording the behavior of the primary and reflected shocks respectively. The image of the camera slit at the film was about 0.05 mm wide resulting in an image overwrite time of about 0.05 μsec at 0.918 mm μsec^{-1}.

The rotating mirror while revolving reflected the imaged light onto the film for only a small fraction of each revolution. The camera was therefore equipped with a photoelectric synchronizer system which delivered a pulse to the explosive firing circuit at the proper mirror position. In this system a small beam of light was relayed by reflection at the mirror surface from a source to a photomultiplier tube when the mirror was in a given position. Closing of the main firing switch energized the small bulb that served as the light source. The delay between the firing pulse originating at the photomultiplier and the time at which the camera began writing was determined by the position of the source and photomultiplier tube assembly.

Meinel Spectrograph

The spectrograph used throughout these experiments was a medium-dispersion grating instrument generally referred to by those familiar with it as the Meinel spectrograph. The history and detailed construction

of the instrument have been fully described by Harrington[10]. A photograph of the assembled spectrograph presented in the NRL Report is reproduced here in Fig. 4.

The basic optical design formulated by Dr. A. B. Meinel can best be described as that of a modified Wadsworth type stigmatic instrument. Some of the pertinent optical characteristics of the spectrograph were as follows:

1. Aperture

   Collecting, f/6.1

   Imaging, f/3.5

2. Spectral ranges

   First order, 3317 Å to 8468 Å

   Second order, lower limit of photographic emulsion to 4234 Å

3. Usable slit height, 22 mm

4. Average reciprocal dispersion of entire focal plane

   First order, 20.6 Å mm^{-1}

   Second order, 10.3 Å mm^{-1}

5. Wavelength resolution with 50 μ slit, 0.5 Å

6. Internal magnification, 0.492

7. Grating features

   Plane replica type, 1200 lines mm^{-1}

   Theoretical resolution of first order spectrum, 183600

   Ruled area, 127 mm groove length by 153 mm width

   Blaze angle, 26° 45'

   Operating blazed wavelength, 7121.5 Å

---

[10] F. D. Harrington, "An f/3.5 Medium-Dispersion Grating Spectrograph," U. S. Naval Research Laboratory Report, NRL-5446 (1960).

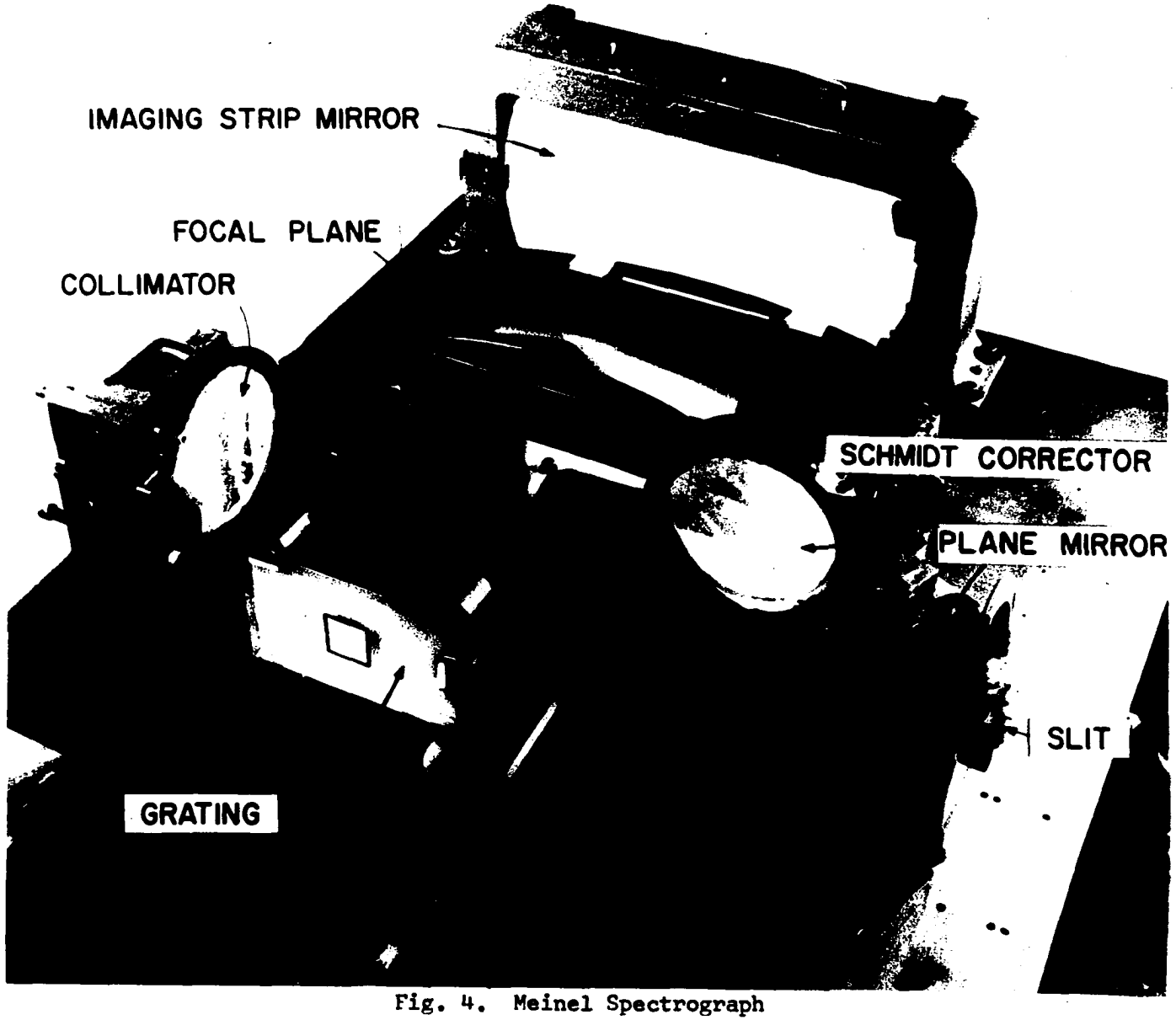

Fig. 4. Meinel Spectrograph

With the aid of Fig. 5, a schematic of the spectrograph, the internal optical path may be traced. Light which entered the slit passed through the hole in the plane mirror and was collimated by the 7.7 in. diameter spherical mirror. The beam was then returned to the plane mirror through which it entered and was reflected to the Schmidt type correcting element. Here the light was again reflected and made incident on the grating. The large segment of a spherical mirror then imaged the diffracted light bundles from the grating onto the focal plane.

A modified form of the interpolation formula of Sawyer[11] was used to describe the spectrograph dispersion curve which was needed to determine the wavelength of unidentified spectral lines occasionally observed on the spectrograms. The modification was expressed as

$$\lambda_{calc} = \lambda_o + Pd \qquad \text{(II-1)}$$

where: λ_{calc} = wavelength as calculated, $\mathring{A}$

λ_o = wavelength of known spectral line, $\mathring{A}$

P = plate factor or average reciprocal dispersion over the focal plane, $\mathring{A}\ mm^{-1}$

d = distance of the unidentified line from the reference line as measured on the spectrogram, positive in the direction of increasing wavelength, mm.

For these experiments a strong line in the HeI spectrum was selected as the reference line and the numerical form of equation (II-1) became

$$\lambda_{calc} = 3888.65 + 20.64d. \qquad \text{(II-2)}$$

---

[11] R. A. Sawyer, Experimental Spectroscopy (Prentice Hall, Inc., New York, 1946), p. 237.

LASL-AEC-OFFICIAL

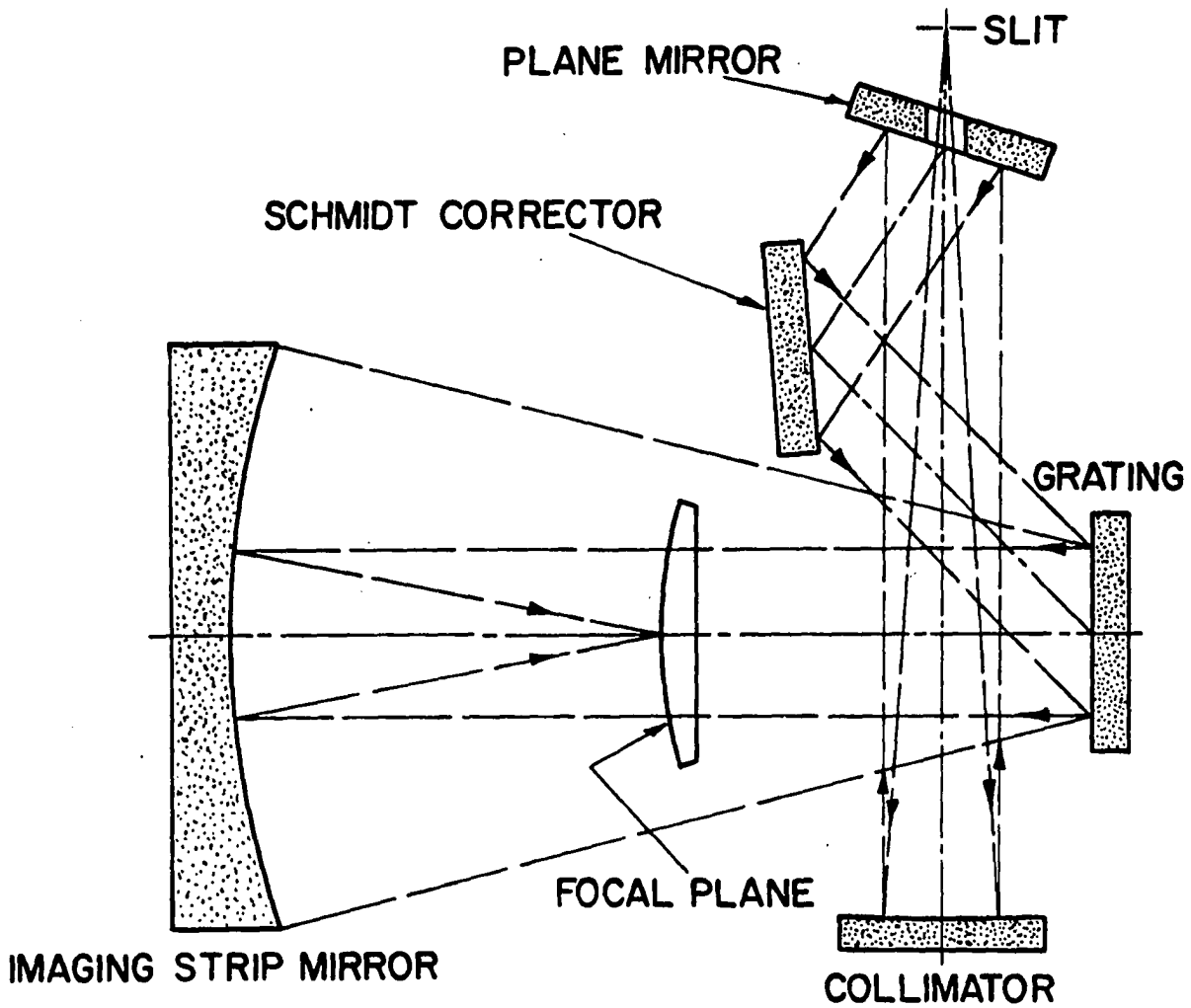

Fig. 5. Meinel Spectrograph Optical Diagram

LASL-AEC-OFFICIAL

However, the grating dispersion changed slowly with the angle of diffraction, so that a correction to equation (II-2) was necessary. A correction curve, presented in Fig. 6, was obtained by measurement of spectrograms of both the helium and mercury spectra. The true wavelength of the unknown line, λ, was therefore determined by reference to the correction curve and the relation

$$\lambda = \lambda_{calc} + \Delta\lambda. \qquad \text{(II-3)}$$

The optical elements external to the spectrograph consisted of an objective lens and a high-speed rotating mirror. An image of that region of the shock tube being studied was swept down the slit at speeds from 1.5 mm μsec^{-1} to 3.0 mm μsec^{-1}. The mirror, driven by an air turbine, was equipped with a synchronizing system similar in operation to that of the smear camera.

Unwanted fogging of the spectrograms by daylight was prevented by a solenoid-operated mechanical shutter positioned over the slit. The shutter opened for less than a second as the main firing switch was closed.

Electrodeless Discharge

An electrodeless discharge was used to place helium reference spectra on each spectrogram. In addition to providing dispersion curve data for each film, these references were used to define the time and dispersion axes when the spectrograms were aligned for analysis by the microdensitometer.

The discharge was established in a helium-filled quartz tube about 4 in. long and 3/8 in. in diameter. The tube had been filled to a pressure of 8 mm Hg after being evacuated to a pressure of about 10^{-6} mm Hg and

LASL-AEC-OFFICIAL
LASL-AEC-OFFICIAL

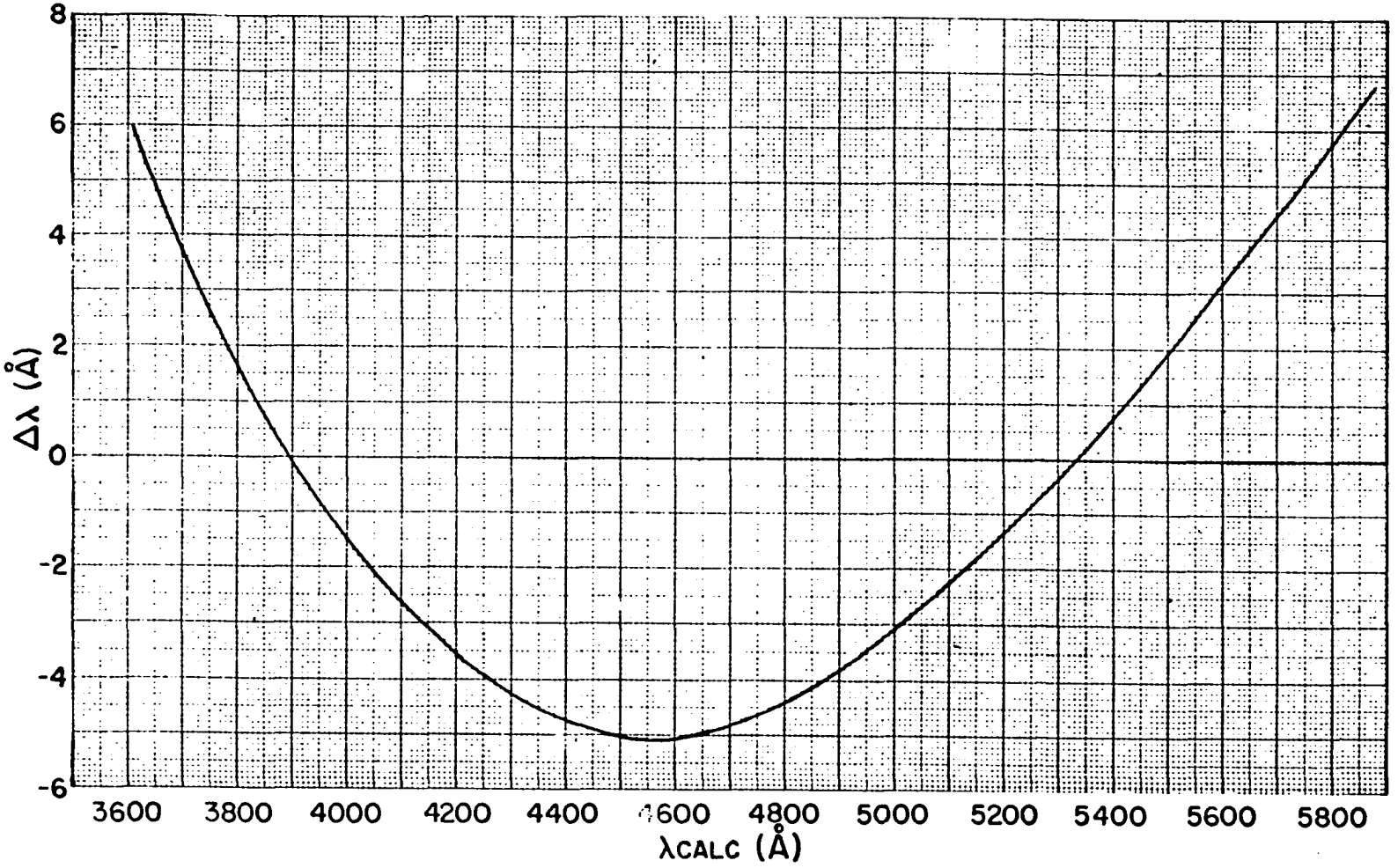

Fig. 6. Correction Curve for Meinel Spectrograph

flamed to a red heat. Excitation of the gas was maintained by microwaves from a commercial Microtherm diathermy machine[12].

Photographic Material

Kodak Royal-X Pan film was used in the smear camera experiments because of its extremely fast photographic speed. The films were developed with intermittent agitation for 10 minutes in Kodak DK-50 Developer.

Spectrogram films were cut from Kodak Royal Pan sheet film. Although slightly less fast, Royal Pan had desirably smaller grain size than Royal-X Pan and a fairly flat response over the visible portion of the spectrum. The spectrograms were brush developed for 8 minutes in Kodak DK-50 Developer.

Microdensitometer

A microdensitometer is a photometric device designed to determine the reduction in the intensity of a light beam transmitted through a small restricted area of a photographic emulsion. The varieties of microdensitometer design have been generally discussed by Harrison, Lord, and Loofbourow[13] and Strasheim[14]. Certainly several of the modern commercial microdensitometers are quite adequate for the densitometry of spectrograms if the measured spectral lines are of some length so that the scanning beam can be made relatively large. However, a beam that was small on both axes was necessary for the densitometry of the time-resolved Meinel spectrograms in order to result in the required time resolution as well as

---

[12] Model CMD-4 manufactured by Raytheon Manufacturing Co., Waltham, Mass.

[13] G. R. Harrison, R. C. Lord, and J. R. Loofbourow, Practical Spectroscopy (Prentice Hall, Inc., New York, 1948), p. 350.

[14] A. Strasheim, Spectrochim. Acta 4, 489 (1952).

the appropriate wavelength resolution. This requirement for small beam size and necessity for precision in measuring small changes in the low transmitted intensity that was a result thereof could not be satisfied by available commercial microdensitometers.

However, a new automatic microdensitometer which could be used became available. The instrument designed by Steinhaus, Engleman, and Briscoe[15] of LASL was more than capable of meeting the stated requirements by providing a scanning beam of dimensions 96 microns on the time axis by 38 microns on the dispersion axis. A self-explanatory sketch of the optical system of the microdensitometer is given in Fig. 7. The output of the photomultiplier system was recorded by a paper chart recorder.

---

[15] D. W. Steinhaus, R. Engleman, and W. L. Briscoe, "Design and Operation of a New Automatic Comparator for Measurement of Spectra," Los Alamos Scientific Laboratory Report, LA-3100 (1964).

LASL-AEC-OFFICIAL
LASL-AEC-OFFICIAL

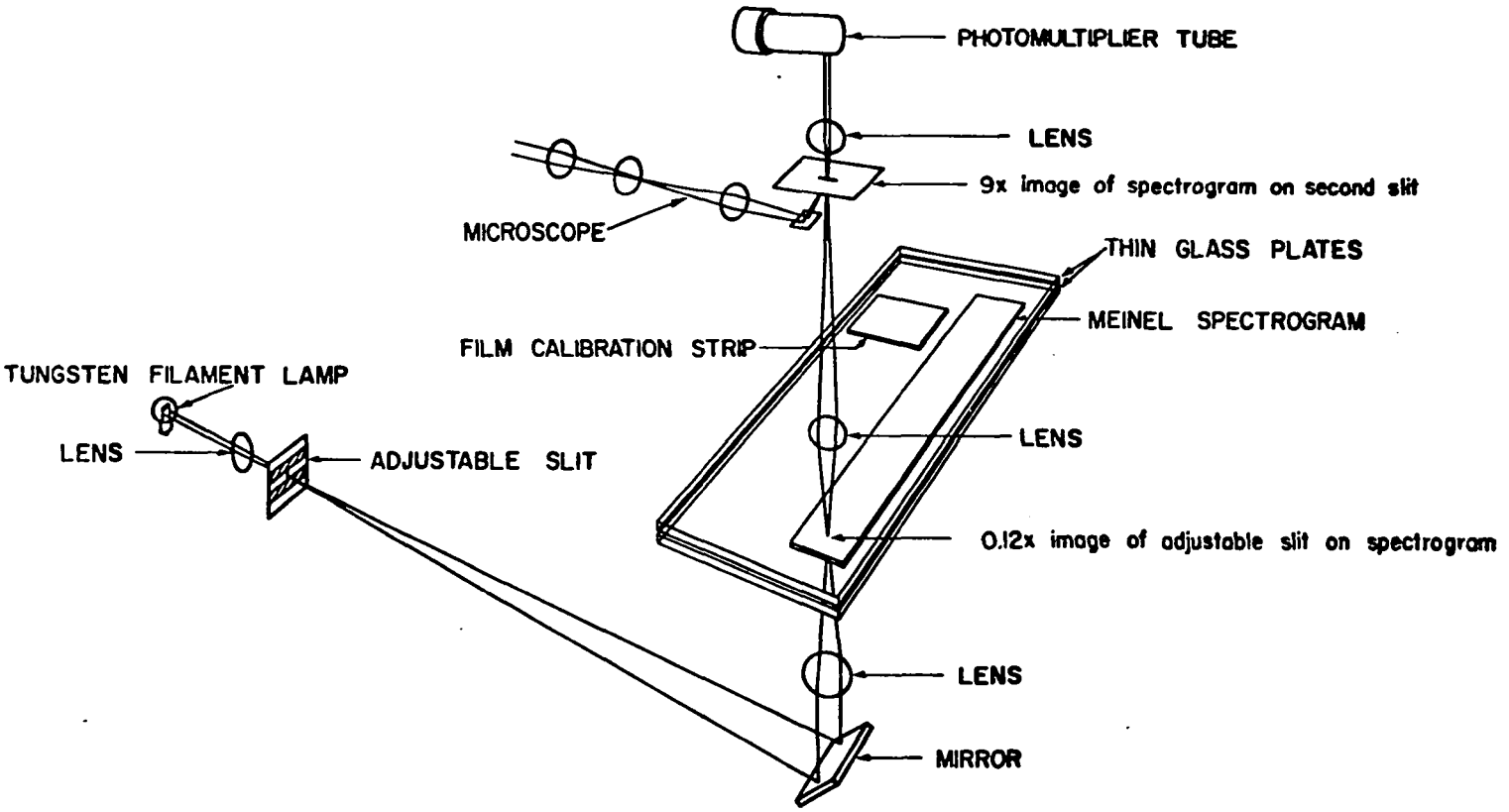

Fig. 7. Microdensitometer

CHAPTER III

EXPERIMENTAL PROCEDURE

A detailed knowledge of the hydrodynamic behavior of the high-explosive shock tube was required in addition to the spectroscopic investigation of the kinetics of helium ionization, as only a fraction of the necessary information on the state of the relaxing gas could be obtained from the spectrograms themselves. The values of the remainder of the state variables required to specify the kinetic system were to be predicted by theoretical calculations based on one-dimensional shock hydrodynamics.

As is discussed in the Appendix in some detail, a solution of the appropriate equations which would specify the pertinent state variables could be found given the initial state of the unshocked gas and the value of one additional observed quantity. In this case the quantity which was most easily observed and measured was the incident shock velocity. Familiar smear camera techniques were used not only to observe the incident shocks but were also employed to evaluate the validity of the one-dimensional calculations by providing an observed reflected shock velocity for comparison with that predicted theoretically.

Simultaneous recording of velocities with the smear camera and the exposure of the spectrograms was prevented by experimental difficulties inherent in the synchronization of the two independent rotating-mirror

instruments. Therefore, the following description of the experimental procedures is in effect divided into two sections. The first section covers those experiments designed to observe the shock velocities and other behavior apparent on the smear camera photographs and the second describes the experiments recorded with the Meinel spectrograph.

Smear Camera Experiments

The arrangement of the apparatus employed in those experiments recorded by the smear camera is shown schematically in Fig. 8. After being removed from the high-vacuum system, the shock tube was placed on a steel-covered concrete pad and viewed by the smear camera from a reinforced concrete building which also housed the electronic control circuits and the experimenters.

Alignment of the tube was such that its axis was imaged along the slit of the camera. A plane mirror was positioned to provide a view directly down the tube. The particular optical requirements of each experiment determined the distance from the viewing window to the tube. In those experiments intended to observe the incident shock, the tube was located as shown in the schematic with its entire length in the field of view. The tube was located closer to the window with only the final one-tenth of its length visible if the interest was primarily in the reflected shock behavior.

The gas sample bulb was removed from the tube following optical alignment in order that the gas sample be as nearly as possible representative of the gas in the tube at the time of firing. The sample was retained and delivered at a later time to Dr. E. D. Loughran of LASL for mass spectrometric analysis. Thus the impurity concentration was recorded for each experiment.

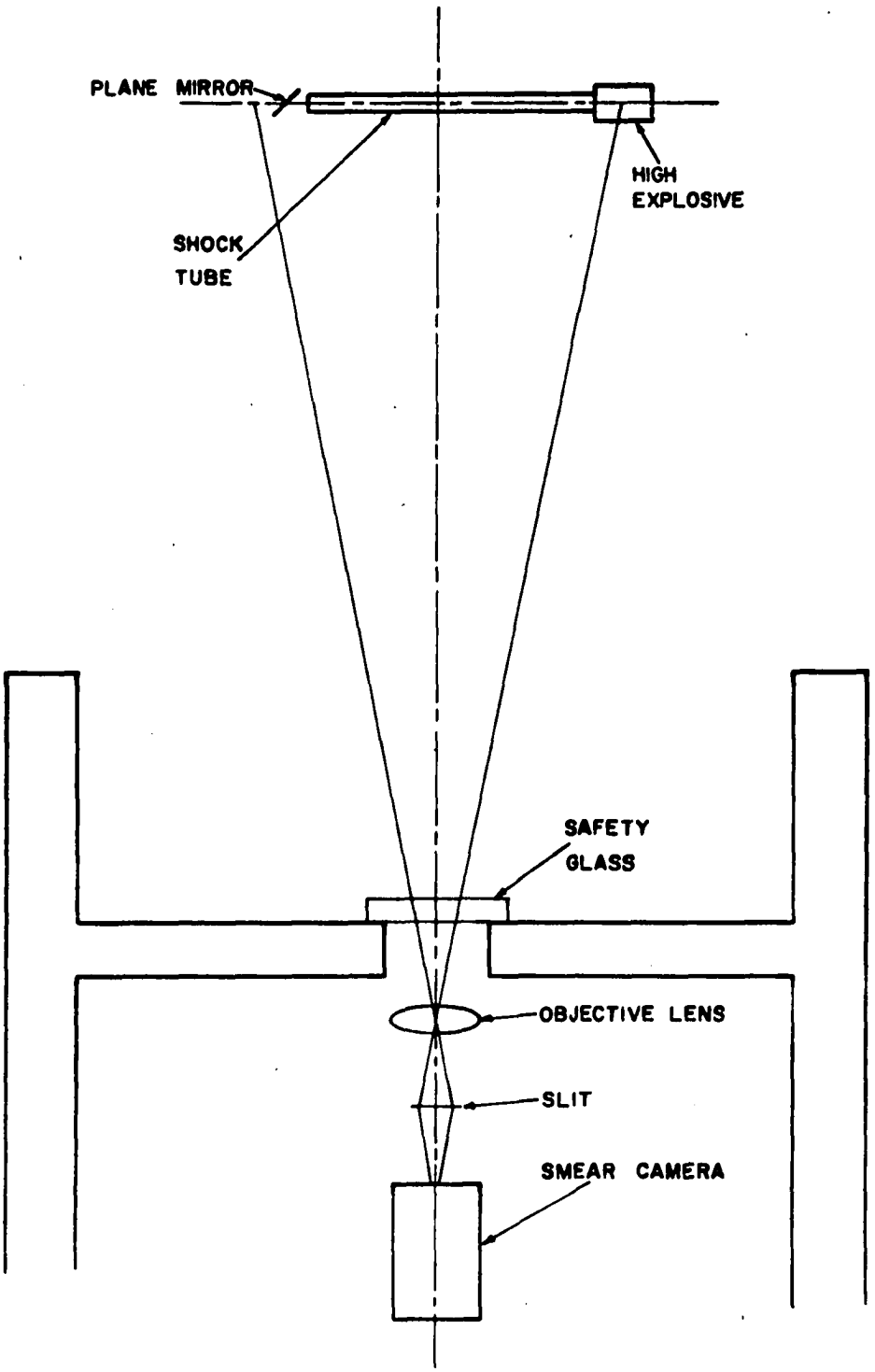

Fig. 8. Arrangement for Smear Camera Experiments

LASL-AEC-OFFICIAL
LASL-AEC-OFFICIAL

The firing circuit was then armed, the camera mirror brought to speed, the high-explosive components detonated, and the resulting film developed. Camera speed was adjusted so that the shock trace would make an angle of about 45° on the film record for best reading accuracy, while the synchronizer assembly was positioned such that the event of interest would be totally recorded on the film.

In pure helium the luminosity of the incident shock was below that necessary to produce an image on the film in the view along the tube axis. Therefore only an average velocity could be determined, this by measuring the transit time between the onset of light as the shock left the explosive and the abrupt intensity increase observed in the end view with shock relfection at the end plate. In order to measure possible shock attenuation, advantage was taken of a phenomenon observed by several shock tube investigators but first identified by Rosa[1] and Turner[2]. If trace amounts of organic gas (for these experiments less than 1% by volume of C_2H_2) were added to the helium, a brief burst of molecular light occurred at the incident shock front. Typical examples of the smear camera photographs of the incident shocks in both pure and doped helium are shown in Fig. 9.

The doping technique was not necessary in order to record the behavior of the reflected shocks. For the purpose of reproduction, however, the position of the faintly luminous reflected shock front has been accented by the dashed line in a typical photograph presented in Fig. 10.

---

[1] R. J. Rosa, Phys. Rev. 99, 633 (1955).

[2] E. B. Turner, Phys. Rev. 99, 633 (1955).

The firing circuit was then armed, the camera mirror brought to speed, the high-explosive components detonated, and the resulting film developed. Camera speed was adjusted so that the shock trace would make an angle of about 45° on the film record for best reading accuracy, while the synchronizer assembly was positioned such that the event of interest would be totally recorded on the film.

In pure helium the luminosity of the incident shock was below that necessary to produce an image on the film in the view along the tube axis. Therefore only an average velocity could be determined, this by measuring the transit time between the onset of light as the shock left the explosive and the abrupt intensity increase observed in the end view with shock relfection at the end plate. In order to measure possible shock attenuation, advantage was taken of a phenomenon observed by several shock tube investigators but first identified by Rosa[1] and Turner[2]. If trace amounts of organic gas (for these experiments less than 1% by volume of C_2H_2) were added to the helium, a brief burst of molecular light occurred at the incident shock front. Typical examples of the smear camera photographs of the incident shocks in both pure and doped helium are shown in Fig. 9.

The doping technique was not necessary in order to record the behavior of the reflected shocks. For the purpose of reproduction, however, the position of the faintly luminous reflected shock front has been accented by the dashed line in a typical photograph presented in Fig. 10.

---

[1] R. J. Rosa, Phys. Rev. 99, 633 (1955).

[2] E. B. Turner, Phys. Rev. 99, 633 (1955).

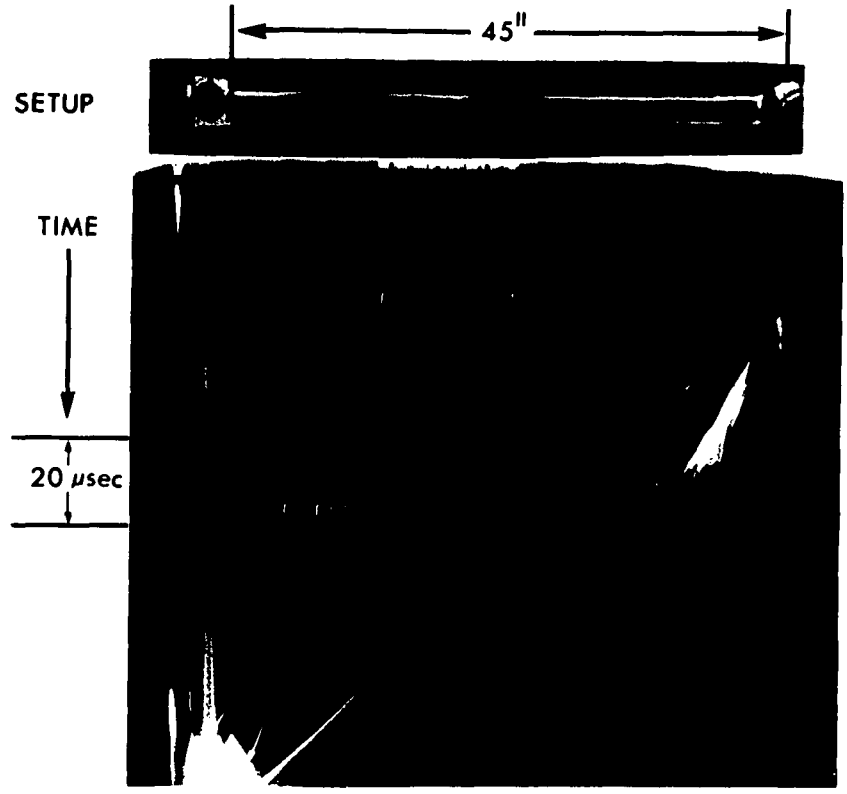

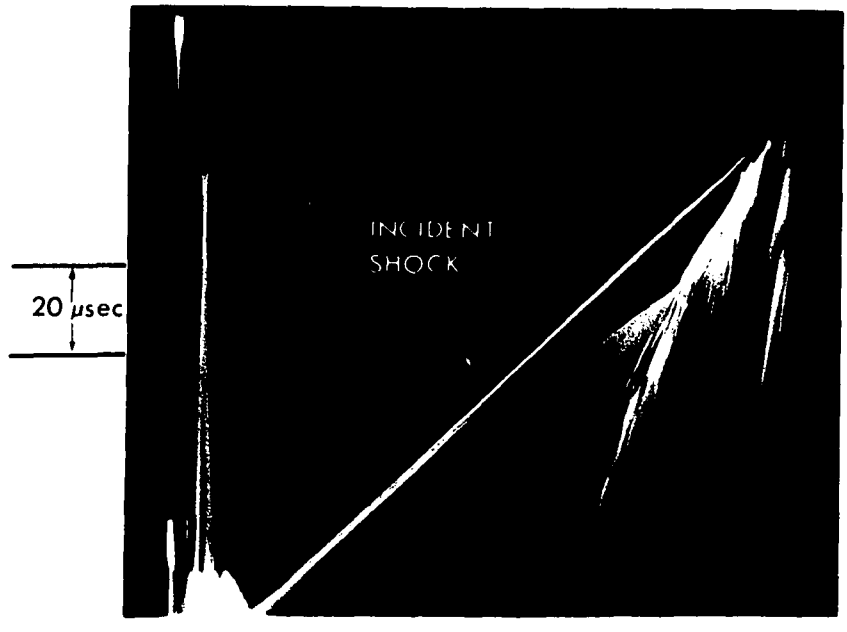

Fig. 9. Smear Camera Records of Incident Shock

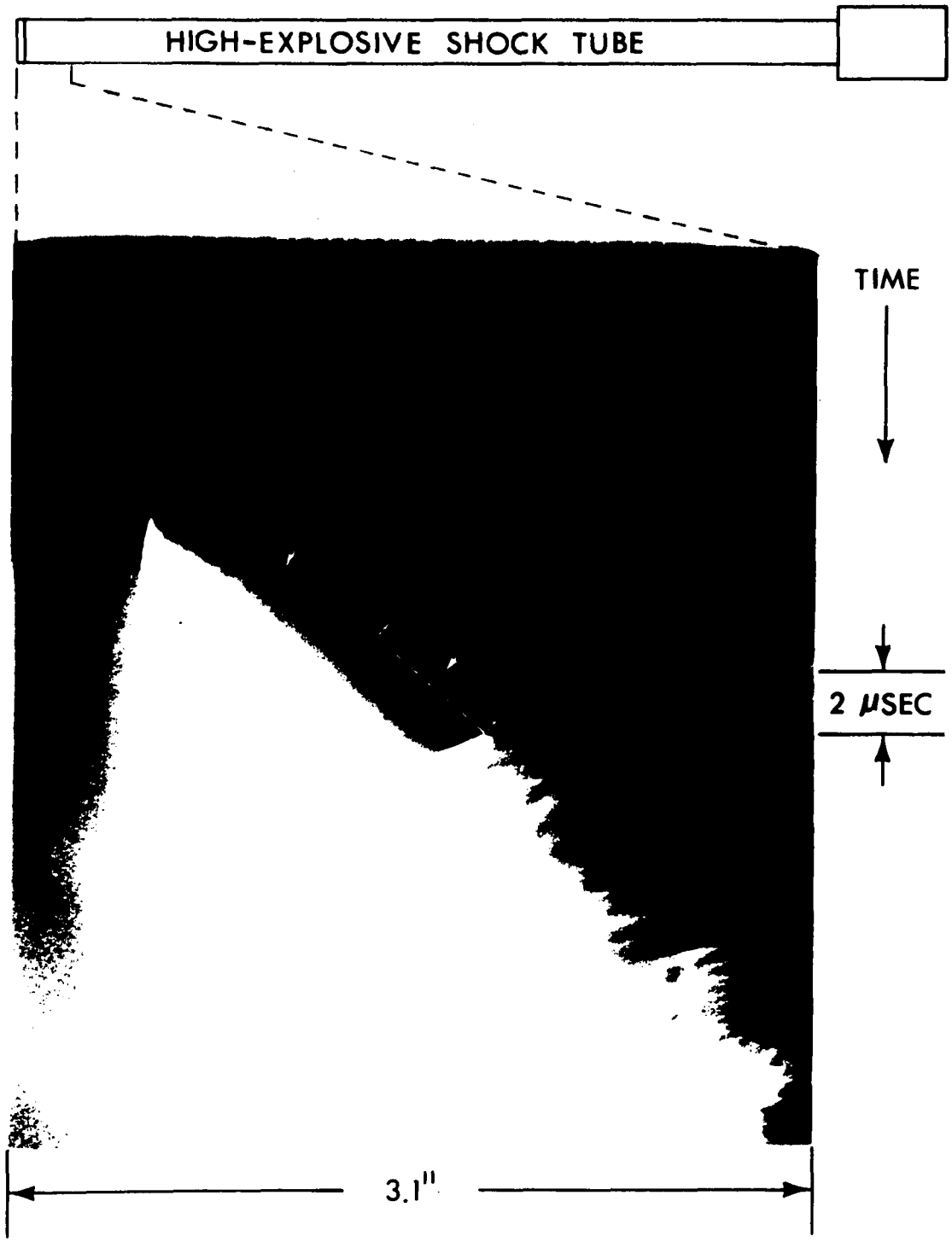

Fig. 10. Smear Camera Record of Reflected Shock

Spectrograph Experiments

The arrangement of apparatus used in the spectrograph experiments is shown in Fig. 11. For clarity, the position of the spectrograph itself has not been included in the figure and only the location of the spectrograph entrance slit has been specified. The pictured location of the shock tube, remote from the front of the concrete building, was necessary because an adjacent firing would have ruptured the thin glass viewing window.

The objective lens formed a horizontal image of the tube slit across the vertical spectrograph slit causing a narrow spectrum characteristic of the imaged light to be formed at the spectrograph film plane. As the rotating mirror turned (Section A-A), the image of the tube slit was swept down the spectrograph slit and the position of the spectrum at the film plane moved proportionately. Hence transient behavior of the light emitted from the tube at the position defined by the intersection of the tube slit and the spectrograph slit projected to the tube (Section B-B) was recorded on the spectrogram as a function of time. The distance from the end plate at which the projected spectrograph slit crossed the shock tube axis was determined from the smear camera photographs to be sufficient for the establishment of steady-state flow following the shock reflection.

Optical alignment followed the placement of an optical pattern at the tentative location of the shock tube axis. The plane relay mirror was positioned and the objective lens was adjusted to focus the pattern over the spectrograph slit. The pattern was then removed and a marker moved first several inches before and then several inches behind the position previously occupied by the pattern. At each marker position the optic axis was determined by moving the marker back and forth until its image

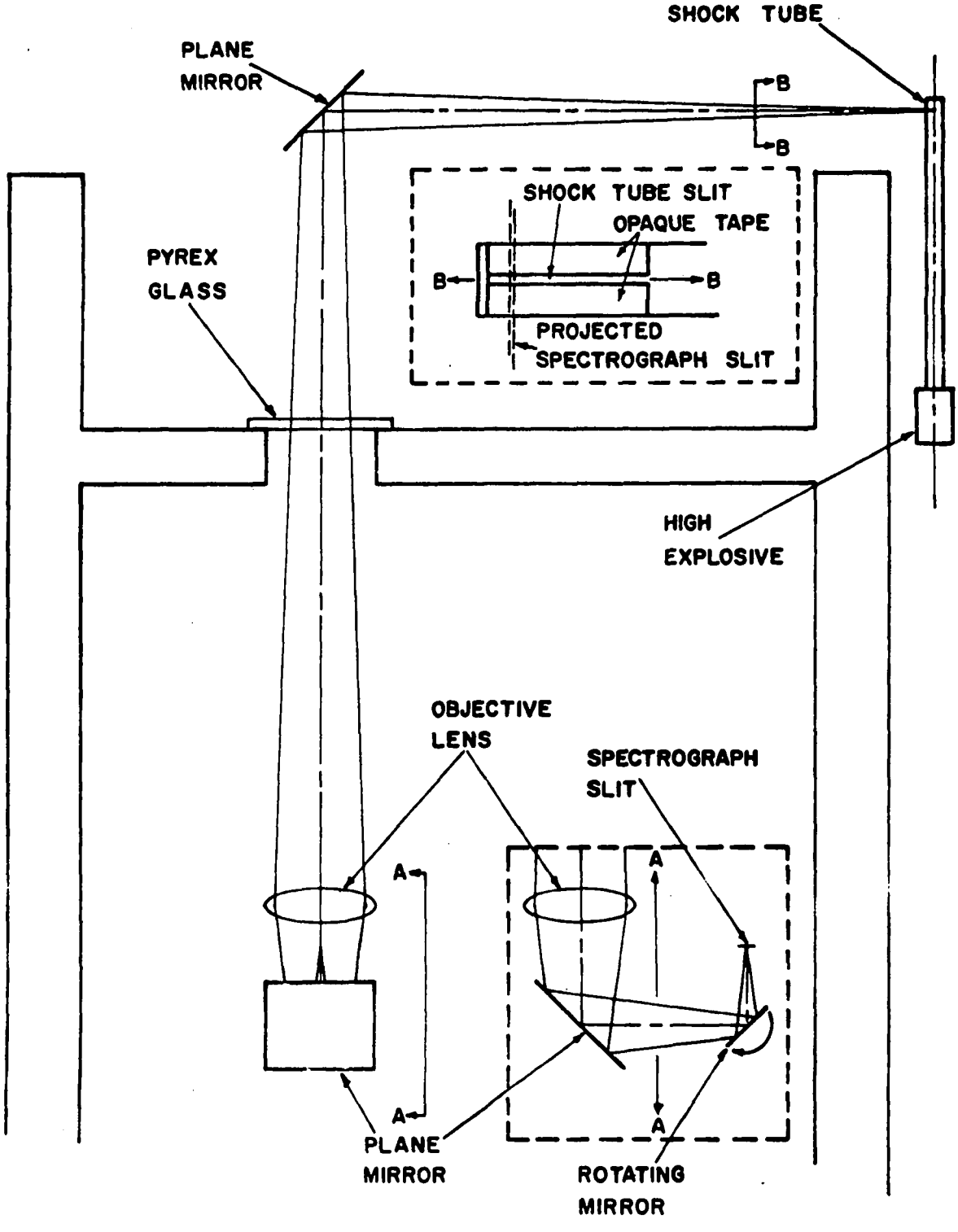

Fig. 11. Arrangement for Spectrograph Experiments

LASL-AEC-OFFICIAL
LASL-AEC-OFFICIAL

fell directly over the slit. This procedure was possible as a result of the extended depth of field of the objective lens. The shock tube axis was then placed normal to this established optic axis at the position previously occupied by the optical pattern.

The rotating-mirror synchronizer was adjusted so that the light emitted from the relaxation zone behind the reflected shock front would be centered in the approximately 14 μsec total writing time recorded on the spectrogram.

Reference spectra were placed on the spectrograms prior to each experiment. The light emitted from the electrodeless helium discharge was made incident on the spectrograph slit which was covered except for small sections at the extreme top and bottom. The two references, each about 0.4 mm high, did not extend into the central 10 mm of the film on which the light from the relaxation zone was recorded. Some typical time-resolved spectrograms, one for each set of experimental conditions experienced in this research, are presented in Fig. 12. In these experiments the tube slit was 3 mm high, the spectrograph slit was 60 μ wide, the mirror writing speed was 1.5 mm μsec^{-1} on the slit, and the magnification of the external optics was 0.0826 or 0.0513 when the objective lens was an f/5 achromatic or an f/5.3 quartz lens respectively.

Spectrogram Film Calibration

Calibration of the photographic emulsion with respect to relative light intensity in the vicinity of the helium spectral lines was necessary for the measurement of the line shapes (intensity vs. wavelength). For a detailed description of the properties of photographic emulsions one may

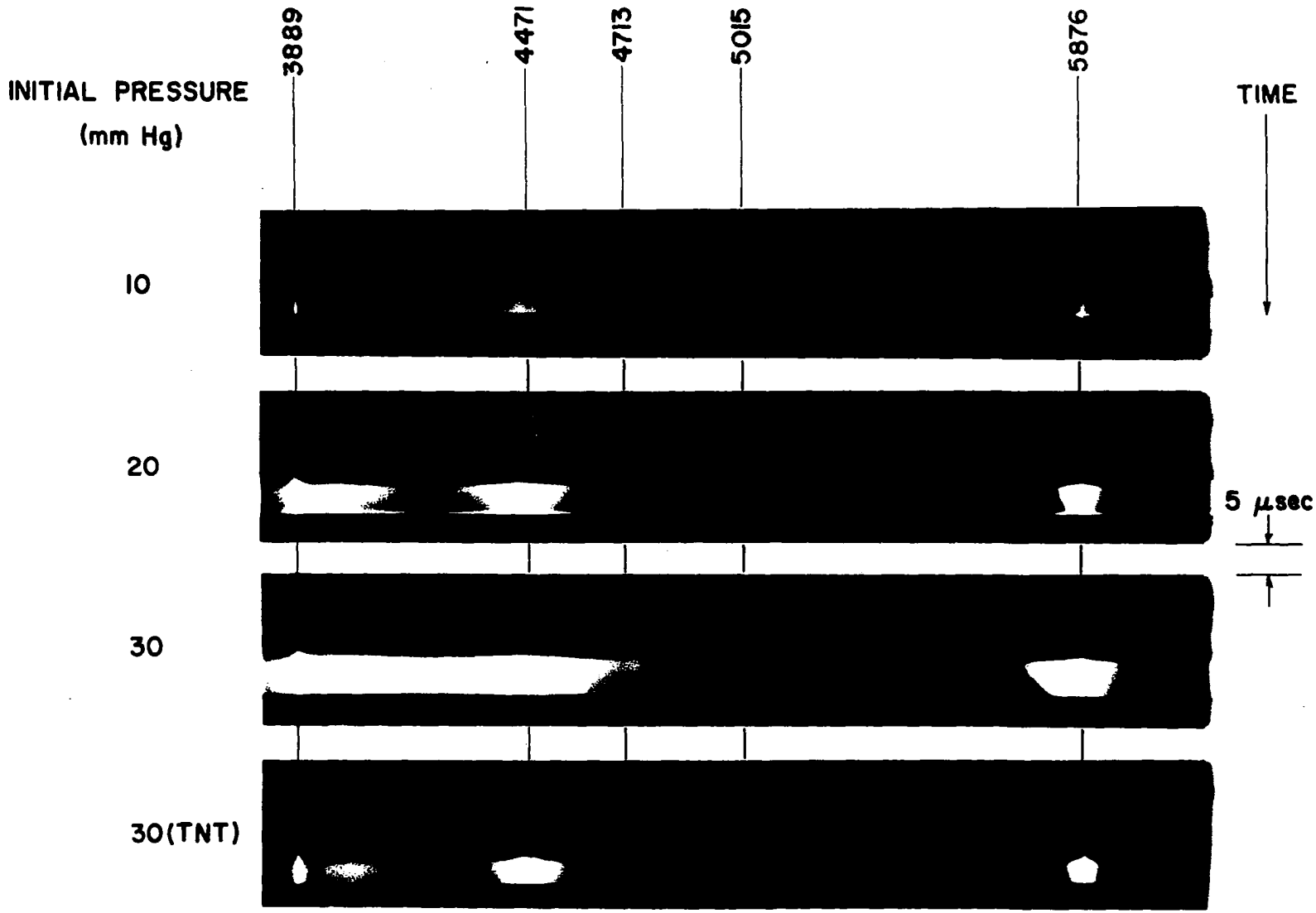

Fig. 12. Time-Resolved Spectrograms

consult the book by Mees[3] and the various Eastman Kodak technical publications. For the present discussion, however, only the following photographic parameters need be defined:

$O = I_o/I$ = opacity

I_o = intensity of a measuring light beam incident on the exposed emulsion

I = intensity of the transmitted measuring beam

$D = \log O$ = photographic density

E = exposure or the time integral of the intensity of the exposing light

In general all emulsions exhibit a similar relationship between the density and the logarithm of the exposure, the plot of which is referred to as the characteristic or Hurter and Driffield curve[4]. For a given exposure time, knowledge of the characteristic curve for the emulsion in use was sufficient to determine line shapes from the density vs. wavelength measurements made with the microdensitometer. The shape of these curves can vary, however, as a function of film development, wavelength of the exposing light, and exposure time. The exposure and processing of the calibration film from which the curves were obtained were therefore as similar as possible to that experienced by the experimental spectrograms.

A calibration film was exposed by the argon bomb light source just preceding each experiment. First, the bomb was placed at the position to be occupied by the shock tube in the subsequent experiment but with its axis normal to what would be the direction of the tube axis. An image of

---

[3] C. Mees, The Theory of the Photographic Process (Macmillan Company, New York, 1942).

[4] F. Hurter and V. Driffield, J. Soc. Chem. Ind. 9, 455 (1890).

the horizontal bomb slit was then focused over the vertical spectrograph slit. About midway in the period of light emission from the bomb, the image of the bomb slit was swept down the spectrograph slit at such a speed as to make the ratio of the slit height to the writing speed equal to that of the shock tube experiment. The exposure time for any point down the calibration film was therefore equal to that of the experimental film, and errors introduced into the calibration as a result of failure of film reciprocity at these short exposure times (0.165 μsec) were avoided. The calibration film was retained and developed with the experimental film so that differences in developer strength and temperature or development time would not influence the calibration.

The actual determination of the shape of the characteristic curve required variation of the exposure by the exposing light and measurement of the changes in the photographic density that these variations produced. The variation of exposure was accomplished by placing a seven-step filter[5] over the spectrograph slit. The intensity of the argon bomb was found to be constant over the 3 μsec time required to sweep down the filter. The image writing speed was constant and the amount of transmitted light which passed through each step was known relative to the clear or density 0 step from the filter calibration. The exposure at each step was therefore proportional in a known way to the exposure corresponding to the clear step. This information together with the densitometric measurement of each step on the exposed film was sufficient to establish the shape of the characteristic curve.

---

[5]Model 16-830 purchased from the Jarrell-Ash Company, Newtonville, Mass. Each step, produced by the evaporation of rhodium on crystal quartz, was 1.2 mm wide. The density range was from 0 to 1.2 in steps of approximately 0.2.

The values of the exposure along the log exposure (or log intensity axis since the exposure time was constant) of the characteristic curve were only relative since no absolute calibration was involved in this technique. The curve did, however, describe the relationship between film density and relative intensity which was required for the data reduction. A curve was established for each of several wavelengths along the calibration film, but no effort was made to compare relative intensities between wavelengths.

In some cases, in order to bring the exposure of the calibration film into the same range as that of the experimental film, a 0.4 neutral density filter was placed over the argon bomb slit. A representative calibration film showing the continuous nature of the light in the regions near the helium lines of interest is presented in Fig. 13.

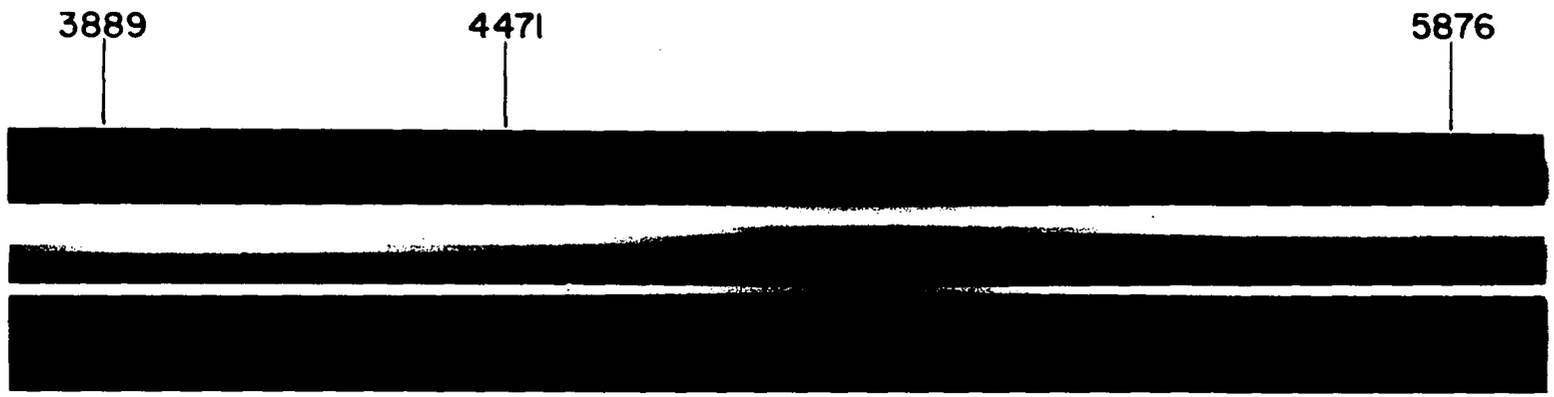

Fig. 13. Film Calibration Spectrogram

CHAPTER IV

EXPERIMENTAL RESULTS AND ANALYSIS OF DATA

Qualitative Results

In addition to the determination of the shock velocities, measurements of the smear camera records resulted in the collection of other information pertinent to the kinetics experiments. These observations were essential to establishing the validity of the one-dimensional shock calculations, determining the range of initial conditions which would result in a spectrally measurable relaxation zone, and evaluating the effect of both wall and gas-borne impurities on the relaxation.

Smear camera photographs taken by Seay[1] early in the history of the high-explosive shock tube sometimes showed the existence of nonplanar shock waves. At that time and throughout this research, the primary evidence as to the wave planarity was obtained by observing the end view of the tube at the moment the incident shock was reflected. The time of reflection as a function of distance along the tube diameter was readily measured as a result of the abrupt increase in light intensity at shock reflection. Apparently the care exercised in the assembly of each tube was rewarding, as only one obviously nonplanar shock was observed in the near sixty smear camera records obtained in the course of this investigation.

---

[1]Seay, op. cit., p. 30.

A rough estimate of the length of the ionization relaxation zone was obtained by visual inspection of smear camera photographs. Referring again to Fig. 10, the reflected shock front was observed to decelerate from an initially high velocity near the end plate to a constant steady-state velocity after several millimeters of travel. A noticeable increase in luminosity, interpreted as the approximate location where equilibrium was reached, followed the shock front at some distance. Using the explosive selected as the booster charge for the major part of this work (cyclotetramethylenetetranitramine--generally abbreviated as HMX), it was found that the region between the shock front and the equilibrium "front" at steady-state conditions could no longer be resolved in the photographs for initial tube pressures greater than 30 mm of Hg. On the other hand, the luminosity of this zone was too low to be well recorded on both the smear camera records and the spectrograms if the initial pressure was less than 10 mm of Hg. These results limited the range of initial conditions in which observations could be made.

Throughout this investigation no consistent correlation existed between the gas-borne impurity concentration determined mass spectrometrically and the length of the relaxation zone as observed in the smear camera records or indeed in the spectrograms. In general the impurity ratios were found to be characteristic of the composition of air although in a few instances the presence of unexplainable impurity gases was recorded. In a given series of experiments the concentrations varied from about twice to about one-half of the average total impurities of 600 ppm by volume for an initial tube pressure of 10 mm Hg, 400 ppm at 20 mm, and 350 ppm at 30 mm.

The effect of wall-borne impurities on the relaxation was also investigated. A shock reflected from the end plate of a tube which had a thin

A rough estimate of the length of the ionization relaxation zone was obtained by visual inspection of smear camera photographs. Referring again to Fig. 10, the reflected shock front was observed to decelerate from an initially high velocity near the end plate to a constant steady-state velocity after several millimeters of travel. A noticeable increase in luminosity, interpreted as the approximate location where equilibrium was reached, followed the shock front at some distance. Using the explosive selected as the booster charge for the major part of this work (cyclotetramethylenetetranitramine--generally abbreviated as HMX), it was found that the region between the shock front and the equilibrium "front" at steady-state conditions could no longer be resolved in the photographs for initial tube pressures greater than 30 mm of Hg. On the other hand, the luminosity of this zone was too low to be well recorded on both the smear camera records and the spectrograms if the initial pressure was less than 10 mm of Hg. These results limited the range of initial conditions in which observations could be made.

Throughout this investigation no consistent correlation existed between the gas-borne impurity concentration determined mass spectrometrically and the length of the relaxation zone as observed in the smear camera records or indeed in the spectrograms. In general the impurity ratios were found to be characteristic of the composition of air although in a few instances the presence of unexplainable impurity gases was recorded. In a given series of experiments the concentrations varied from about twice to about one-half of the average total impurities of 600 ppm by volume for an initial tube pressure of 10 mm Hg, 400 ppm at 20 mm, and 350 ppm at 30 mm.

The effect of wall-borne impurities on the relaxation was also investigated. A shock reflected from the end plate of a tube which had a thin

layer of calcium evaporated onto the inside walls was compared to those reflected in clean, well-baked tubes at initial pressures of 10 mm. To be determined was the ability of the shocks to ionize the wall-borne impurities and as a result accelerate the helium ionization by supplementing the electron concentration in the relaxation zone. If such a process were present in the clean tubes, the gross amounts of calcium in this tube would greatly enhance the effect and shorten the relaxation zone appreciably. There was no significant difference between the appearance of the relaxation zone in the coated tube and that observed in similar smear camera photographs taken of the clean tubes.

Shock Velocity Data

The mean value of the average incident shock velocities at each of the three initial pressures is presented in Table 1 together with an unbiased estimate of the standard deviation of the data. The booster charge was HMX except for the entry specifically noting the use of the less-powerful explosive trinitrotoluene[2]. In those tubes where the incident shock was made visible by impurity doping, the average velocities were not significantly different from those measured in pure helium.

The accuracy to which the average velocity could be measured was limited only by the errors in the measurement of the tube length, l, and the shock transit time, t. Estimating these errors as no greater than 1 mm and 0.1 μsec respectively, the maximum error in the measured average velocity, l/t, for any given experiment may be expected to be

---

[2]The notation (TNT) is continued for the remainder of this work to denote those experiments using this less-powerful explosive.

TABLE 1

MEASURED AVERAGE INCIDENT SHOCK VELOCITY

Initial Pressure (mm Hg)	No. of Shots	Mean Velocity (mm μsec^{-1})	Standard Deviation (mm μsec^{-1})
10	4	13.01	0.02
20	4	12.93	0.09
30	4	12.84	0.10
30 (TNT)	3	10.86	0.12

$$dv = \sqrt{\left(\frac{\partial v}{\partial l}\, dl\right)^2 + \left(\frac{\partial v}{\partial t}\, dt\right)^2} = \sqrt{\left(\frac{dl}{t}\right)^2 + \left(\frac{l dt}{t^2}\right)^2}$$

which amounted to about 0.02 mm μsec^{-1} for the worst set of time and length measurements.

The observed systematic decrease in the measured incident shock velocity with increasing initial pressure in HMX boostered tubes was apparently statistically significant and somewhat greater than might be readily explained by physical reasoning. It was expected that velocity differences produced by changes in initial pressure of this magnitude would be of the order of the measurement error and therefore not detectable. These observed velocities were nonetheless accepted at face value.

As was stated previously, both the reflected shock velocities and the spectral characteristics were determined in experiments completely independent from those in which the incident shock velocities were measured. It was therefore necessary to predict an uncertainty for the mean of the incident velocity in these additional shots. This problem, the difference between two means, has been treated by Brownlee[3], Ostle[4], Anderson and Bancroft[5], and others. The difference between $\bar{U}_o$, the mean incident velocity actually measured in the n_o shots, and $\bar{U}_n$, the mean velocity of n shots in a series where either the reflected shock velocities were measured or the emission spectra recorded, will be normally distributed about zero with a standard deviation of

---

[3] K. A. Brownlee, Industrial Experimentation (Chemical Publishing Company, New York, 1953), p. 34.

[4] B. Ostle, Statistics in Research (Iowa State College Press, Ames, 1954), p. 83.

[5] R. L. Anderson and T. A. Bancroft, Statistical Theory in Research (McGraw-Hill Book Company, Inc., New York, 1952), p. 80.

$$s_m = s_o\sqrt{\frac{1}{n_o} + \frac{1}{n}}$$

if it is assumed that all measurements to be taken are from a single normal distribution with standard deviation s_o. The quantity

$$t = \frac{\overline{U}_o - \overline{U}_n}{s_o\sqrt{\frac{1}{n_o} + \frac{1}{n}}}$$

is a t distribution with $n_o + n - 2$ degrees of freedom. However, since only n_o measurements of the incident velocity were actually made, the degrees of freedom are limited to $n_o - 1$ in this calculation. Referring to standard statistical tables for this distribution[6], it is found that the probability is 90% that the difference $\overline{U}_o - \overline{U}_n$ is between

$$\pm s_o\sqrt{\frac{1}{n_o} + \frac{1}{n}}\ t_{0.9}$$

where $t_{0.9}$ is 6.31, 2.92, 2.35, 2.13, 2.02, 1.94 for degrees of freedom equal to 1 through 6 respectively.

The error limits reported for the calculated reflected shock properties, velocities in Table 2 and equilibrium electron densities in Figs. 22 through 26, correspond to the changes in the properties resulting from the variation of $\overline{U}_n$ through the 90% confidence interval for the mean of the incident shock velocity. The values of $\overline{U}_o$, s_o, and n_o used in the calculations of the intervals were obtained from the appropriate entries in Table 1.

The mean values and standard deviations of the reflected shock velocities in 59 mm diameter tubes measured from smear camera records like Fig. 10

---

[6] B. Ostle, op. cit., p. 451.

are presented in Table 2. Although there existed uncertainties in measurement of each of the parameters used to determine the reflected velocities (camera writing speed, optical magnification, and the angle between the steady-state reflected shock front and the time axis of the film), the error associated with the angle measurement completely dominated the other two terms in magnitude. On this basis, the maximum error in the measurement of the reflected velocity was estimated to be about ± 2%.

The reflected velocities obtained from the hydrodynamic calculations described in the Appendix are also presented in Table 2 for comparison with the observed values. The agreement between observed and calculated velocities is quite good at each experiment condition except for the results at initial tube pressure of 10 mm. This agreement is some verification of the ability of one-dimensional shock hydrodynamics to describe the equilibrium state in the high-explosive tube with a diameter of 59 mm providing that the initial pressure is greater than some value between 10 and 20 mm.

A brief digression from the main purpose of this research was made to investigate possible causes for the reflected velocity in tubes at initial pressure of 10 mm being about 10% below that calculated. In supplemental experiments it was found that the incident shock velocity changed by less than 1% of its magnitude but the measured reflected shock velocity approached the calculated value as the shock tube diameter was increased to about 90 mm. These results, together with the agreement between calculated and measured velocities at higher initial pressures and experimental proof of a complete shock reflection[7], led to the conclusion that this discrepancy was due to

---

[7] R. A. Jeffries, L. B. Seely, and R. G. Fowler, Phys. Fluids 7, 1390 (1964).

TABLE 2

MEASURED AND CALCULATED STEADY-STATE REFLECTED SHOCK VELOCITY

Initial Pressure (mm Hg)	No. of Shots	Mean Velocity (mm μsec^{-1})	Standard Deviation (mm μsec^{-1})	Calculated Velocity (mm μsec^{-1})
10	4	3.45	0.15	3.91 ± 0.00
20	5	3.93	0.31	4.04 ± 0.00
30	5	4.18	0.15	$4.12 \begin{smallmatrix} + 0.01 \\ - 0.00 \end{smallmatrix}$
30 (TNT)	4	4.27	0.07	4.21 ± 0.01

boundary layer effects as described by Rudinger[8]. Therefore, although the spectral behavior of the gas behind the reflected shock is reported in the following section, the results at initial pressure of 10 mm in 59 mm tubes have been omitted from further consideration due to the uncertainties in calculating the state of the shocked gas. Only the results of a single experiment at initial pressure of 10 mm using a tube of 95 mm diameter have been included in the kinetic analysis.

Time-Resolved Spectra

The shape of the shock-produced emission spectral lines as a function of time was obtained from microdensitometer traces made in successive scans along the dispersion axis of the spectrogram. These scans were continued at separations along the time axis corresponding to 0.17 μsec until the entire relaxation zone had been traversed and the line shapes were no longer markedly changing with time. A scan across the reference spectra was also made to verify the spectrograph dispersion curve for each spectrogram.

A time-resolved spectrogram and the microdensitometer traces of the film made across the reference spectra and across the relaxation zone at one point in time are shown in Fig. 14. The traces have been drastically reduced in size photographically for comparison with the film. As shown in the figure, the visible shock spectrum contained the allowed HeI lines at 3889 Å (2^3S-3^3P), 4713 Å (2^3P-4^3S), 5015 Å (2^1S-3^1P), and 5876 Å (2^3P-3^3D), a forbidden line at 6069 Å (2^3P-3^3P), and the "allowed-forbidden pair" at 4471 Å (2^3P-4^3D) and 4470 Å (2^3P-4^3F) superimposed over a mixture of continuum radiation and other less intense, heavily broadened lines.

---

[8] G. Rudinger, Phys. Fluids 4, 1463 (1961).

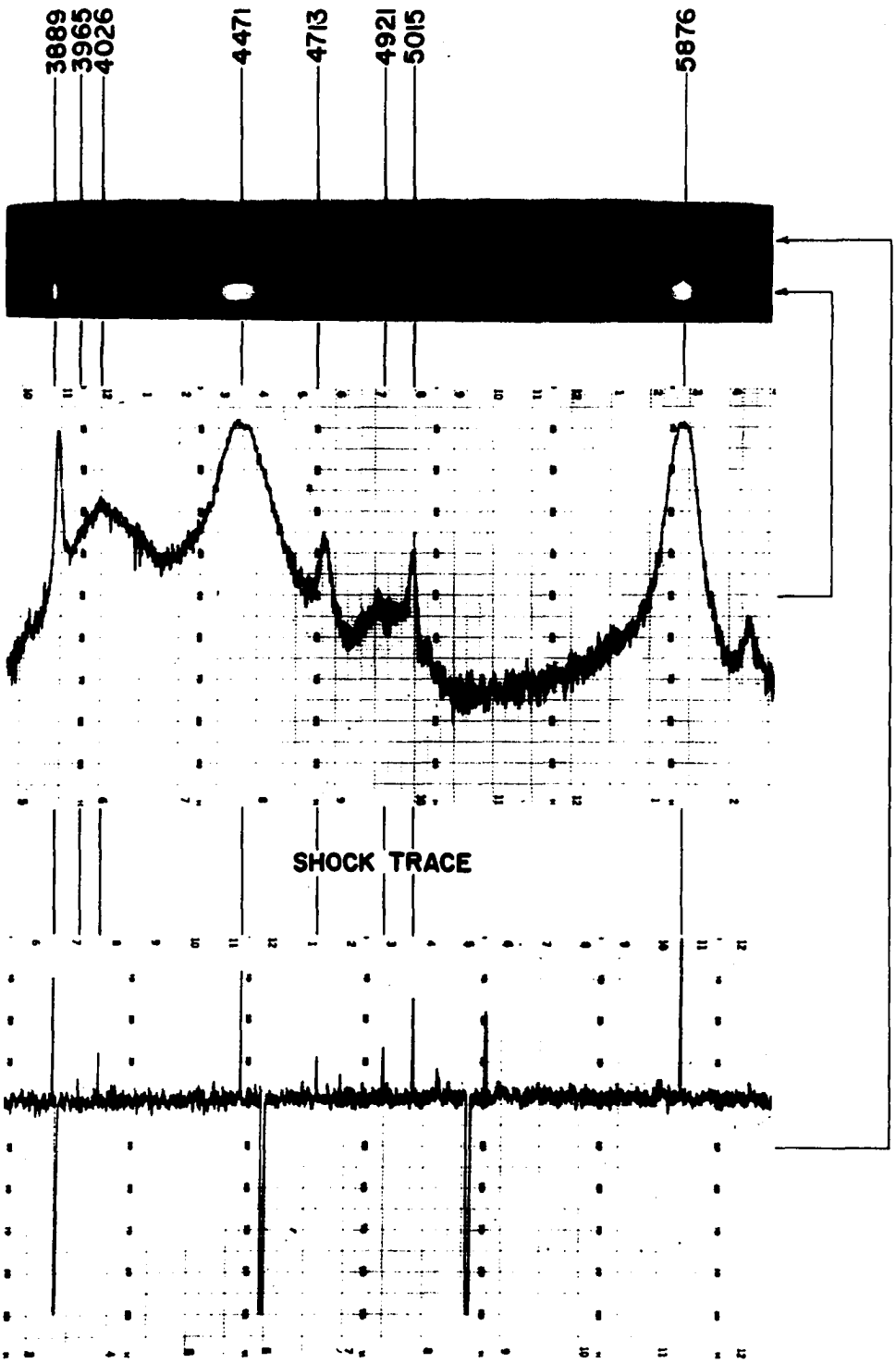

Fig. 14. Densitometry

The reduction of the information contained on the traces consisted primarily of the determination of the half-widths (full spectral line width at half-maximum intensity) of the more intense emission lines. No attempt was made to measure shift of the lines, for to do so would have required placing reference spectra on that portion of the film where the relaxation zone was recorded and would have obscured the line shapes there.

Detailed analysis of the spectrograms proceeded as follows: In conjunction with the tracings made on the experimental films and without change in the optics or electronic adjustments of the microdensitometer, traces were made of the calibration film at several wavelengths. The characteristic curves constructed from the traces were then used to transform the density-wavelength tracing of the experimental film into an intensity-wavelength plot of the region containing the spectral line of interest. The response of the emulsion was assumed to be constant over this region and equal to its value at the wavelength of the unperturbed line. Except for the wavelength region below about 3850 $\AA$ where the transmissivity of the objective lens began to decrease, the reflectivity of the spectrograph elements and the transmissivity of the external optics and shock tube were essentially constant making this intensity-wavelength information representative of the source within the shock tube.

In order to determine the shape of a specific line, a base intensity due to the sum of continuum and nearby relatively weak line radiation was subtracted from the total intensity-wavelength plot of the region about the line. The base was assumed to follow a smooth curve between the minima bounding the line. The difference was then replotted and the width at half-maximum intensity measured. Special consideration was given the determination of the maximum intensity of the 4471 $\AA$ line which exhibited

asymmetries similar to those previously observed for the hydrogen line H_β[9]. The maximum intensity was taken to be the average of the maxima of the blue and red peaks. Typical profiles of the lines at 3889 Å, 4471 Å, and 5876 Å are presented in Figs. 15 through 17[10]. The half-width for each of the three lines of interest was measured from the profiles obtained from each trace made through the relaxation zone. At this point, use was made of theoretical calculations which allowed the direct determination of the charged particle density of the plasma from the half-widths of these heavily broadened spectral lines.

At the conditions experienced in this research, the spectral line profiles were determined primarily by the interactions of the light-emitting atoms with the surrounding particles. Natural and Doppler broadening were orders of magnitude less and could be safely neglected. The most important of the particle interactions was that between the radiating system and the plasma electrons and ions. Since the electric microfields of the charged particles were involved, this type of broadening is referred to as Stark broadening. Recent improvements in the theoretical treatment of Stark broadening have resulted in the ability to determine accurately the electron density of a plasma from the line profiles alone. The theoretical calculations which led to the results for neutral helium emission used here have been completely described and copiously referenced in the recent book by Griem[11]. Differences exist in the details of the calculations

---

[9] H. R. Griem, Z. Physik 137, 280 (1954).

[10] Specifically, these profiles were obtained from the densitometric tracing of Fig. 14. Since no data on line shift were obtained the location of the zero for these profiles is arbitrary.

[11] H. R. Griem, Plasma Spectroscopy (McGraw-Hill Book Company, Inc., New York, 1964), Ch. 4.

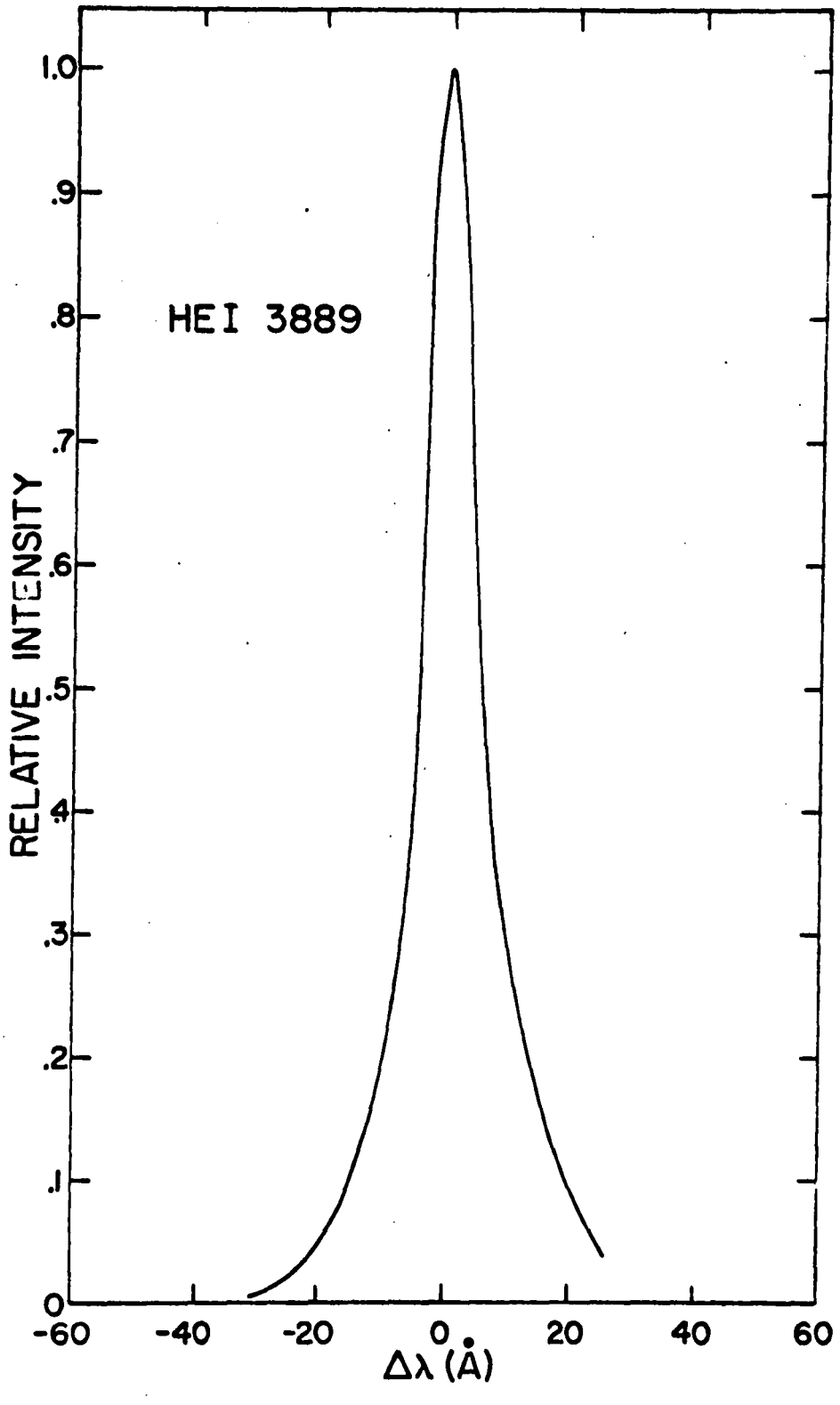

Fig. 15. Observed Line Shape, HeI 3889

LASL-AEC-OFFICIAL
LASL-AEC-OFFICIAL

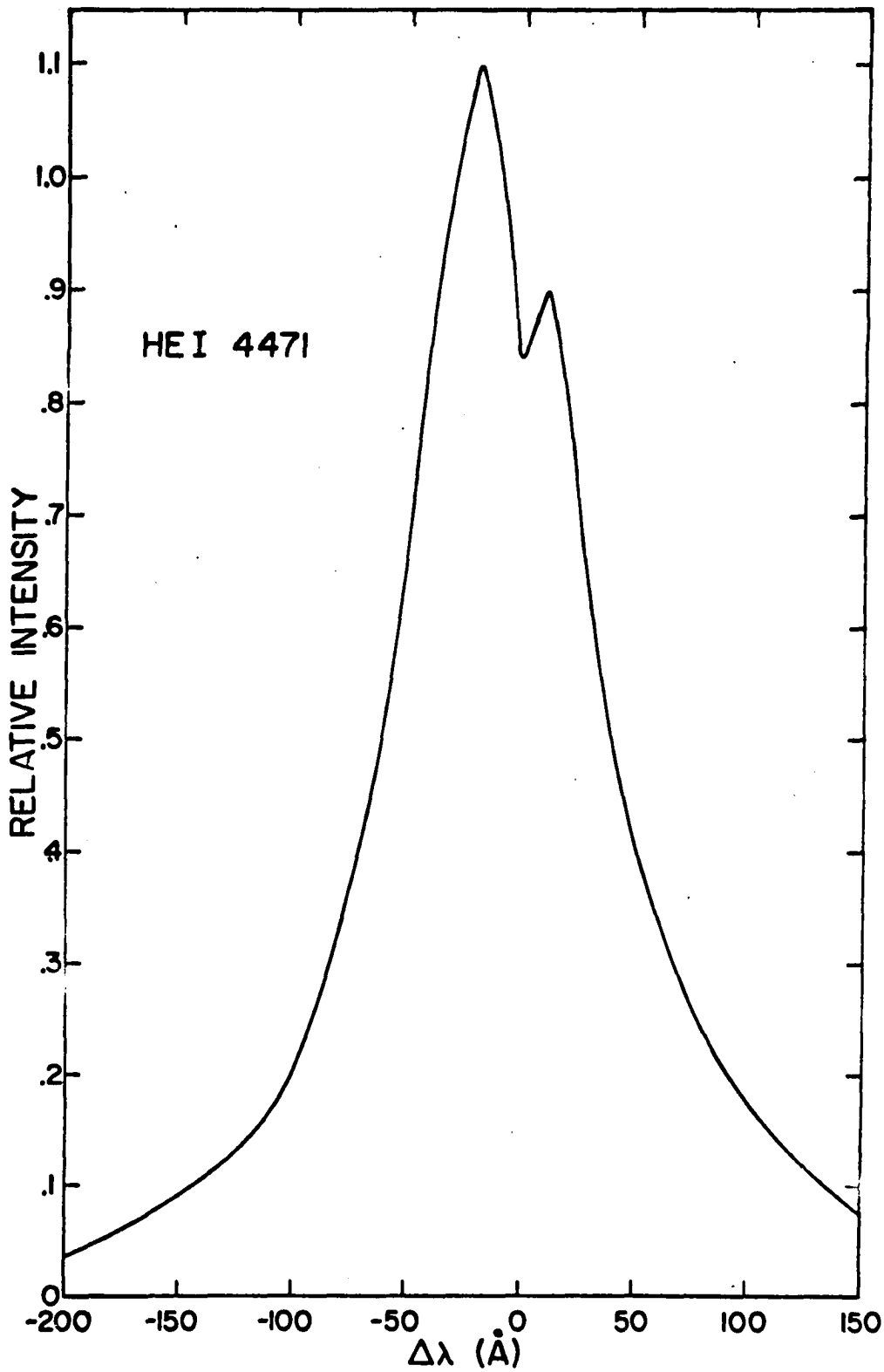

Fig. 16. Observed Line Shape, HeI 4471

LASL-AEC-OFFICIAL
LASL-AEC-OFFICIAL

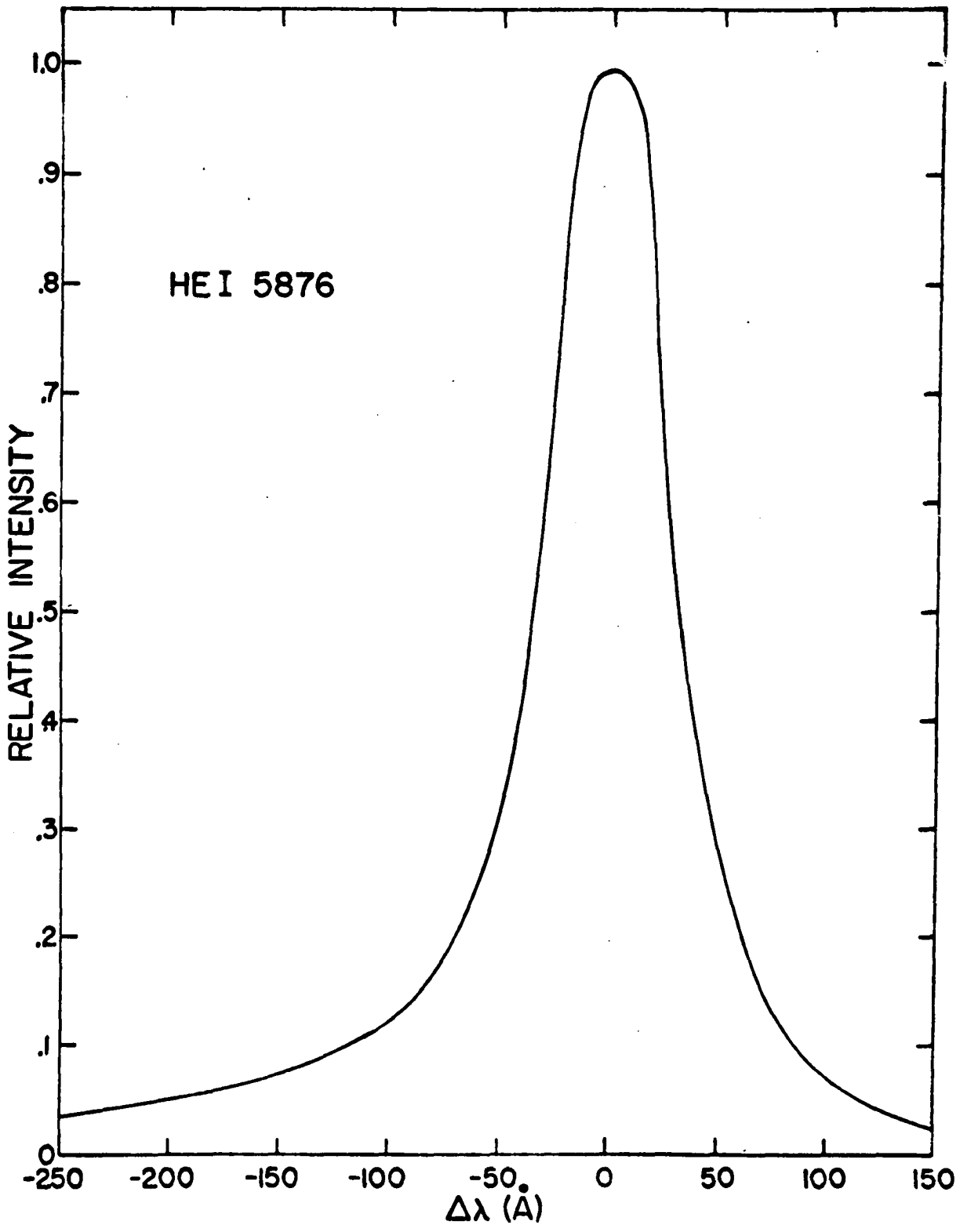

Fig. 17. Observed Line Shape, HeI 5876

LASL-AEC-OFFICIAL

concerning the isolated lines at 3889 Å and 5876 Å, i.e. lines resulting from transitions between levels whose components with different orbital momenta were energetically well separated, and the line at 4471 Å, which was considered to be hydrogenic in nature with degeneracy in the energy of each level of the transition. The differences result in the electron density being almost directly proportional to the half-width of the isolated lines but proportional to the three-halves power of the half-width of the hydrogenic line. Accuracy of the theoretical results which are given below is estimated by Griem to be 20% and 10% for the isolated and hydrogenic lines respectively.

For the isolated helium lines, 3889 Å and 5876 Å, the (full) half-width is given by[12]

$$\delta_{1/2} = [1 + 1.75\alpha\,(1 - 0.75R)]\,w \qquad \text{(IV-1)}$$

where $\delta_{1/2}$ = (full) half-width, Å

α = calculated parameter which characterizes the quasi-static ion broadening

R = parameter characterizing the ion field distribution function

w = electron impact (full) half-width, Å.

The parameter R is given by

$$R = 6^{1/3}\,\pi^{1/6}\,\varepsilon[e]^{1/6}\,(kT)^{-1/2} \qquad \text{(IV-2)}$$

where ε = the electronic charge (4.8×10^{-10} esu)

$[e]$ = electron number density, cm^{-3}

k = Boltzmann constant, ergs $°K^{-1}$

T = temperature, °K

---

[12] H. R. Griem, Phys. Rev. 128, 515 (1962).

while the values of α and w are obtained from tables prepared for each helium line[13]. The $\delta_{1/2}$ - [e] relationships for these two lines are presented in Figs. 18 and 19 for several temperatures.

For the hydrogenic line at 4471 Å, a less complicated relation exists between the half-width and the electron densities for the temperatures and electron densities experienced in these experiments. This relation is[14]

$$\delta_{1/2} = 1.80 \times 10^{-10} [e]^{2/3} \qquad \text{(IV-3)}$$

the plot of which is presented in Fig. 20.

The suitability of using these results in the reduction of data taken in the nonequilibrium relaxation zone is substantiated by the fact that the line profiles do not depend critically on the electron and ion velocity distribution or the temperature, so that the existence of local thermal equilibrium is not a necessary condition. The half-width history of the three lines through the relaxation was therefore transformed using these results into electron density-time information. For 3889 Å and 5876 Å the curves for 2×10^4 °K were used. A typical plot of the results of this type of analysis is given in Fig. 21.

Examination of Fig. 21 shows substantial agreement throughout the relaxation zone between the electron densities indicated by the lines at 3889 Å and 4471 Å. The electron densities indicated by the 5876 Å line are in agreement with those obtained from the 3889 Å and 4471 Å profiles early in the relaxation but increase to unreasonable values as the reaction proceeds to equilibrium. This departure from agreement with results obtained

---

[13] H. R. Griem et al., Phys. Rev. 125, 177 (1962).

[14] H. R. Griem et al., "Stark Broadening of Hydrogen and Hydrogenic Neutral and Ionized Helium Lines in a Plasma," U.S. Naval Research Laboratory Report, NRL-5805 (1962).

LASL-AEC-OFFICIAL

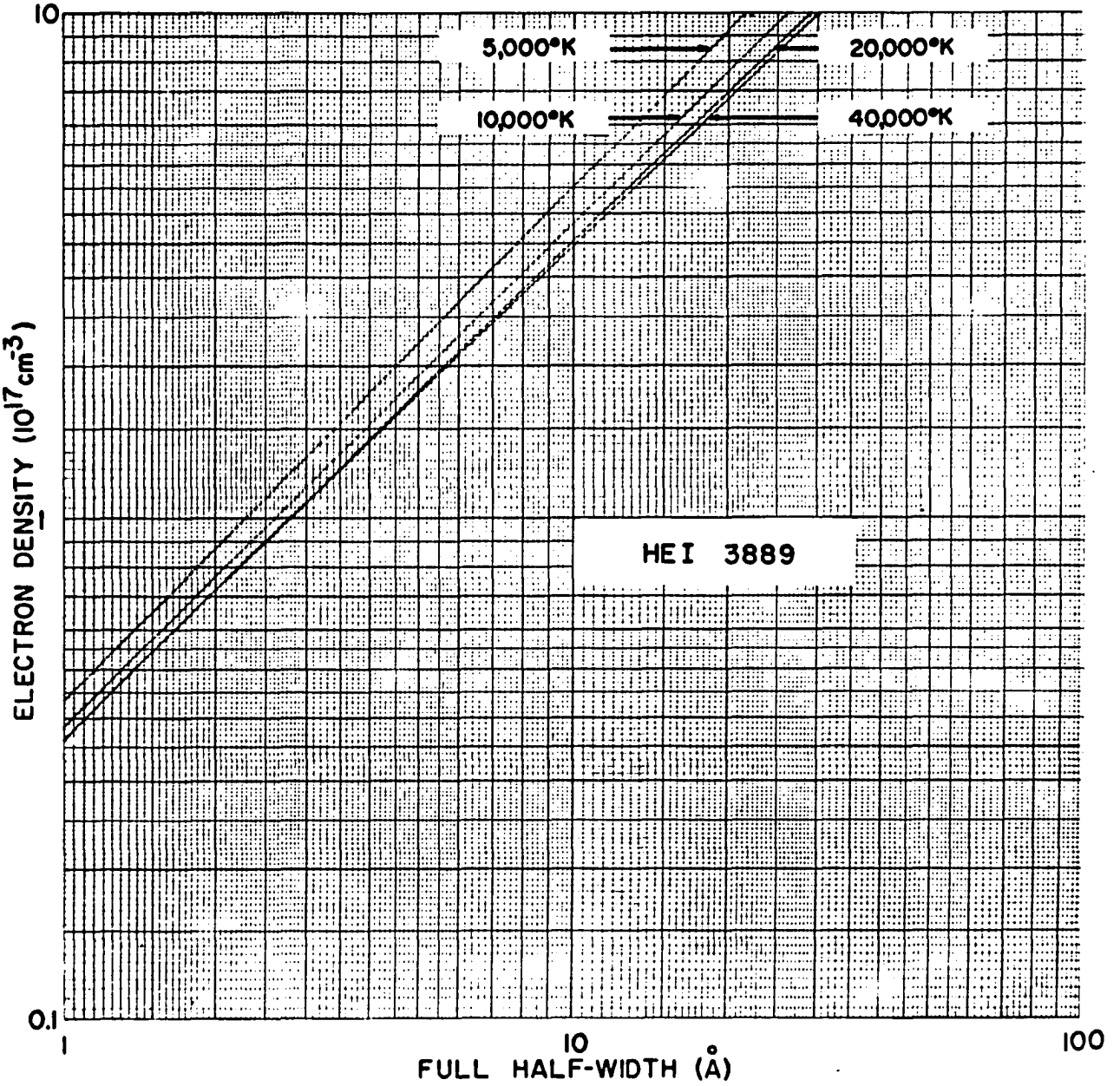

Fig. 18. Stark Broadening of HeI 3889

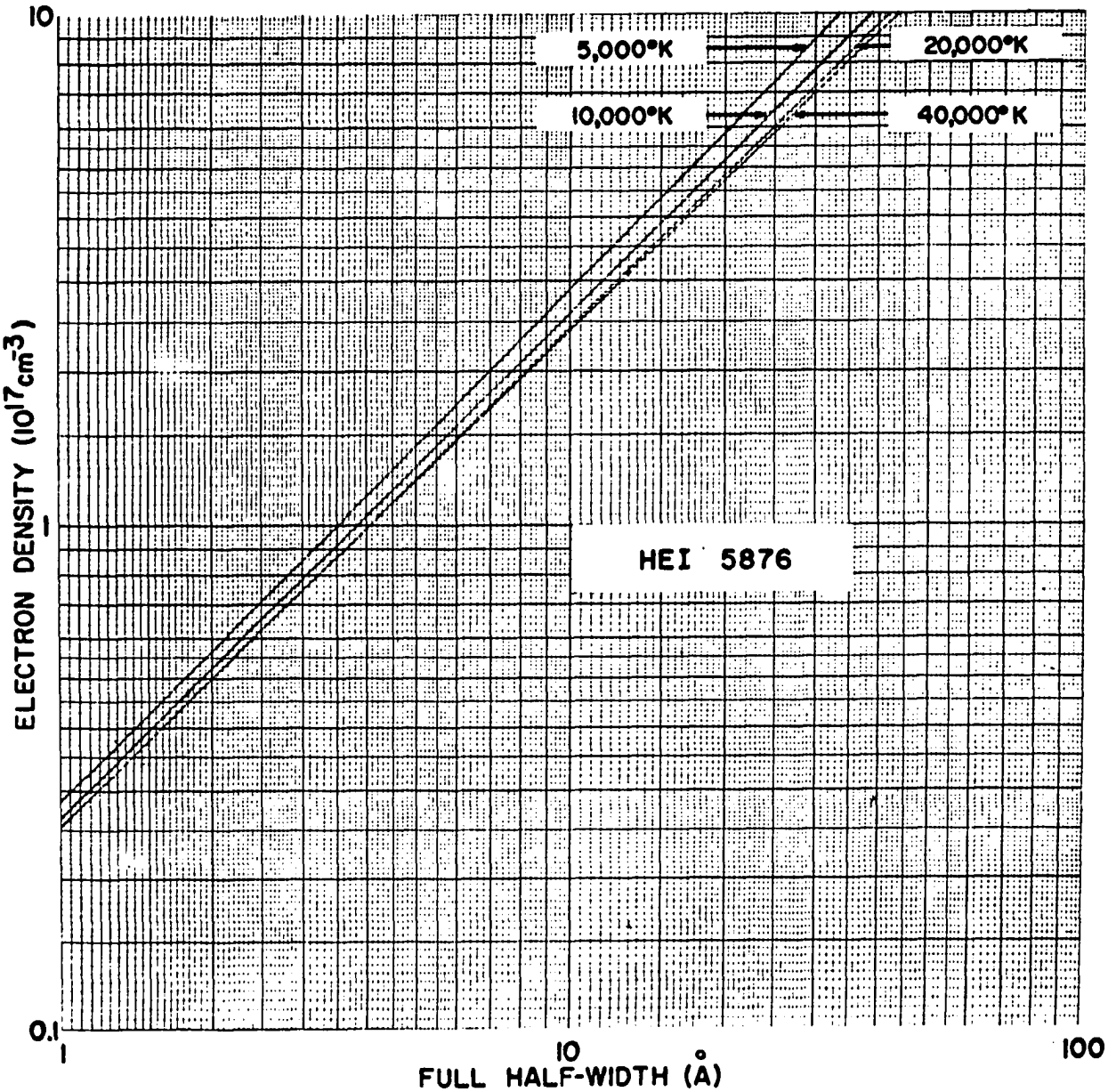

Fig. 19. Stark Broadening of HeI 5876

LASL-AEC-OFFICIAL

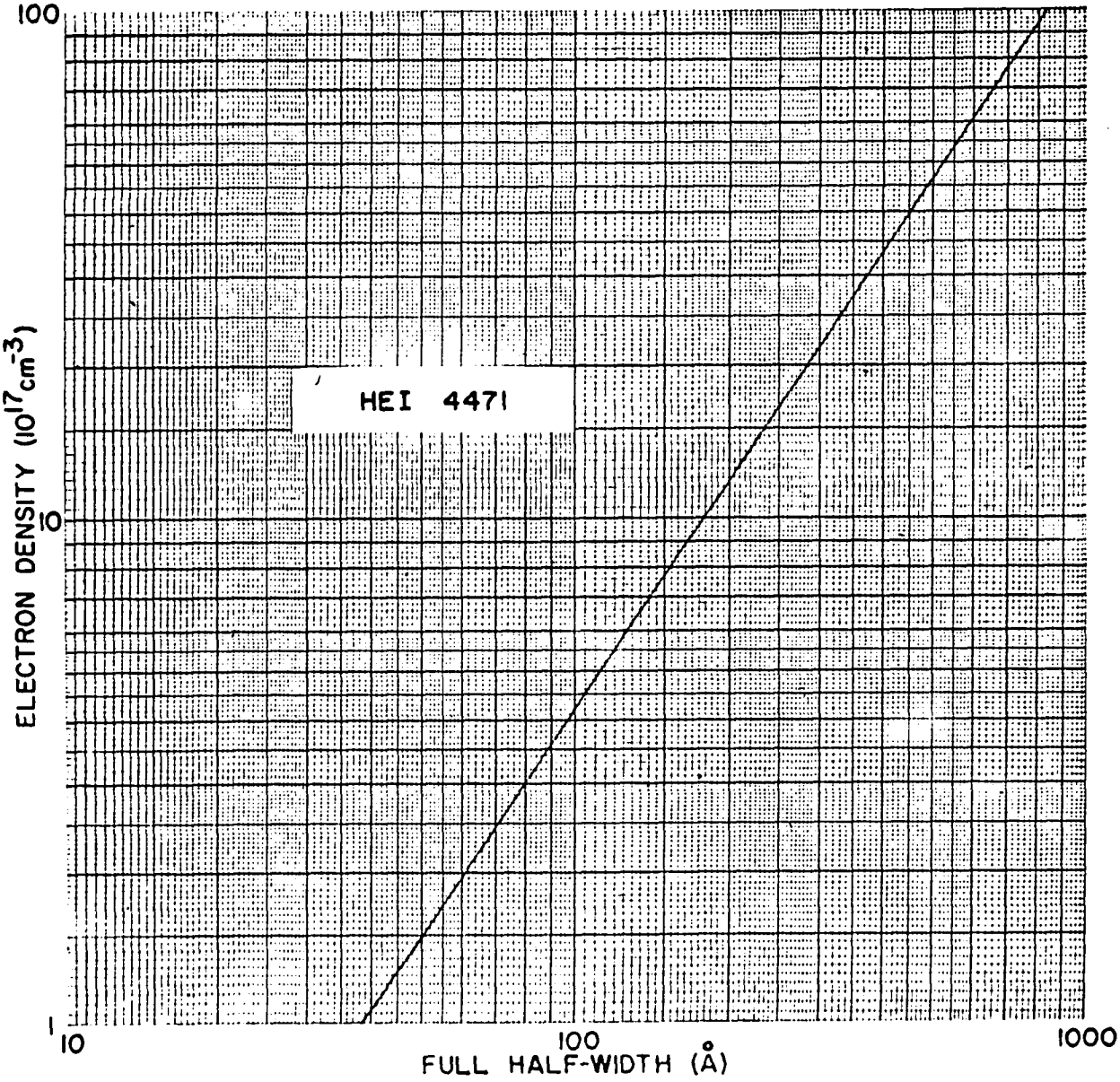

Fig. 20. Stark Broadening of HeI 4471

LASL-AEC-OFFICIAL

LASL-AEC-OFFICIAL

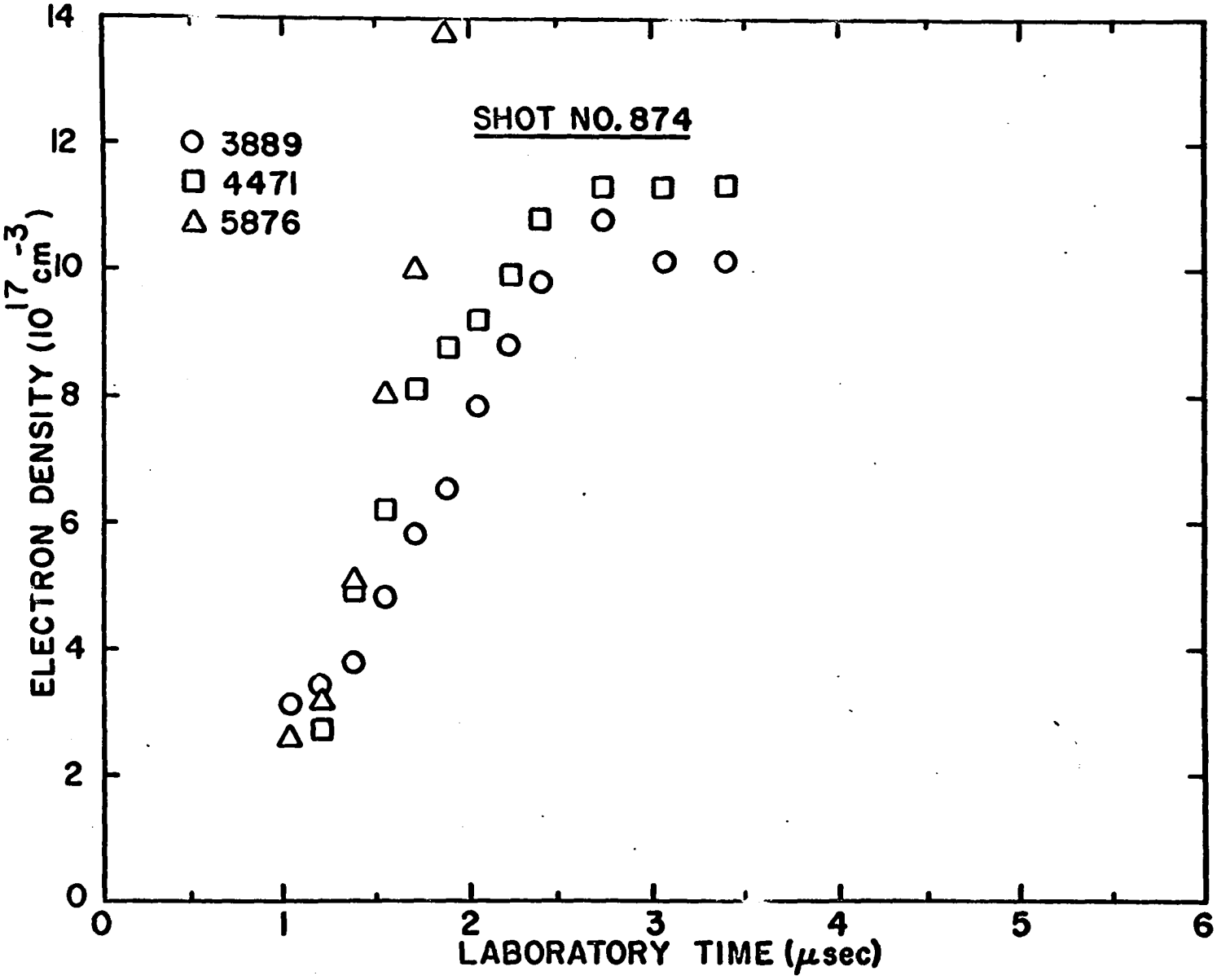

Fig. 21. Relaxation Zone, Comparison of Measurements from Three Spectral Lines

from the other lines is attributed to self-absorption of the 5876 Å line which is the most intense of the HeI emission spectrum.

The agreement between the electron densities indicated by the 3889 Å and 4471 Å lines was observed only in the concluding experiments of this research. The majority of the experimental analyses showed the electron density histories obtained from the 3889 Å line to be both unreproducible and in disagreement with those indicated by the other lines. This behavior was found to be caused by a significant change in the focal length of the f/5 "achromatic" objective lens as the wavelength of the imaged light approached the violet end of the visible spectrum. Since the optical system external to the spectrograph was focused visually and the human eye is most sensitive to light of wavelength near 5000 Å at low levels of lumination[15], the image of the light emitted from the shock tube at 3889 Å was apparently out of focus on the spectrograph slit. Replacement of the "achromatic" lens with an f/5.3 quartz objective lens resulted in the agreement evident in Fig. 21. The lens change had no effect on the results obtained from the lines at 4471 Å and 5876 Å.

Of the three lines in the spectrum that were intense enough to be recorded on the spectrograms over an appreciable fraction of the relaxation zone, the profiles of two lines were generally not suitable for use in the data reduction. Little or no information came from analysis of the 3889 Å line since the lens change came late in the research. Furthermore, the profile of the 5876 Å line varied from the optically-thin profile required for the analysis early in each relaxation zone. The kinetic analysis which follows in Chapter V is therefore primarily based on the information obtained

---

[15] O. Stuhlman, An Introduction to Biophysics (John Wiley and Sons, Inc., New York, 1943), p. 117.

by the analysis of the line at 4471 Å. Two additional features that make the use of this line attractive are a claimed accuracy in the theoretical calculations a factor of two better than that for the isolated helium lines and the minimal effect on half-width measurements due to cold boundary layer absorption which if present would occur at the central dip of the profile.

The electron density-(laboratory) time histories of the relaxation as determined from the 4471 Å line for each of the experimental conditions are presented in Figs. 22 through 26. Although several different methods were employed, all attempts to establish the position of the reflected shock front (or time zero) on the spectrograms were unsuccessful. Time zero on the graphs of the electron density histories must therefore be considered to be entirely arbitrary. The results of the several experiments performed for each of the experimental conditions have been effectively averaged by sliding each along the time axis until in the author's judgement best agreement in the superposition was obtained. As discussed previously the calculated equilibrium electron density and its estimated error limits are also indicated on each graph.

Results of a single experiment utilizing an absorption spectroscopy approach may have some bearing on the subsequent discussion of the ionization kinetics. As shown in Fig. 27, a plane mirror was placed behind the shock tube so that light emitted from a small volume close to the end plate would be reflected back through the tube on the optic axis defined by the spectrograph optics. The shock tube was then fired and the resulting time-resolved spectrogram analyzed in a manner identical to that of the other spectrograph experiments. At early times the spectrogram was exposed only by the light emitted by the gas which was at equilibrium behind the reflected

LASL-AEC-OFFICIAL

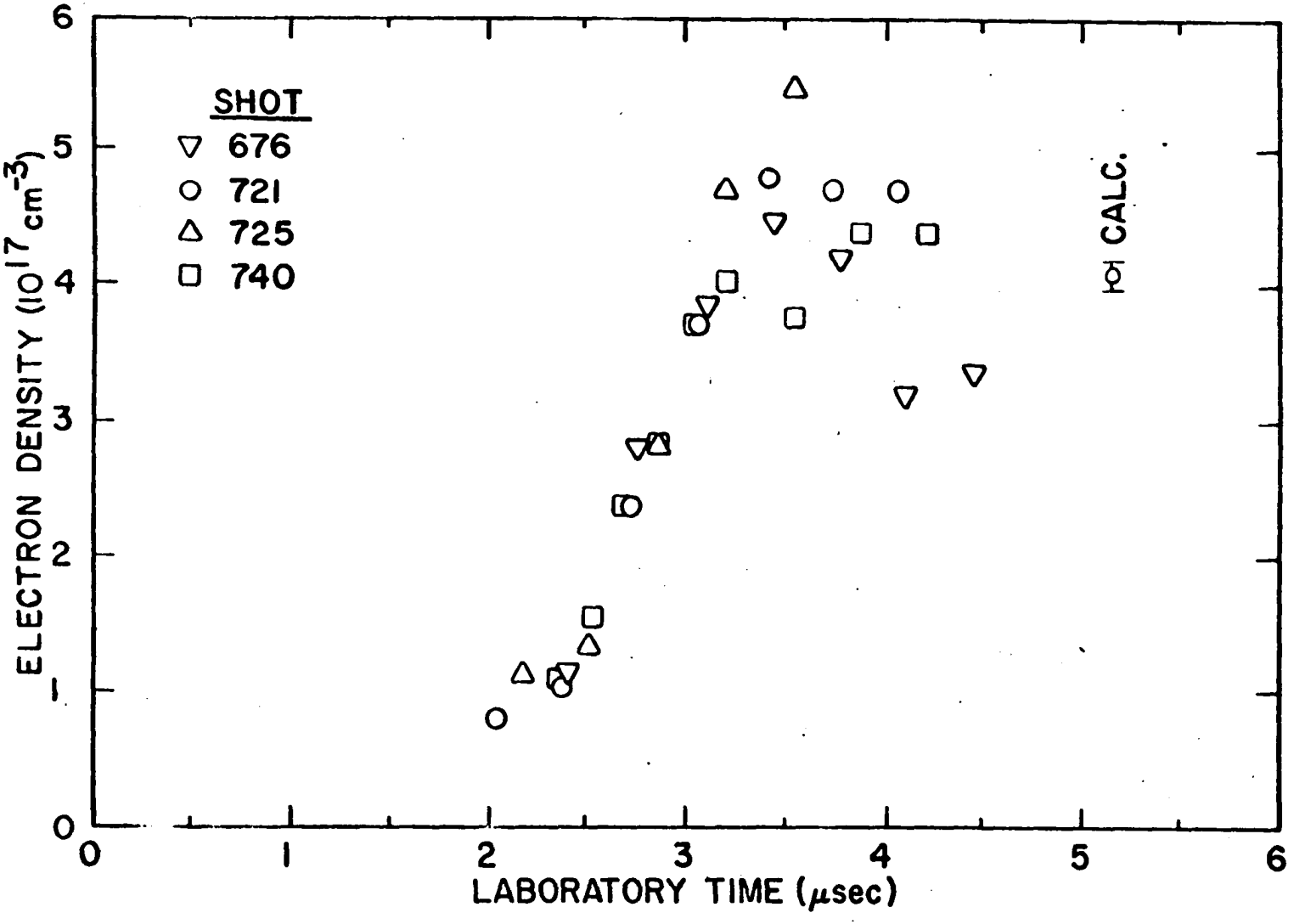

Fig. 22. Relaxation Zone, P_o = 10 mm

LASL-AEC-OFFICIAL

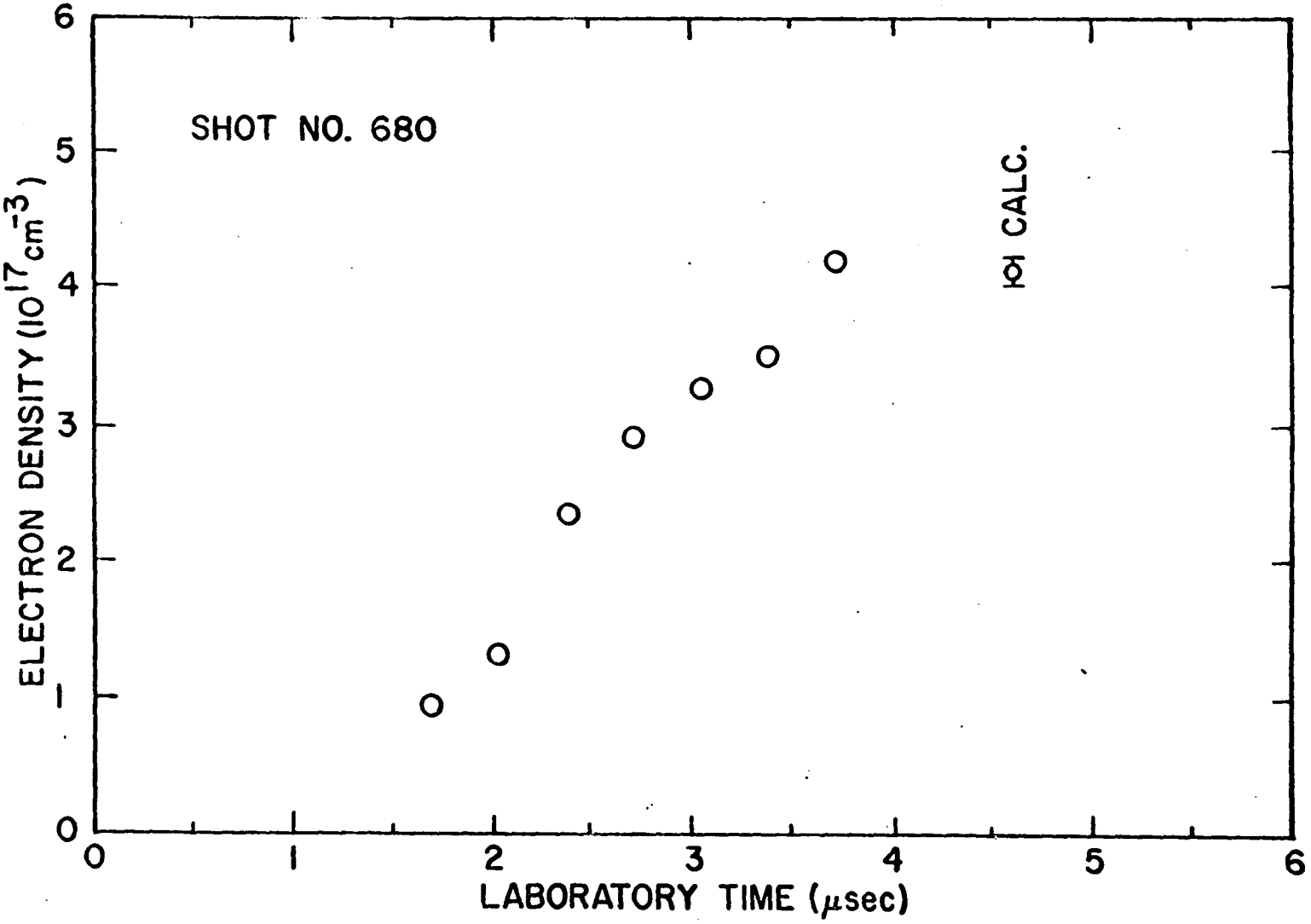

Fig. 23. Relaxation Zone, P_o = 10 mm - Large Diameter Tube

LASL-AEC-OFFICIAL
LASL-AEC-OFFICIAL

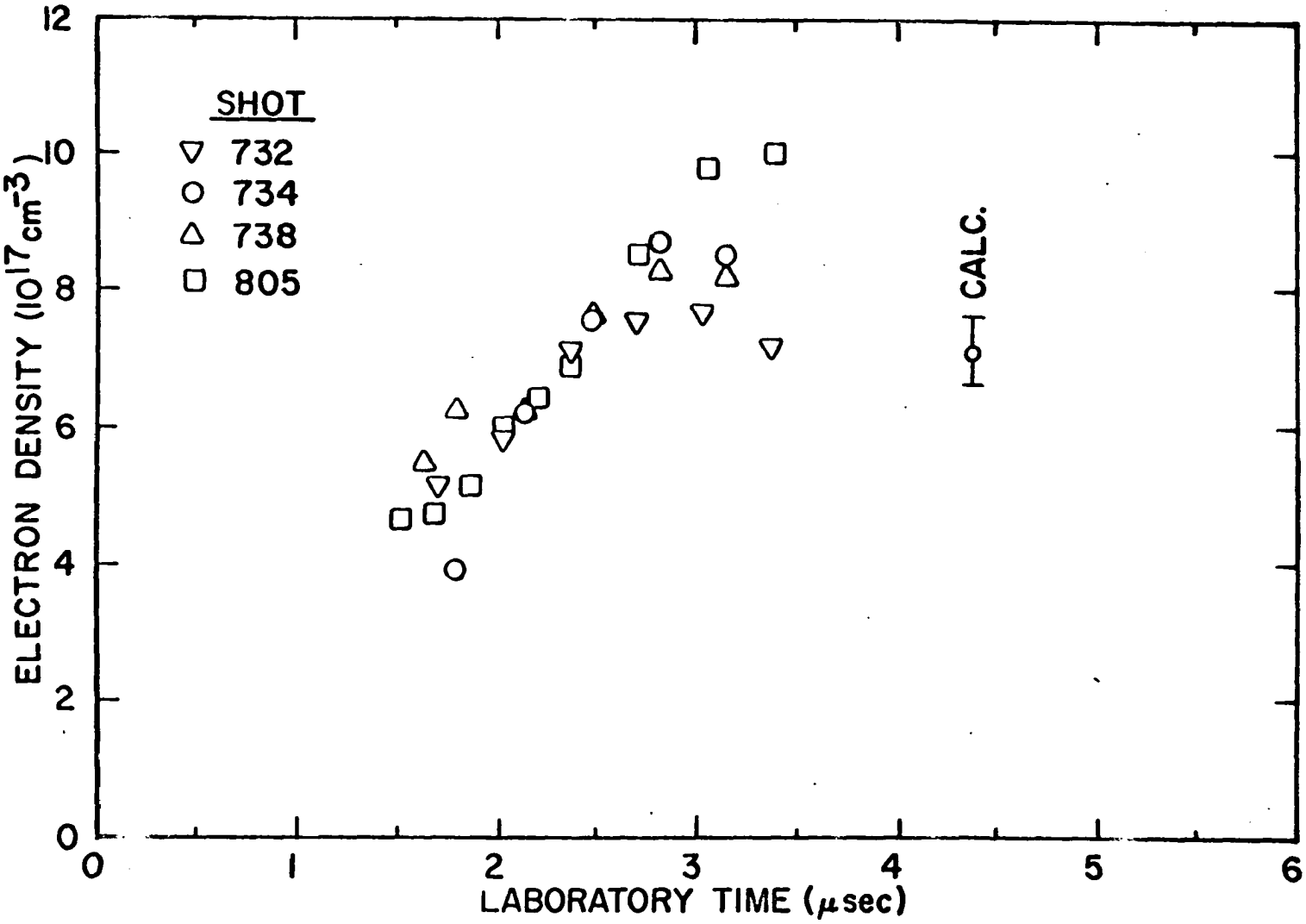

Fig. 24. Relaxation Zone, P_o = 20 mm

LASL-AEC-OFFICIAL

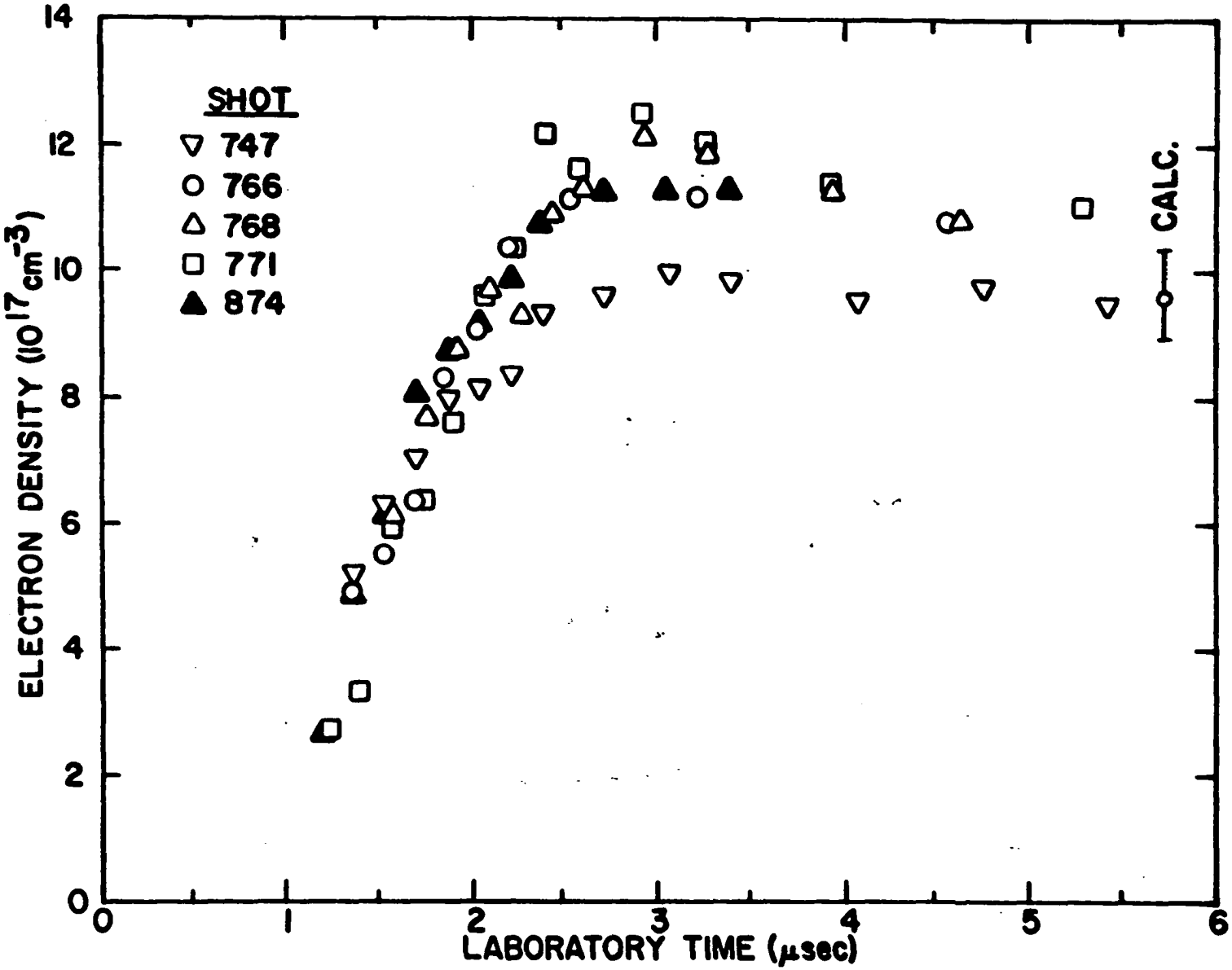

Fig. 25. Relaxation Zone, P_o = 30 mm

LASL-AEC-OFFICIAL
LASL-AEC-OFFICIAL

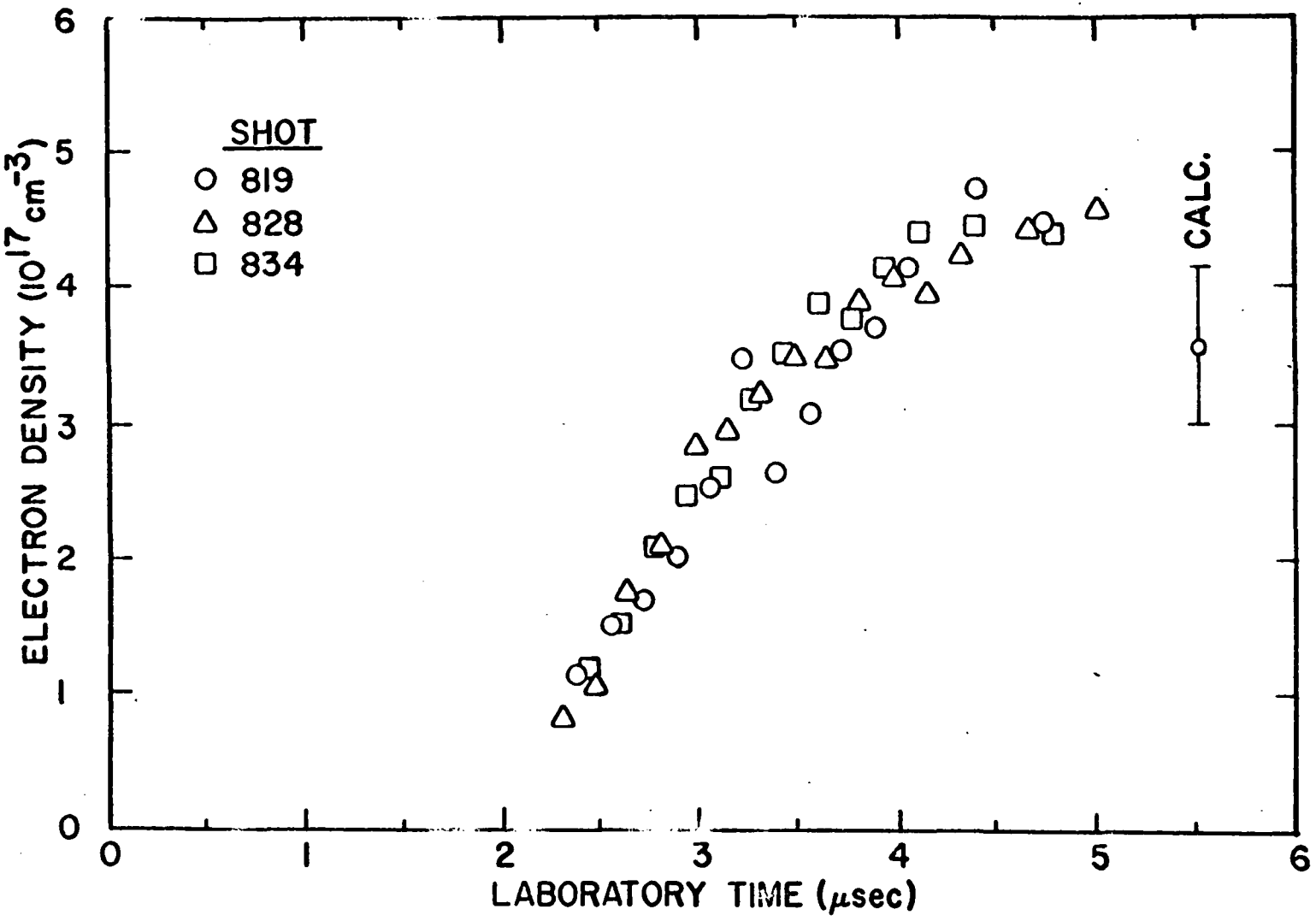

Fig. 26. Relaxation Zone, P_o = 30 mm (TNT)

LASL-AEC-OFFICIAL
LASL-AEC-OFFICIAL

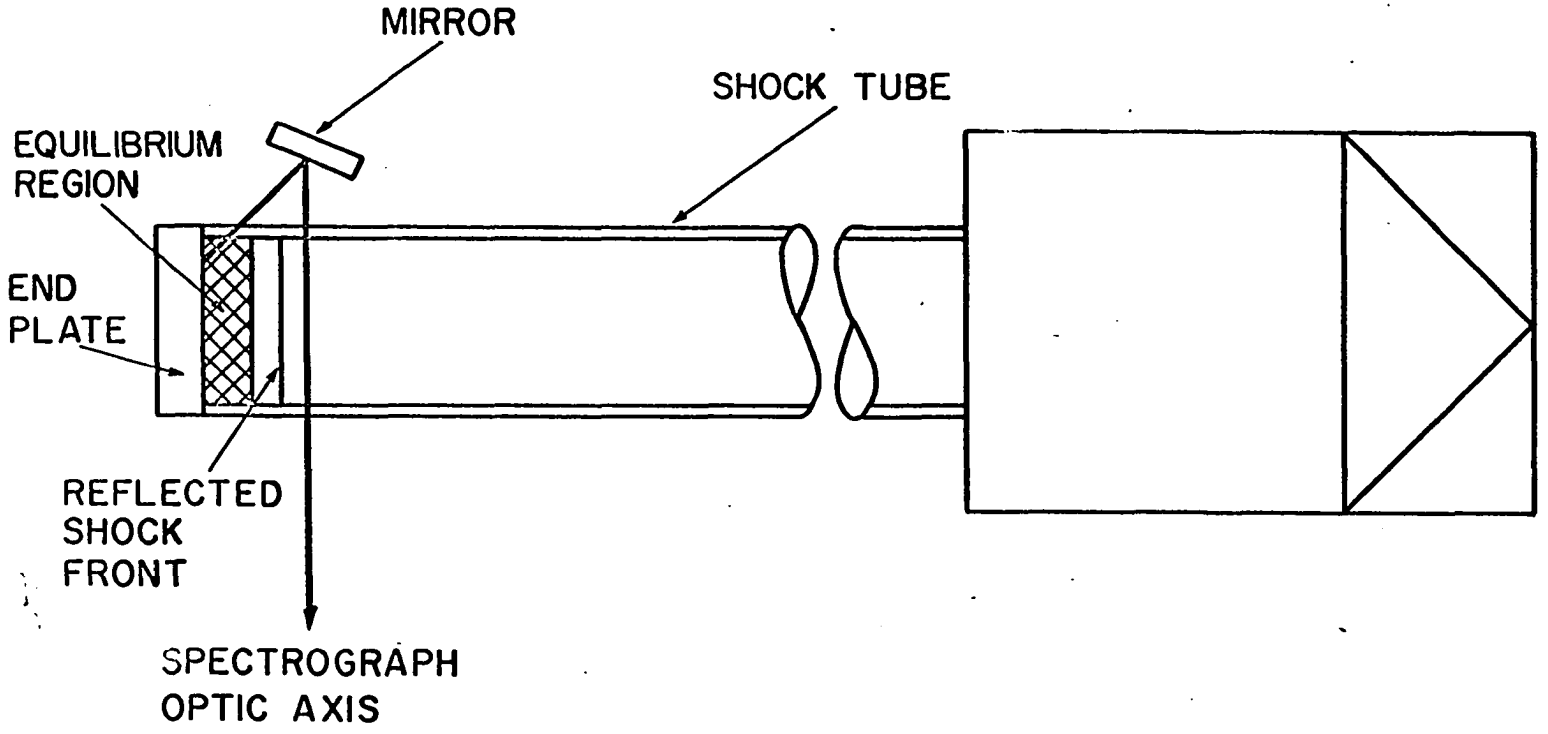

Fig. 27. Arrangement for Absorption Experiment

shock adjacent to the end plate. The intensity of the back light, however was considerably less than that resulting from a normal view of the equilibrium region and only that portion of the spectrogram around the intense line at 5876 Å was exposed. At some later time the reflected shock front and following relaxation zone passed through the region of the tube illuminated by the back light. The electron density-time behavior of the relaxation as indicated by the 4471 Å line profile was unchanged from those experiments without the mirror. However, the back light at 5876 Å was observed to be centrally absorbed, in much the same way as would result from a cold gas layer, from early times after passage of the shock front until the electron density had reached about half of its equilibrium value. Hydrodynamic calculations indicate that the gas temperature directly behind the reflected shock front was as much as 7000° higher than that of the gas at equilibrium behind the shock. The observed absorption of the back light by the gas in the relaxation zone is possibly a manifestation of either excited state populations in the zone vastly different from those predicted by Boltzmann factors or electron temperatures lower than those calculated.

The systematic error introduced into the observed line shapes as a result of instrumental broadening can be considered to originate primarily from two sources: the intrinsic broadening of a spectrograph with finite resolving power and the broadening resulting from the use of a microdensitometer beam of finite width. In this case the sum of these contributions may be conservatively approximated by an instrumental broadening factor with Gaussian profile of half-width 1 Å. A factor of this magnitude will not influence to any degree the observed shape of the extremely wide line at 4471 Å but could perhaps be significant in the measurement of the narrowest

line observed, 3889 Å. An estimate of the error in the determination of electron density from the 3889 Å line artificially broadened by the instrumental factor can be readily obtained if a Gaussian profile with its half-width given by equation (IV-1) is assumed for the true line shape. Analysis of the observed line shape will then predict an electron density 10% high at $[e] = 7.2 \times 10^{16}$ cm^{-3} but less than 1% high at [e] greater than 2.5×10^{17} cm^{-3}. Errors of this magnitude were negligible in the analysis.

Of far greater significance in the determination of the systematic error was the time resolution, or more precisely the time averaging, of the recorded line profiles. Ideally each scan across the time axis of a spectrogram would generate spectral line profiles that were characteristic of the plasma conditions at some instant subsequent to the shock. Due to the experimental technique and method of data reduction, however, the profiles actually measured were the result of an integral of the time-dependent particle emission over a finite time interval.

Contributions to the size of the time interval resulting from the experimental technique came from two sources. First, as a result of the rotating mirror instrumentation, a given point on the spectrograph slit and therefore a corresponding point on the time axis of the spectrogram were illuminated by light emitted from the shock tube from the instant the sweeping image of the tube slit came to the point until the image had completely swept over the point. The point on the time axis was therefore exposed throughout this overwrite time given by

$$\Delta t_t = \frac{S_t M}{W}$$

where S_t = tube slit height

M = magnification of external optics

W = writing speed down the spectrograph slit.

Δt_t was equal to 0.165 μsec for all but the final spectrograms obtained where it was equal to 0.102 μsec. The second contribution to the interval size of an experimental origin arises as the result of light being collected from a section of the tube which had finite thickness in the direction along the tube axis. The thickness was determined by the projection of the spectrograph slit on the shock tube. At any instant as the relaxation zone moved through the section, the particles included in the section have been shocked for different durations and hence have varying characteristic emission. The contribution to the interval of light integration from this source is equal to

$$\Delta t_s = \frac{S_s}{M(U_R)}$$

where S_s = spectrograph slit width

U_R = reflected shock velocity, laboratory coordinates.

For $U_R = 4.1\ \mu sec^{-1}$, Δt_s was generally equal to 0.177 μsec or equal to 0.285 μsec in the final experiments.

Conservatively estimated, the light which produced a profile measured at some point on the spectrogram time axis was the sum of all emission occurring in the interval $\pm (\Delta t_t + \Delta t_s)$ about the time corresponding to that point.

Adding to this interval of $2(\Delta t_t + \Delta t_s)$ was the measurement error, Δt_d which resulted from the use of a microdensitometer beam of finite size to scan the spectrograms. Considering the term Δt_d to be independent of the other terms, the total length of the interval over which the emitted light

was integrated to effect a given measured line profile was estimated equal to

$$\Delta t = \sqrt{[2(\Delta t_t + \Delta t_s)]^2 + \Delta t_d^2}$$

or 0.696 μsec for most experiments.

This integration of the light over an interval in time was the primary source of error in the results. Since both the line half-width and peak intensity were in general changing in an unknown manner throughout the interval, there was no unique unfolding of an observed line profile to recover the true profile at each instant. An estimation of the error involved in using the half-width of the observed line profiles for the determination of the electron density therefore reduced to a consideration of how well an observed profile represented the average of the true profiles in the interval. Near equilibrium, the peak intensities and the half-widths were changing relatively slowly, so that the observed profile was probably quite a good average over the interval. On the other hand, in that region of the relaxation where the change of electron density with time was large, both the peak intensities and half-widths were significantly increasing in magnitude through the interval. The extreme example of this type of behavior would be a vanishingly small intensity and half-width at the early time side of the interval but a very large intensity and half-width at later time. In this case an observed profile measured on the spectrogram for some given time could actually be appropriate for conditions as much as $\Delta t/2$ or 0.348 μsec later.

The kinetic analysis of the experimental data described in Chapter V is based on measurement of the slopes of the electron density histories, Figs. 23 through 26. It follows from the above discussion of the profile

averaging mechanism inherent in the experimental technique that, intermediate in the relaxation zone, an observed electron density-time curve could be less steep than that appropriate for the actual rate of change of electron density. On the other hand, the slopes were measured at only one point on each of these curves. There is no reason to expect that the details of the process which averages the true profiles in the interval Δt into an observed profile would change drastically between successive densitometer scans only 0.17 μsec apart on the spectrograms. With no further information available about the mode by which the time-dependent line profiles summed to result in an observed profile, it is difficult to evaluate the present experimental accuracy in the determination of the actual electron density rate at some position in the ionization relaxation zone. As a conservative estimate, therefore, the measured rates are considered accurate within a factor of two. Since the experimental error was estimated to be of such magnitude, no further increase in the size of the error estimate as a result of using theoretical half-width calculations for the analysis of the observed integrated profiles was necessary.

Some evidence of the effect of averaging the time-dependent line profiles over a finite time interval can be seen in Fig. 28, a plot of the observed distance between the maxima of the blue and the red intensity peaks versus the half-width of the 4471 Å line. A least-squares fit of all the data to a straight line through the origin was found to have a slope of 0.265 as compared to a slope of 0.417 theoretically predicted in NRL-5805[16]. This discrepancy can be partially attributed to the averaging of the narrow lines with wider ones which would have the effect of filling in the central

---

[16]Griem et al., op. cit.

LASL-AEC-OFFICIAL
LASL-AEC-OFFICIAL

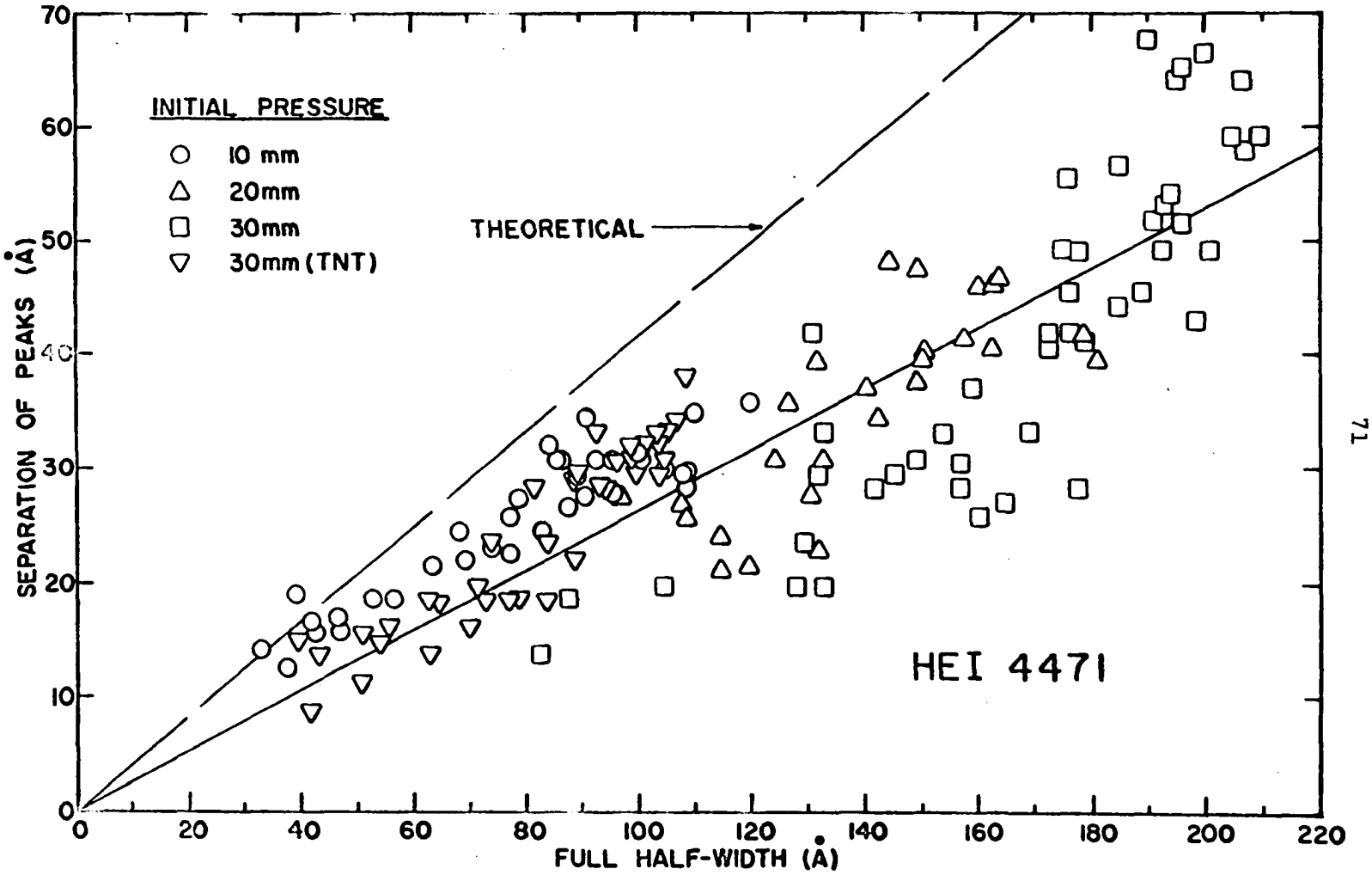

Fig. 28. Separation of Intensity Peaks vs. Half-Width, HeI 4471

dip of the profile and decreasing the distance between peaks. Close examination of this plot shows that at the upper end of each set of data for a given experimental condition, corresponding to data taken near equilibrium, the disagreement between the observed and calculated relationship was reduced. The slope through these near-equilibrium points was about 0.3.

CHAPTER V

IONIZATION KINETICS

A reaction rate is defined in terms of the time rate of change of concentration of a reactant involved in that reaction. The rate of a reaction with stoichiometric equation

$$wW + xX \rightarrow yY + zZ$$

may be specified by either $-d[W]/dt$, $-d[X]/dt$, $d[Y]/dt$, or $d[Z]/dt$. The bracketed upper case letters are number densities of the reactants denoted by upper case letters and the lower case letters are stoichiometric coefficients of the reaction equation. For a common type of reaction whose rate is proportional to a product of powers of m number densities, the rate of change of species C is expressed by

$$d[C]/dt = k_i \prod_{j=1}^{m} [C_j]^{n_j}.$$

The order of the reaction is defined as $n = \sum_{j=1}^{m} n_j$, and the order with respect to concentration $[C_j]$ is merely n_j. An experimental kinetic investigation generally has as its objective the determination of each reactant together with its order and the evaluation of the rate constant, k_i, for that specific reaction.

Both the electron density histories of the relaxation obtained from the spectrograms and the results of detailed hydrodynamic calculations were required to formulate a quantitative description of the ionization reaction in shocked helium. The calculations were first needed to transform the observed electron density rates into a form suitable for kinetic analysis.

In most shock tube experiments, observations of phenomena occurring in the tube are made at some position fixed in the laboratory. Such was the case in the present experiments where the spectrographic observations were made a few centimeters from the tube end plate. As a result of particle flow past this position at a speed slower than that of the shock front, a transformation of laboratory observations of time-dependent particle properties was necessary to relate the observations to particle coordinates. For the rate of change of electron density behind a reflected shock, the appropriate transformation is

$$\frac{d[e]}{dt} = \left(\frac{U_R - u_2}{U_R} \right) \frac{d[e]}{d\tau} \qquad \text{(V-1)}$$

where t = particle time

τ = laboratory time

u_2 = particle velocity behind the relfected shock, laboratory coordinates.

For an endothermic reaction such as the ionization process, U_R and u_2 are opposite in sense so that $(U_R - u_2)/U_R$ is greater than one. In this case the reaction rate is observed in laboratory coordinates to be slower than it actually is in particle coordinates. For comparison, consider reactions occurring behind an incident shock. The rates here are always observed to be faster than the true particle rates regardless of the nature of the reaction.

Next, the data were corrected for an effect on the observed rates caused by the density gradient behind the reflected shock. The rate to be considered in the kinetic analysis is that due to the ionization process alone. However, as the relaxation proceeded the mass density, ρ, behind the shock was increasing to its equilibrium value. As a result, the total rate of change in electron density, d[e]/dt, included a term due to this compression. The rate at constant volume is given by

$$\left(\frac{\partial[e]}{\partial t}\right)_\rho = \frac{d[e]}{dt} - \left(\frac{\partial[e]}{\partial \rho}\right)_t \frac{d\rho}{dt}$$

$$= \left(1 - \frac{[e]}{\rho} \frac{d\rho}{d[e]}\right) \frac{d[e]}{dt} . \qquad \text{(V-2)}$$

The reactant number densities and temperature present in the relaxation zone behind the reflected shock were varied by changing the initial tube pressure and the strength of the exciting shock. The kinetic analysis which follows consists of a correlation of the magnitude of $(\partial[e]/\partial t)_\rho$ to such changes in state of the relaxing gas. Values of the state variables which were pertinent to the kinetic analysis are presented in graphical form for each experimental condition in Figs. 32 through 39.

Three species, neutral helium atoms, helium positive ions, and electrons were considered to be possible reactants in the ionization process. Local charge neutrality was assumed making the positive ion density numerically equal to the electron density. The existence of helium molecular ions in the plasma was viewed as unlikely since the gas temperature was approximately equal to the ion binding energy of near 2eV[1]. Consideration of impurity atoms which might enter into very early processes[2] was also

---

[1] E. Mason and J. Vanderslice, J. Chem. Phys. 29, 361 (1958).

[2] H. Petschek and S. Byron, Ann. Phys. (N. Y.) 1, 270 (1957).

inappropriate because the initial condition for the experiments was a gas already partially ionized by the incident shocks.

Initial kinetic analysis involved determination of the order to which the reactants entered the reaction. Comparison of the electron density histories for those experiments using the HMX booster explosive showed a steepening of the electron density-time curves as the initial tube pressure was increased. An increase in initial pressure implied of course an increase in reactant densities. However, it was probable that the reaction was also temperature dependent and the calculations indicated different temperature profiles through the compared relaxation zones. Quantitative comparisons of reaction rates to reactant densities were therefore made at positions in the several relaxation zones which the calculations indicated were at common temperature.

The electron density rates at a temperature of 2.25×10^4°K were obtained for each experiment using HMX by measuring the slope of the electron density-time curve at the electron density present when the relaxing gas was at this temperature. The electron density rates at constant volume for each experiment and the slope measurements from which they were obtained are presented in Table 3. The values of the state variables required to calculate the rates from the slope measurements are also tabulated for each experimental condition.

Notice from the table that the mass density and number densities of neutral helium atoms and electrons present in the relaxation zones at 2.25×10^4°K are almost directly proportional to the initial tube pressure. As a result of this relationship, the ratio of electrons to neutrals was almost constant regardless of initial pressure and a unique determination

LASL-AEC-OFFICIAL

TABLE 3

RELAXATION ZONE DATA

Initial Pressure (mm Hg)	T (10^4 °K)	[e] (10^{17} cm^{-3})	[He] (10^{18} cm^{-3})	u_p (10^5 cm sec^{-1})	ρ (10^{-5} g cm^{-3})	$d\rho/d[e]$ (10^{-23} g)	Shot	$d[e]/d\tau$ (10^{23} cm^{-3} sec^{-1})	$(\partial[e]/\partial t)_\rho$ (10^{23} cm^{-3} sec^{-1})
10	2.25	3.05	4.12	0.35	2.92	2.7	680	1.07	0.837
20	2.25	5.95	8.10	0.21	5.73	2.8	732	3.73	2.77
							734	4.13	3.07
							738	3.84	2.86
							805	3.69	2.74
30	2.25	8.60	11.95	0.13	8.50	2.9	747	5.68	4.13
							766	6.20	4.51
							768	5.09	3.70
							771	10.0	7.27
							874	3.70	2.69
30 (TNT)	2.00	2.90	10.3	0.15	7.06	4.2	819	2.47	2.13
							828	1.62	1.39
							834	2.03	1.75

of the specific order to which each of these species entered the reaction was precluded. However, since both the neutral and electron number densities were proportional (within about 2%) to the mass density in all experiments using HMX, the overall order could be determined as follows.

The general form assumed for the helium ionization reaction is

$$a[He] + b[He^+] + c[e] \underset{k_1}{\overset{k_2}{\rightleftharpoons}} d[He] + f[He^+] + g[e]$$

which proceeds with forward and reverse rate constants, k_1 and k_2, according to the kinetic equation

$$\left(\frac{\partial[e]}{\partial t}\right)_\rho = k_1 [He]^a [He^+]^b [e]^c - k_2 [He]^d [He^+]^f [e]^g$$

or

$$\left(\frac{\partial[e]}{\partial t}\right)_\rho = k_1 [He]^a [He^+]^b [e]^c - k_2 [He]^{a-1} [He^+]^{b+1} [e]^{c+1},$$

because for every ionization event the neutral density is decreased by one and the positive ion and electron densities are increased by one.

At equilibrium the net ionization rate is zero. The ratio of the rate constants, k_1/k_2, is therefore equal to the equilibrium constant given by the Saha equation for helium:

$$\frac{k_1}{k_2} = K(T) = 9.66 \times 10^{15}\ T^{3/2} e^{-2.85 \times 10^5/T}\ cm^{-3}.$$

The rate equation may now be rewritten as

$$\begin{aligned}\left(\frac{\partial[e]}{\partial t}\right)_\rho &= k_1 \left\{[He]^a [e]^{b+c} - \frac{1}{K(T)} [He]^{a-1} [e]^{b+c+2}\right\} \\ &= k_1 \left\{[He]^a [e]^{b+c} \left(1 - \frac{1}{K(T)} \frac{[e]^2}{[He]}\right)\right\}\end{aligned} \qquad \text{(V-3)}$$

recalling that $[He^+] = [e]$.

At the positions in the relaxation zones where the slopes of the electron density histories were measured

$$[He] \approx 1.41 \times 10^{23}\rho \text{ cm}^{-3}$$

$$[e] \approx 1.04 \times 10^{22}\rho \text{ cm}^{-3}$$

and $$K(T) = 1.02 \times 10^{17} \text{ cm}^{-3}.$$

Equation (V-3) evaluated at this position becomes

$$\frac{(\partial[e]/\partial t)_\rho}{(1-7.43 \times 10^{3}\rho)} = k_1 (1.41 \times 10^{23})^a (1.04 \times 10^{22})^{n-a}\rho^n \qquad \text{(V-4)}$$

where $a + b + c = n$ is the total order of the ionization reaction.

A least-squares fit of the left-hand member of equation (V-4) versus ρ^n gives $n = 2.27 \pm 0.86$. The error limits are plus or minus one standard deviation. The values obtained for both the total order and the standard deviation would be slightly less if the results of Shot 771, which deviated considerably from the mean, were neglected.

The temperature dependence of the reaction rate constant cannot be determined from equation (V-3) without specific knowledge of the order of each reactant. The magnitude of this dependence can be estimated, however, by deriving an equation of the type of (V-4) for the reaction occurring at lower temperature in tubes using TNT booster explosives and comparing it with equation (V-4).

The results of experiments using TNT boostered tubes were analyzed as above except that the slopes of the electron density histories were measured at the electron density calculated to be present when the relaxing gas temperature was 2.0×10^{4}°K. The slopes measured from histories of these experiments and the results of the hydrodynamic and rate calculations are also presented in Table 3. Proceeding as before, at the position where

the slopes of the electron density histories were measured

$$[He] = 1.46 \times 10^{23}\rho \text{ cm}^{-3}$$

$$[e] = 0.411 \times 10^{22}\rho \text{ cm}^{-3}$$

and $$K(T) = 1.77 \times 10^{16} \text{ cm}^{-3}.$$

The equation for these conditions analogous to (V-4) is

$$\frac{(\partial[e]/\partial t)_\rho}{(1-6.54 \times 10^{3}\rho)} = k_1 (1.46 \times 10^{23})^a (0.411 \times 10^{22})^{n-a} \rho^n. \qquad \text{(V-5)}$$

Evaluating equations (V-4) and (V-5) at conditions corresponding to initial tube pressures of 30 mm and using a value of n = 2, the ratio of rate constants at the two temperatures is

$$\frac{k_1 (2.25 \times 10^{4}\text{°K})}{k_1 (2.0 \times 10^{4}\text{°K})} = 0.40 (2.62)^a. \qquad \text{(V-6)}$$

The quantity $(2.62)^a$, assuming reasonable values for a, is no larger than order 10. Therefore, the temperature dependence of the ionization rate constant is small indeed between temperatures of 2.0 and 2.25×10^{4}°K. A similar conclusion is reached for n = 3.

A knowledge more detailed than that resulting from this research is required to compare the experimental results with theoretical predictions. Specifically, the order to which each reactant entered the reaction must be known. It is of interest, however, to assume a form for the reaction consistent with the experimental observations and compare the results of such an assumption with experimental data of other investigators and theoretical calculations.

An ionization reaction which is physically plausible is one first order in both neutral atoms and electrons, overall second order. The ionization reaction would result from binary collision between atoms and

electrons, and the recombination reaction would be three-body with a free electron acting as the third body. The stoichiometric equation for such reactions is

$$He + e \underset{k_1}{\overset{k_2}{\rightleftarrows}} He^+ + e + e,$$

and the rate equation is

$$(\partial[e]/\partial t)_\rho = k_1 [He] [e] - k_2 [e]^3 \qquad (V\text{-}7)$$

where the rate constants are now defined as

k_1 = collisional ionization rate constant, $cm^3\ sec^{-1}$

k_2 = three-body recombination rate constant, $cm^6\ sec^{-1}$.

The rate equation (V-7) in the form of (V-3) is

$$(\partial[e]/\partial t)_\rho = k_1 \left\{ [He] [e] - [e]^3/K(T) \right\}. \qquad (V\text{-}8)$$

Figure 29 is a plot of $(\partial[e]/\partial t)_\rho$ versus the bracketed quantity of equation (V-8). The slope of the solid line, a least-squares fit of the data at 2.25×10^4°K through the origin, gives a value of $1.08 \times 10^{-13}\ cm^3\ sec^{-1}$ for the ionization rate constant at this temperature. The three-body recombination rate coefficient is equal to $k_1/K(T)$ or $1.05 \times 10^{-30}\ cm^6\ sec^{-1}$ at 2.25×10^4°K.

Of particular interest in Fig. 29 is the comparison of the data points at a temperature of 2.00×10^4°K [30 mm (TNT)] to the results at 2.25×10^4°K. Notice that there is no significant difference between the ionization rate constants although the temperatures were different by 2500°. This relationship is, of course, a specific example of the more general result, (V-6). If indeed the ionization reaction is bimolecular between

LASL-AEC-OFFICIAL

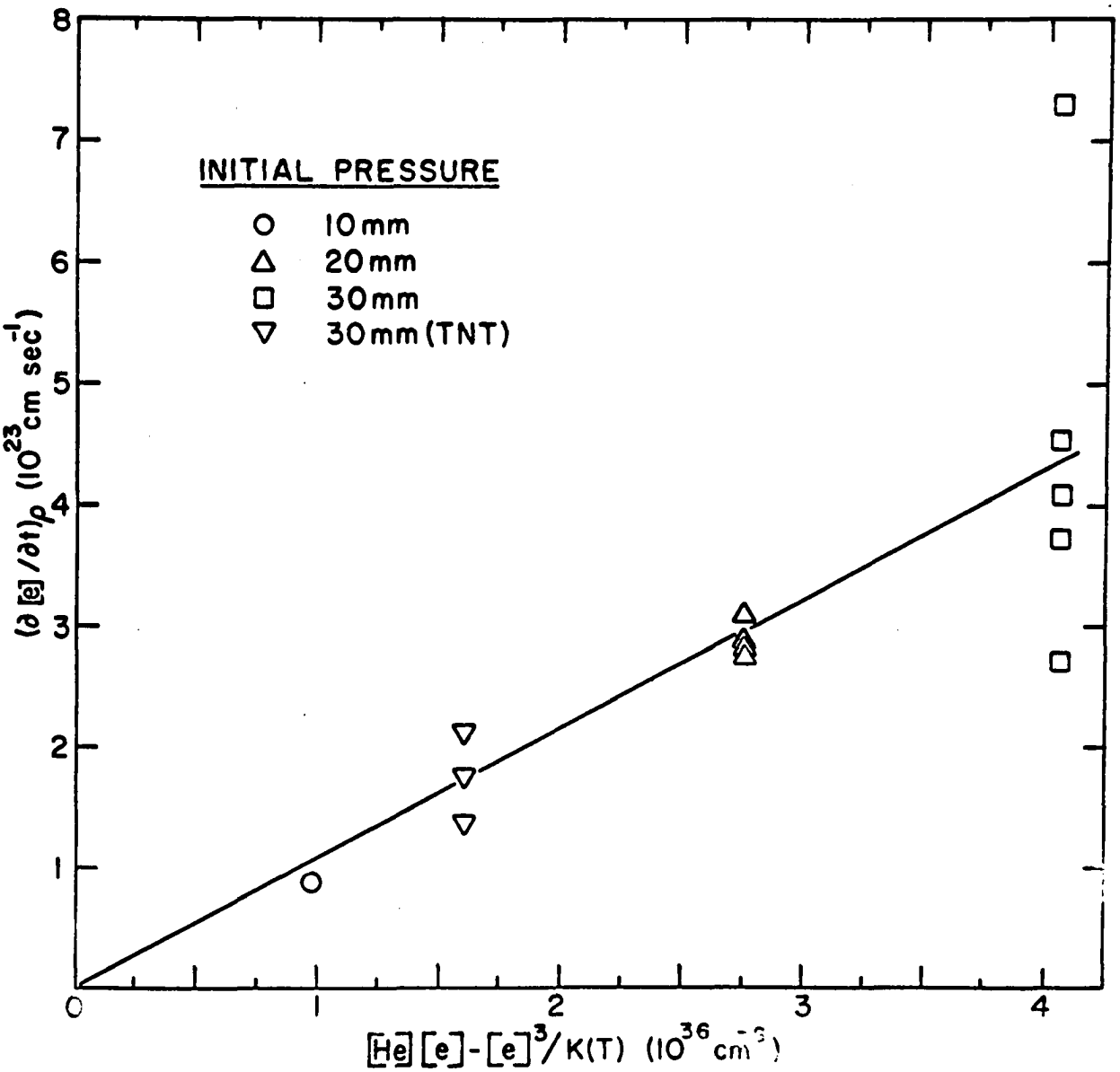

Fig. 29. Ionization Rate Coefficient for Helium

LASL-AEC-OFFICIAL

neutral atoms and electrons and the results of this research may be extrapolated to other temperatures, the ionization rate constant is

$$k_1 = 1.08 \times 10^{-13} \text{ cm}^3 \text{ sec}^{-1} \qquad \text{(V-9)}$$

and the three-body recombination rate constant is

$$k_2 = 1.12 \times 10^{-29} \, T^{-3/2} \, e^{2.85 \times 10^5/T} \text{ cm}^6 \text{ sec}^{-1}. \qquad \text{(V-10)}$$

There is no known experimental investigation of helium ionization under similar conditions to which these results may be directly compared. A theoretical ionization rate constant may be derived, however, using the well-known cross section for helium ionization by electron impact as determined in beam experiments.

The bimolecular rate constant required is equal to the product of the ionization cross section and the electron velocity averaged over the appropriate velocity distribution. The value for the ionization cross section near threshold is given for electron impact by the results of Smith[3], Fox[4], and Asundi[5] to be

$$\sigma = 8.1 \times 10^{-7} \, \Delta E \text{ cm}^2 \qquad \text{(V-11)}$$

where ΔE is the energy in ergs above the ionization potential of helium, 24.6 eV or 3.94×10^{-11} ergs. Expressing the electron velocity and its distribution function in energy units, the rate constant is given by

---

[3] P. T. Smith, Phys. Rev. 36, 1293 (1930).

[4] R. E. Fox, J. Chem. Phys. 35, 1379 (1961).

[5] R. K. Asundi, in Comptes Rendus de la VI Conference Internationale sur les Phenomenes D'Ionisation dans les Gaz, ed. P. Hubert and E. Cremieu-Alcan, Vol. I, p. 29 (1963).

$$\overline{\sigma v} = \frac{1.15 \times 10^{-6}}{\sqrt{m_e}} \int_{3.94 \times 10^{-11}}^{\infty} E^{1/2} (E - 3.94 \times 10^{-11}) f(E)\, dE \qquad \text{(V-12)}$$

where m_e = electron mass

E = electron kinetic energy

$f(E)$ = the electron energy distribution function.

Assuming a Maxwell-Boltzmann distribution for the electrons, equation (V-12) may be integrated to give

$$\overline{\sigma v} = 4.28 \times 10^{7} (3.94 \times 10^{-11} + 2kT) (kT)^{1/2} e^{-3.94 \times 10^{-11}/kT} \text{ cm}^3 \text{ sec}^{-1}. \qquad \text{(V-13)}$$

This equation is similar to the usual rate constant for bimolecular reactions[6]:

$$\overline{\sigma v} = \text{constant } \sqrt{T}\ e^{-A/kT}.$$

The quantity A is defined as the "activation energy".

The large temperature dependence of this derived rate constant is of course in complete disagreement with the experimental results. Quantitative agreement between the observed value of 1.08×10^{-13} cm^2 sec^{-1} and the values of 1.04×10^{-14} and 2.02×10^{-15} obtained from (V-13) for temperatures of 2.25×10^{4} and 2.00×10^{4}°K respectively is also poor.

In their investigation of the ionization of shocked argon, Petschek and Byron[7] have proposed that, following an initial reaction which results in the production of free electrons, the rate-determining process is a bimolecular reaction between ground state atoms and electrons resulting in

---

[6] A. A. Frost and R. G. Pearson, Kinetics and Mechanism (2nd ed.; John Wiley and Sons, Inc., New York, 1961), Chap. V.

[7] Petschek and Byron, op. cit.

excitation to the first excited state. The ionization rate constant then could be dependent on the cross section for excitation to the excited state assuming that all atoms which reach this state are subsequently ionized. Although it too will exhibit a strong temperature dependence, a rate constant for helium ionization analogous to that presented by Petschek and Byron for argon may be derived for numerical comparison to these results. The cross section near threshold for electronic excitation to the 2^3S helium state is[8,9]

$$\sigma^* \simeq 6.5 \times 10^{-6} \Delta E \text{ cm}^2 \qquad \text{(V-14)}$$

where ΔE is now the electron's energy in ergs above the first excited state at 19.8 eV or 3.17×10^{-11} ergs. As before, the rate constant follows from

$$\overline{\sigma v^*} = \frac{9.2 \times 10^{-6}}{\sqrt{m_e}} \int_{3.17 \times 10^{-11}}^{\infty} E^{1/2} (E - 3.17 \times 10^{-11}) f(E)\, dE \qquad \text{(V-15)}$$

which integrates to

$$\overline{\sigma v^*} = 3.44 \times 10^8 (3.17 \times 10^{-11} + 2kT) (kT)^{1/2} e^{-3.17 \times 10^{-11}/kT} \text{ cm}^3 \text{ sec}^{-1}. \qquad \text{(V-16)}$$

This relationship is numerically equal to 1.88×10^{-12} and 2.18×10^{-13} $\text{cm}^3 \text{ sec}^{-1}$ at 2.25×10^4 and 2.00×10^4°K. The observed ionization rate constant was therefore intermediate in magnitude between those derived here utilizing experimentally determined ionization and excitation cross sections.

---

[8] H. Maier-Leibnitz, Z. Physik 95, 499 (1936).

[9] G. J. Shultz and R. E. Fox, Phys. Rev. 106, 1179 (1957).

Several investigations of helium recombination are reported in the literature[10-12] but were performed at temperatures about a factor of ten lower than those achieved in the present research. The rate coefficients observed in the lower temperature experiments, collected and tabulated in references 11 and 12, have been transformed from the two-body form in which they were presented into three-body coefficients and plotted in Fig. 30. The results of recent theoretical treatments of the recombination process are also plotted in the figure. The rate coefficients indicated by the dashed line were obtained by Mankin and Keck[13] from a classical treatment of the three-body process which is claimed to be valid up to temperatures of 11,000°K. The coefficients calculated by Bates, Kingston, and McWhirter for recombination in a hydrogen plasma which is either totally optically-thin[14] or optically-thick only to resonance radiation[15] are indicated in the figure by the dot-dashed and dot-dot-dashed lines respectively. These coefficients calculated for hydrogen are also valid for helium plasma according to Bates and Kingston[16]. The observed agreement between experimental and theoretical rate coefficients for temperatures near 1000°K is

---

[10] R. W. Motley and A. F. Kuckes, in Proceedings of Vth International Conference on Ionization Phenomena in Gases, ed. H. Maecker (North-Holland Publishing Company, Amsterdam, 1962), Vol. I, p. 651.

[11] E. Hinnov and J. G. Hirschberg, Phys. Rev. 125, 795 (1962).

[12] F. Robben, W. B. Kunkel, and L. Talbot, Phys. Rev. 132, 2363 (1963).

[13] B. Mankin and J. C. Keck, Phys. Rev. Letters 11, 281 (1963).

[14] D. R. Bates, A. E. Kingston, and R. W. P. McWhirter, Proc. Roy. Soc. A 267, 297 (1962), Table 6 for $[e] \to \infty$.

[15] D. R. Bates, A. E. Kingston, and R. W. P. McWhirter, Proc. Roy. Soc. A 270, 155 (1962), Table 5 for $[e] \to \infty$.

[16] D. R. Bates and A. E. Kingston, Proc. Roy. Soc. A 279, 32 (1964).

strong evidence of the three-body mode of recombination in partially ionized helium with temperatures in this range and electron densities which may or may not be restricted to the region observed in the low temperature experiments, $\sim 10^{13}$ cm^{-3}.

The rate coefficients obtained in the present research with the assumption of three-body recombination are indicated in Fig. 30 by the solid line plot of equation (V-10). Clearly equation (V-10) predicts a rate coefficient much too large at temperatures around 1,000°K where the values of the coefficient are well documented and in good agreement. At temperatures near 20,000°K, numerical agreement between the coefficients observed here and the calculations of Bates et al. is also poor, the present results being one or two orders of magnitude less than the calculations would indicate. The present results, however, are similar to the conclusions of Camac and Feinberg[17] who have presented a plot for the argon recombination rate coefficient similar to Fig. 30. These authors propose that the rate coefficient for argon may be well described by the Mankin and Keck calculations up to about 3,000°K, but at higher temperatures the details of the recombination process change, and a coefficient with exponential temperature dependence similar to equation (V-10) is valid. The temperature at which the rate coefficient changes from the $T^{-9/2}$ to the exponential temperature dependence would supposedly be a function of the specific gas that is recombining, because the exponent of the higher temperature coefficient is a function of an excited state energy and/or the ionization potential of that gas.

---

[17] M. Camac and R. M. Feinberg, "Thermal Conductivity of Argon at High Temperatures," AVCO-Everett Research Laboratory Report, BSD-TDR-63-250 (1963).

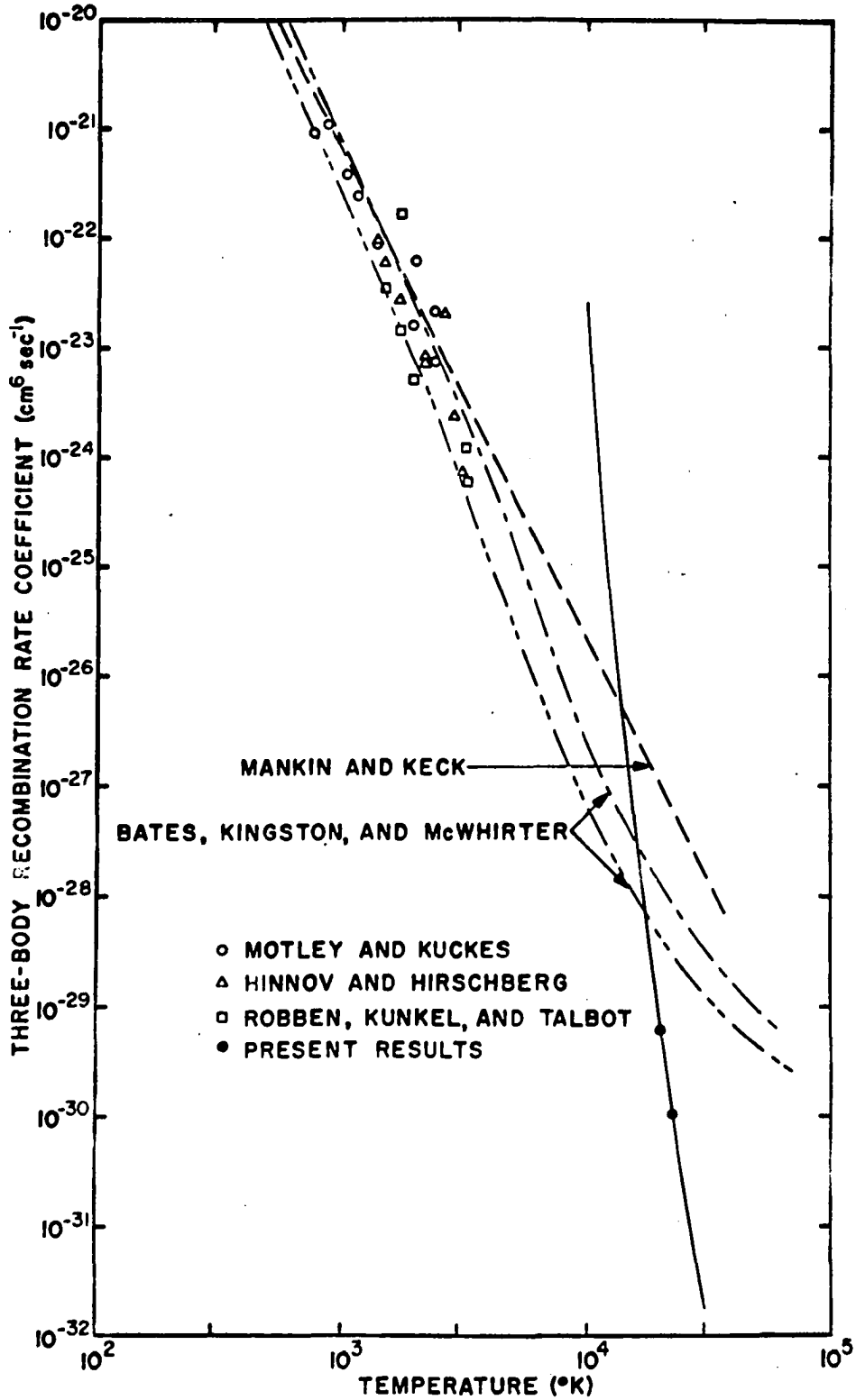

Fig. 30. Three-Body Recombination Rate Coefficient for Helium

LASL-AEC-OFFICIAL
LASL-AEC-OFFICIAL

CHAPTER VI

SUMMARY, CONCLUSIONS, AND RECOMMENDATIONS FOR FUTURE EXPERIMENTS

During the course of this research, experimental techniques involving the use of the high-explosive shock tube were developed to allow an investigation of the kinetics of ionization of strongly shocked helium. Some of the methods were refinements of techniques used earlier by Seay[1] in an investigation of the equilibrium properties of a sample of partially ionized helium also produced in the high-explosive tube. Other new procedures were required in order to observe this transient phenomenon occurring over a period of only a few microseconds.

In this investigation, the ionization relaxation was observed as it proceeded to equilibrium behind the shock reflected from the tube end plate. Changes of the initial tube pressure and strength of the exciting shock produced variations in the behavior of the ionization reaction which were correlated to the state of the gas behind the reflected shock. Due to limitations imposed by the use of photographic film as a recording medium and the time resolution of the experimental equipment, informative observations could be made only of relaxation zones with electron densities between 10^{17} and 10^{18} cm^{-3} and temperatures near 2 eV. The sum of the information obtained, shock velocities from smear camera records, histories of the electron density from time-resolved spectrograms, and quantitative

---

[1] Seay, op. cit.

values of the state variables from theoretical hydrodynamic calculations, was analyzed in an attempt to resolve the detailed nature of the ionization relaxation.

To the author's present knowledge, the current research is the first to employ time-resolved spectroscopy in conjunction with recently improved Stark broadening calculations in a detailed investigation of ionization kinetics. The accuracy of the results obtained by this spectroscopic technique could be evaluated at only one position in the relaxation zone, specifically at equilibrium behind the reflected shock. At the equilibrium position, however, agreement between electron densities determined spectroscopically and those obtained from one-dimensional shock calculations was good. This agreement would have been improved slightly had the lowering of the ionization potential resulting from plasma interactions been included in the hydrodynamic calculations.

The experimental results obtained from spectroscopic observation of the ionization relaxation were highly reproducible from shot to shot. In addition to being reproducible, the electron densities indicated by measurement of the HeI spectral line profiles at 3889 $\mathring{A}$ and 4471 $\mathring{A}$ were in mutual agreement throughout the relaxation zone. Electron densities indicated by the line at 5876 $\mathring{A}$ were in substantial agreement with those deduced from the other lines early in the relaxation zone but not at later times when 5876 $\mathring{A}$ was heavily self-absorbed.

An analysis of the experimental data showed that the ionization rate was proportional to the 2.27 ± 0.86th power of the plasma mass density and essentially temperature independent. However, it was not possible to identify positively the rate-determining species or their specific order in the

reaction. Assuming that the ionization reaction was bimolecular between neutral helium atoms and electrons, the rate was observed to be temperature independent with an effective ionization rate constant equal to 1.08×10^{-13} cm^3 sec^{-1}. A three-body recombination rate constant was also evaluated based on this model and found equal to 1.04×10^{-30} cm^6 sec^{-1} at 2.25×10^4°K. It was estimated that the observed values for these rate constants were accurate within a factor of two.

The most striking feature of this research is the observed temperature independence of the ionization rate constant. This result depends strongly on the ability of simple hydrodynamic calculations to describe accurately the state throughout the relaxation zone. The calculative assumption of equal temperature for all species must therefore be examined. If this assumption is unjustified and the electrons, positive ions, and atoms possess significantly different temperatures in the relaxation zones, most likely the electron temperature is kinetically most important in the ionization and recombination processes. Under such circumstances a possible explanation for the observed temperature independence may be proposed providing that the electron temperature is actually less than that of the atoms and ions behind the reflected shock front. Consider first the situation in the observed fast reactions, i.e., the reactions generated by the HMX explosives. Here the reaction zones are short and quite possibly the electrons have not yet had time to reach the higher ion and atom temperatures at the position in the relaxation zones where the electron density rates were measured. On the other hand, in the comparatively slow reactions generated in the TNT boostered tubes, presume that the electrons have had sufficient time to approach the ion and atom temperatures at the position of rate measurement. With this reasoning, the

electron density rates may actually have been measured at the same electron temperature even though the large particle temperatures were significantly different between the two sets of experiments. It is pertinent to note that, if the rates were actually measured in the HMX experiments at an electron temperature less than 2.25×10^4°K, the ionization rate constant observed equal to 1.08×10^{-13} cm^3 sec^{-1} agrees within experimental error with the value of 2.18×10^{-13} cm^3 sec^{-1} derived for the bimolecular rate constant for excitation to the first excited helium state, equation (V-16), for a temperature of 2.0×10^4°K. A bimolecular reaction between neutral atoms and electrons which results in excitation to the first excited state has been observed by several investigators to be the rate-limiting process in the ionization of shocked argon following very early reactions which produce initial quantities of electrons[2-4].

A poor choice of parameters (neutral atom and electron number densities) with which the observed rates were compared could possibly be another source of the unexpected lack of temperature dependence in the ionization rate constant. It is quite probable that electrons are one of the rate-determining species, because inelastic collision cross sections for electrons are generally larger than those for atoms and ions[5]. Assuming that the ionization reaction is truly bimolecular, the second reactant may well be one of the excited states. Indeed the results of an experiment performed supplementally to the main course of this research which used light emitted

---

[2]Petschek and Byron, op. cit.

[3]E. A. Brown and G. J. Mullaney, Bull. Am. Phys. Soc. 10, 268 (1965).

[4]H. Wong and D. Bershader, Bull. Am. Phys. Soc. 10, 268 (1965).

[5]H. S. W. Massey and E. H. S. Burhop, Electronic and Ionic Impact Phenomena (Clarendon Press, Oxford, 1952).

from gas at equilibrium near the tube end plate for backlighting the relaxation zone may indicate excited state populations widely different from those predicted by Boltzmann factors. It must be emphasized, however, that due to the temperature independence observed in the assumed neutral atom-electron process, the ratio of a rate-determining excited state reactant density to the ground state neutral density must be either temperature independent or temperature dependent in such a way as to cancel the temperature dependence of the ionization rate constant in the rate equation.

The inability to establish definitely the detailed nature of the ionization process investigated in this research points to the need for further information about the relaxation. Certainly a comprehensive theoretical description of the relaxation zones behind strong shocks is a necessity. Of further help would be knowledge of the excited state populations as they changed through the relaxation zone. This information can be obtained with experimental equipment which measures absolute line intensities with time-resolution. Already at hand are the mechanical components to a system which could be used in conjunction with the Meinel spectrograph and appropriate electronic instrumentation to monitor simultaneously the absolute intensity of several time-dependent spectral lines. The addition of this facility to measure excited state populations to the experimental techniques already proven would produce a very capable system for use in the investigation of many fast relaxation processes occurring in shocked gases.

The high-explosive shock tube may prove to be valuable when used in a manner already in extensive use by investigators using shock tubes of the more conventional diaphragm type. For the study of kinetic process in dilute reactants, the subject material is sometimes put into a "carrier" gas

which is readily shocked in a conventional shock tube. Because of its general availability and its hydrodynamic properties, argon is quite often used as the "carrier" in this type of experiment. The ability to shock helium strongly in the high-explosive tube and the physical properties of helium itself make the use of this system attractive for similar studies.

Preliminary spectrographic experiments using helium as the "carrier" gas in the high-explosive tube and involving the study of the kinetic processes which occur at the incident shock front in trace amounts of organic gases have already been completed with considerable success. Similar investigations into the ionization kinetics of cesium vapor also appear to be practical and interesting.

APPENDIX

HYDRODYNAMIC CALCULATIONS

For the purpose of calculating the equilibrium state of the emitting gas behind a shock, the shock can be considered to be a discontinuous jump between initial and final conditions. The state can then be determined by simultaneous solution of the equations describing conservation of mass, momentum, and energy across the discontinuity and the thermal and caloric equations of state for the shocked gas. Assuming that the observed shocks were indeed one-dimensional and that losses due to heat conduction, radiative cooling, and viscosity may be neglected, the conservation equations across the incident shock moving into the gas initially at rest are

$$\rho_o U_i = \rho_1 (U_i - u_1) \qquad \text{(Mass)} \qquad \text{(A-1)}$$

$$\rho_o U_i^2 + P_o = \rho_1 (U_i - u_1)^2 + P_1 \qquad \text{(Momentum)} \qquad \text{(A-2)}$$

$$1/2\ U_i^2 + H_o = 1/2\ (U_i - u_1)^2 + H_1. \qquad \text{(Energy)} \qquad \text{(A-3)}$$

The corresponding equations across the shock completely reflected back into the gas already shocked by the incident shock are

$$\rho_1 (u_1 - U_R) = \rho_2 (u_2 - U_R) \qquad \text{(A-4)}$$

$$\rho_1 (u_1 - U_R)^2 + P_1 = \rho_2 (u_2 - U_R)^2 + P_2 \qquad \text{(A-5)}$$

$$1/2\ (u_1 - U_R)^2 + H_1 = 1/2\ (u_2 - U_R)^2 + H_2 \qquad \text{(A-6)}$$

where U_i = incident shock velocity

U_R = reflected shock velocity

u_k = particle velocity

ρ_k = mass density

P_k = pressure

H_k = enthalpy per unit mass

and the subscript $\underline{k}$ specifies a particular region as defined in Fig. 31. All velocities are in the laboratory frame and positive in the sense of the incident shock.

Considering each of the three species in the partially ionized gas to be an ideal gas, the appropriate state equations are

$$P_k = (1 + \alpha_k) \frac{\rho_k RT_k}{M} \tag{A-7}$$

and

$$H_k = 5/2\ (1 + \alpha_k) \frac{RT_k}{M} + \alpha_k \frac{RT_{ion}}{M}$$

where R = universal gas constant

T_k = temperature, assumed to be the same for each species

T_{ion} = ionization potential expressed in temperature units

α_k = degree of ionization

M = molecular weight of helium.

For the system of equations describing the state following the incident shock, there are seven unknowns and five equations providing that the initial conditions (region $\underline{0}$) are known. If an additional equation which specifies α_k in terms of the other state variables is known, the solution of the system is unique given the value of one additional variable. The additional variable most easily measured is the incident shock velocity.

LASL-AEC-OFFICIAL

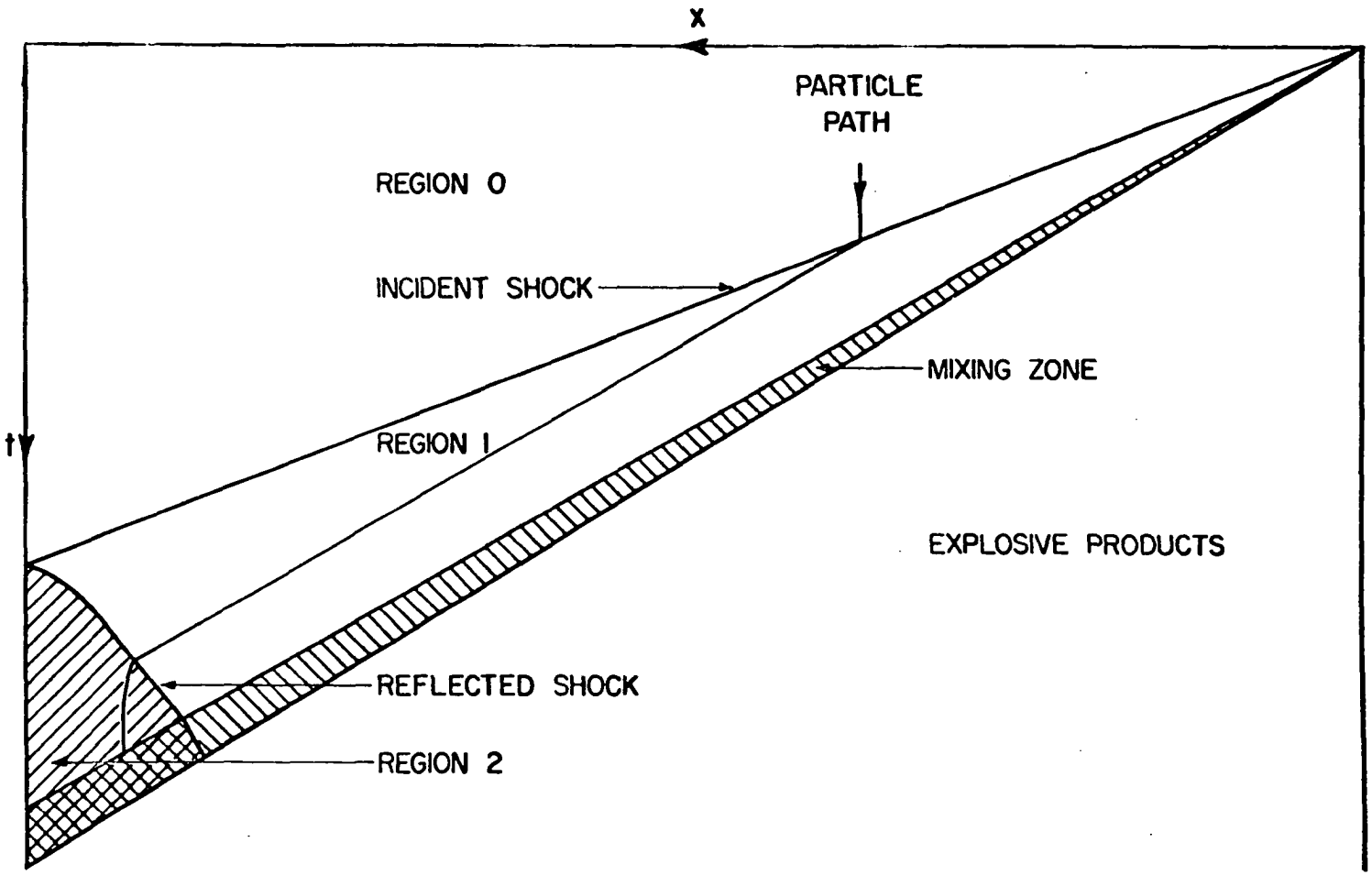

Fig. 31. Schematic Distance-Time Plot of the Shocks Generated in the High-Explosive Shock Tube

A similar situation exists in the system describing the state behind the reflected shock. Here the conditions in region 1 are now known but there still exist only five equations for the seven unknowns. Therefore, the requirement for an equation in α_2 and the value of one of the unknown variables is also valid for unique solution of the system.

The code LASL-HUG written by Bird, Duff, and Schott[1] for the IBM 7090 computer was used to process data according to equations (A-1) through (A-7). Two of the several options offered by the code were used to calculate the state behind the incident and reflected shocks. First, the final state behind each shock was determined by the conditions of chemical equilibrium. This was equivalent to use of one form of the Saha equation for helium ionization:

$$\frac{\alpha_K^2}{(1-\alpha_K^2)} P_k = 1.33\ T_k^{5/2}\ e^{-2.85 \times 10^5/T_k}\ \text{dyn cm}^{-2}. \qquad \text{(A-8)}$$

The equilibrium state behind the incident shock was determined using equation (A-8) for region 1 and the observed values of U_i. The equilibrium state behind the reflected shock was determined using equation (A-8) for region 2 plus the auxiliary condition that the particle velocity at equilibrium behind the completely reflected shock is zero. The equilibrium states calculated for the shocks produced in this research are described in Table 4.

The option which proved essential for the calculation of the state at various positions in the relaxation zone was that which allowed an

---

[1] A detailed description of the code is given in P. F. Bird, R. E. Duff, and G. L. Schott, "HUG, A Fortran-Fap Code for Computing Normal Shock and Detonation Wave Parameters in Gases," Los Alamos Scientific Laboratory Report, LA-2980 (1964).

LASL-AEC-OFFICIAL
LASL-AEC-OFFICIAL

TABLE 4

EQUILIBRIUM SHOCK PROPERTIES

Initial Pressure (mm Hg)	Region	U_i (10^5 cm sec^{-1})	U_R (10^5 cm sec^{-1})	u_k (10^5 cm sec^{-1})	T_k (10^4°K)	P_k (10^6dyn cm^{-2})	ρ_k (10^{-5}g cm^{-3})	$[He]_k$ (10^{18} cm^{-3})	$[e]_k$ (10^{17} cm^{-3})
10	1	13.01		9.91	1.474	2.77	0.898	1.34	0.094
	2		-3.91	0	2.105	15.0	3.16	4.37	4.10
20	1	12.93		9.79	1.479	5.44	1.76	2.64	0.139
	2		-4.04	0	2.170	29.5	6.02	8.38	7.10
30	1	12.84		9.68	1.470	8.00	2.62	3.92	0.159
	2		-4.12	0	2.204	43.2	8.78	12.2	9.65
30 (TNT)	1	10.86		8.08	1.090	5.64	2.50	3.77	0.004
	2		-4.21	0	1.950	30.4	7.31	10.6	3.55

arbitrary specification of the value of α_2. Several values of the degree of ionization intermediate between the equilibrium value calculated for the incident shock and the equilibrium value calculated for the reflected shock were specified in the solutions for the reflected shock properties. The additional variable required for this calculation was the reflected shock velocity obtained from the preceding equilibrium calculations. Assuming that the conservation equations are valid in the relaxation zone behind the reflected shock, equations (A-4) through (A-7) were then solved and the state variables for each specified value of α_2 determined. Graphs of these variables as they changed throughout the relaxation zones are presented in Figs. 32 through 39. In these calculations the degree of ionization directly behind the reflected shock front was assumed equal to that for equilibrium ionization behind the incident shock.

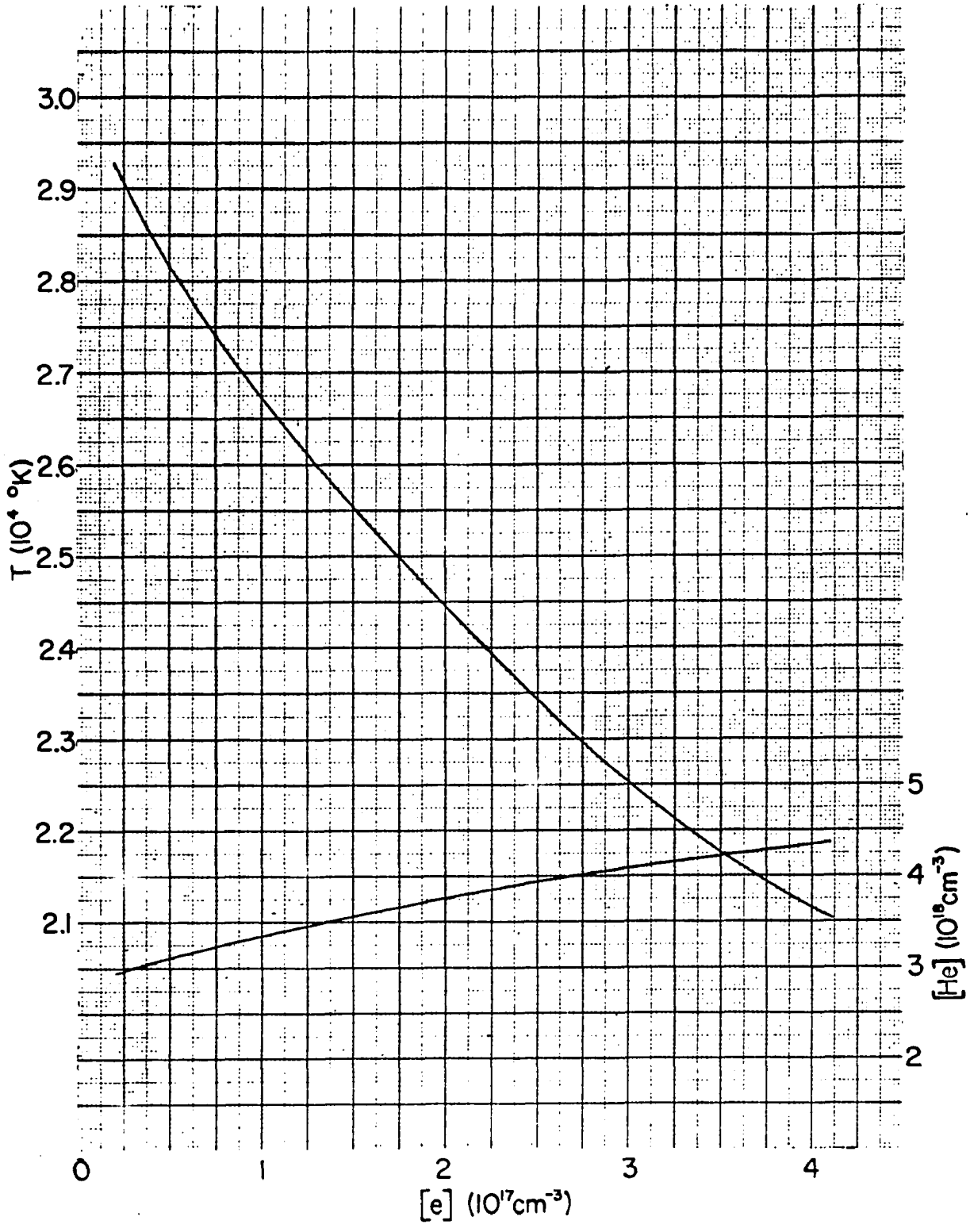

Fig. 32. State of Relaxation Zone, [He] and T, P_o = 10 mm

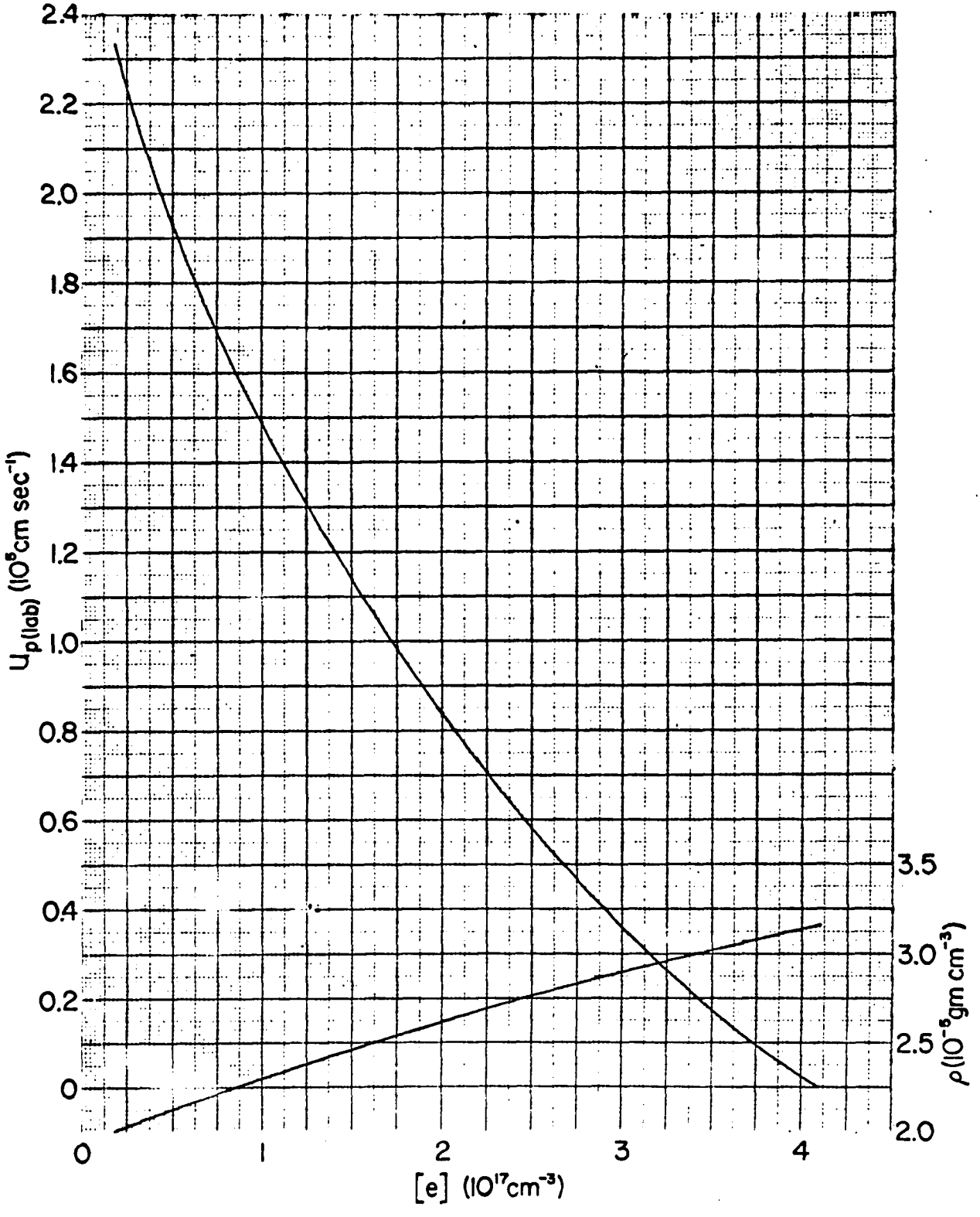

Fig. 33. State of Relaxation Zone, u_2 and ρ, P_o = 10 mm

LASL-AEC-OFFICIAL

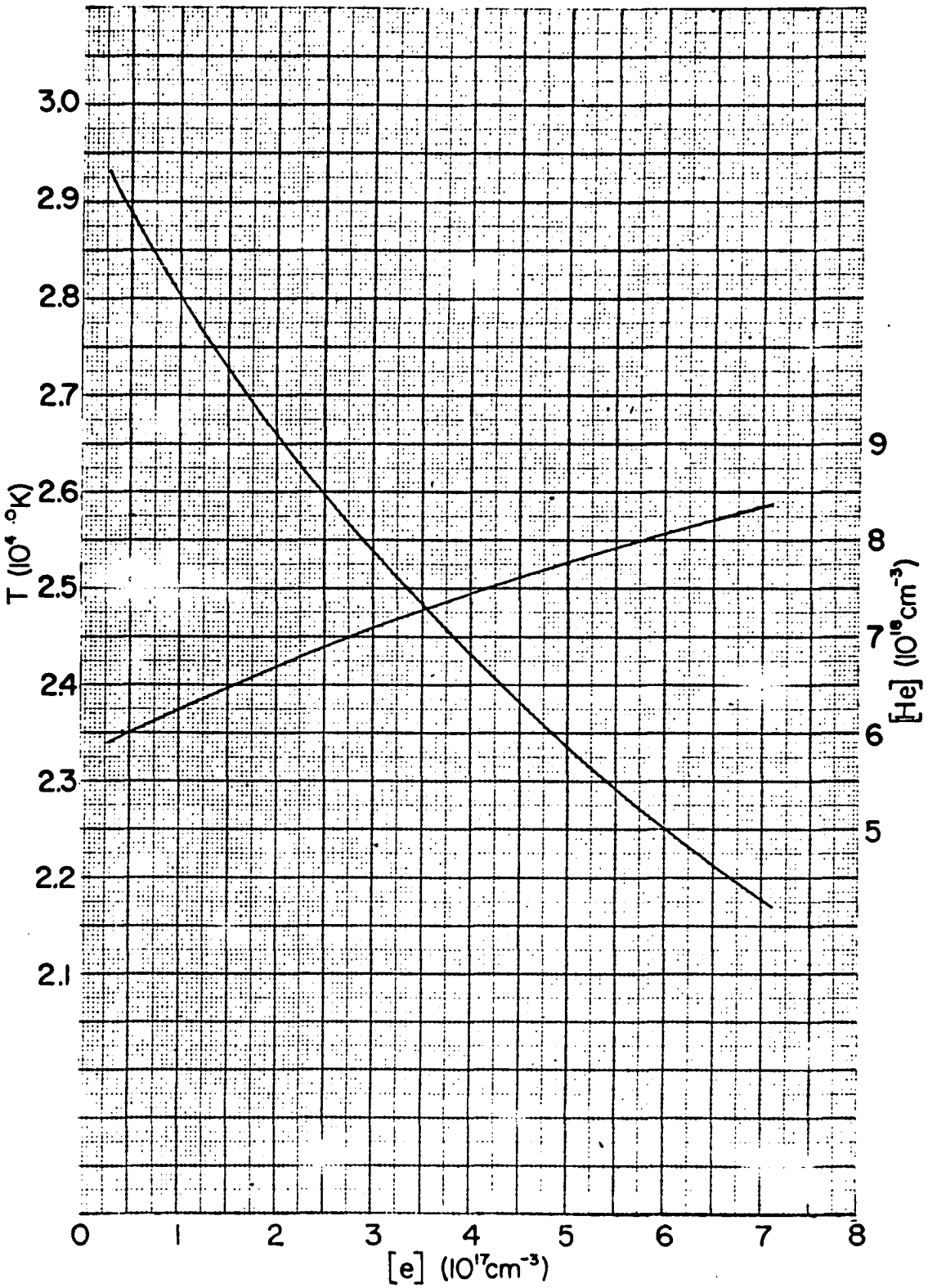

Fig. 34. State of Relaxation Zone, [He] and T, P_o = 20 mm

LASL-AEC-OFFICIAL
LASL-AEC-OFFICIAL

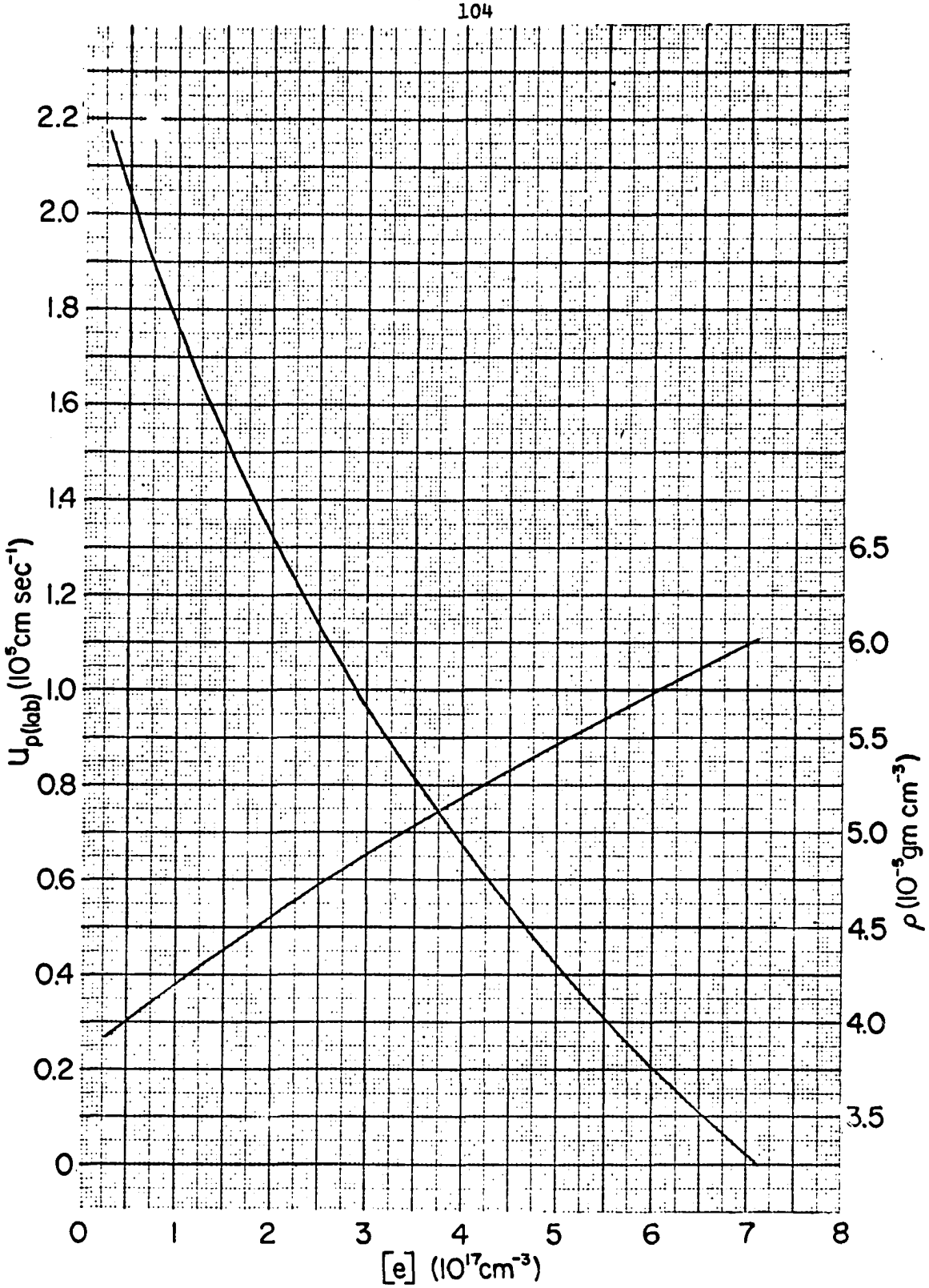

Fig. 35. State of Relaxation Zone, u_2 and ρ, P_o = 20 mm

LASL-AEC-OFFICIAL

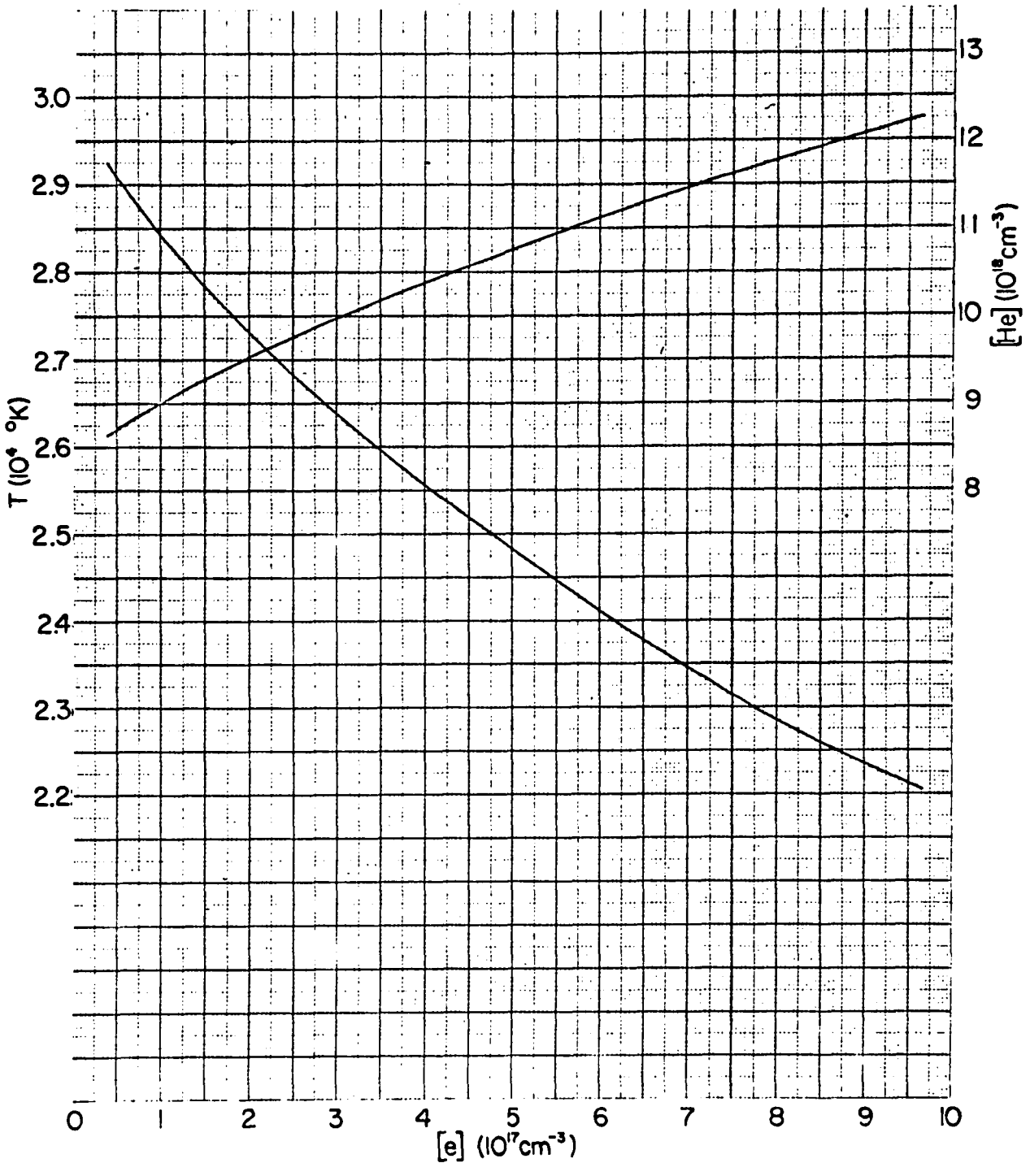

Fig. 36. State of Relaxation Zone, [He] and T, P_o = 30 mm

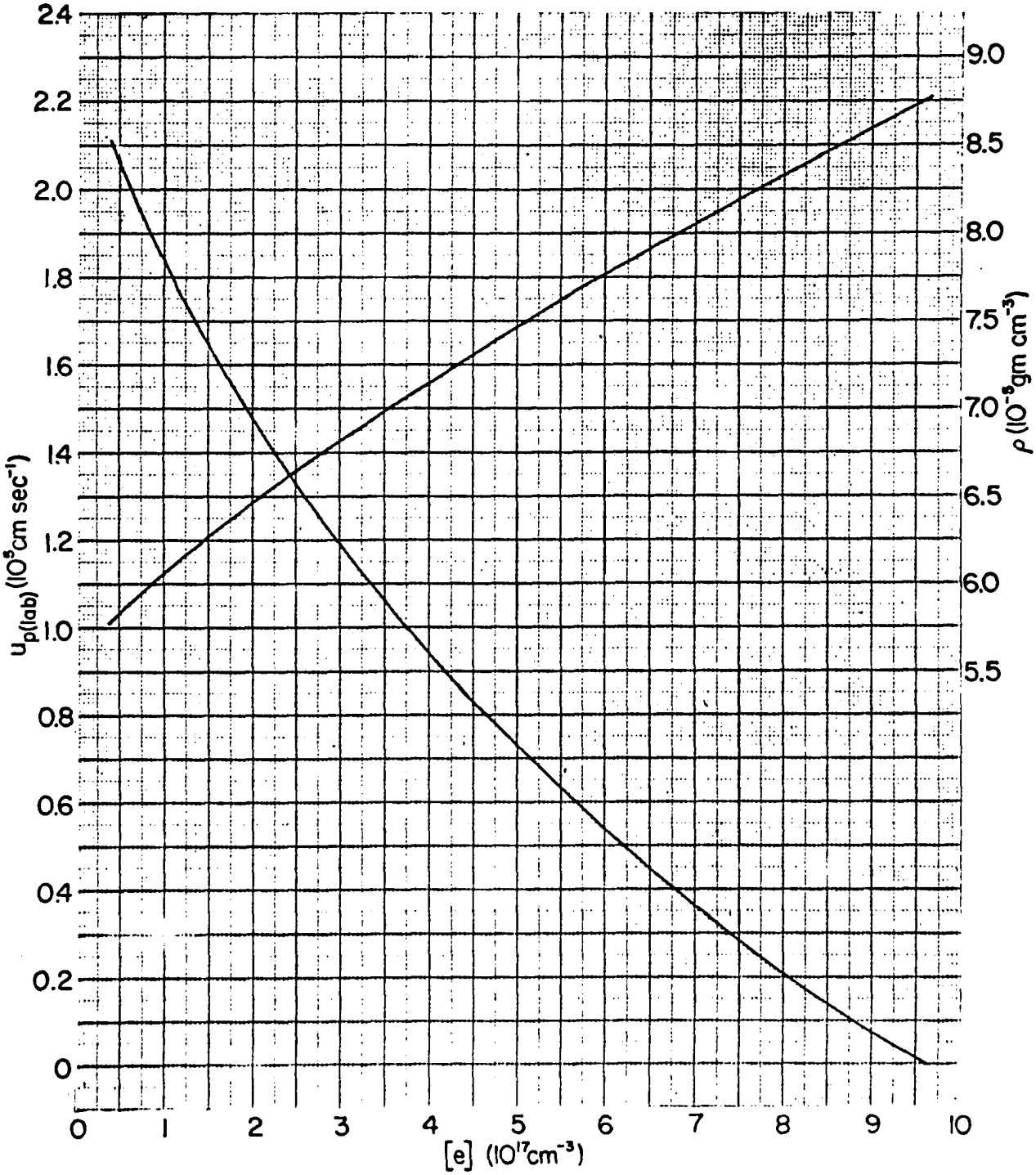

Fig. 37. State of Relaxation Zone, u_2 and ρ, P_o = 30 mm

LASL-AEC-OFFICIAL
LASL-AEC-OFFICIAL

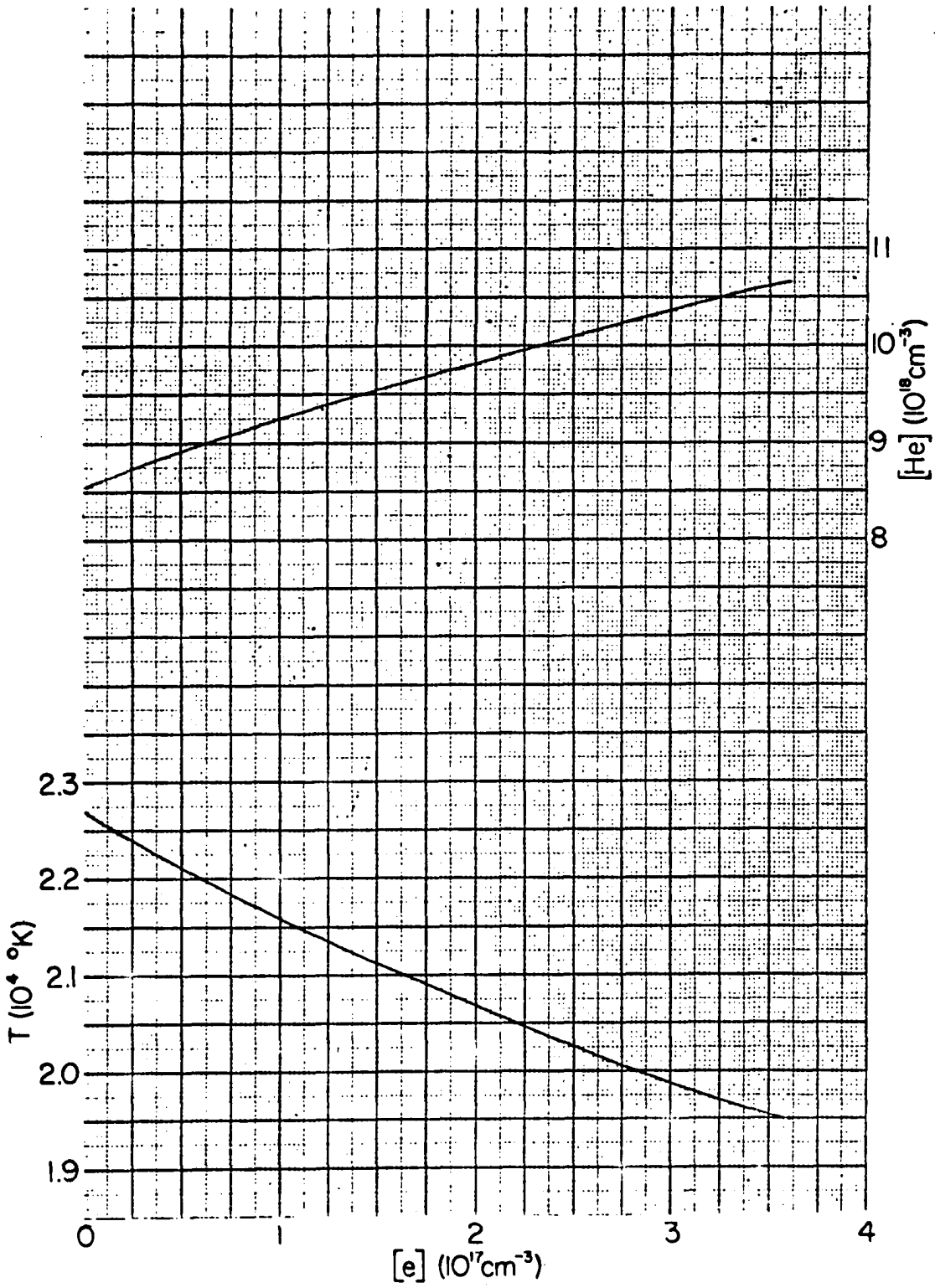

Fig. 38. State of Relaxation Zone, [He] and T, P_o = 30 mm (TNT)

LASL-AEC-OFFICIAL
LASL-AEC-OFFICIAL

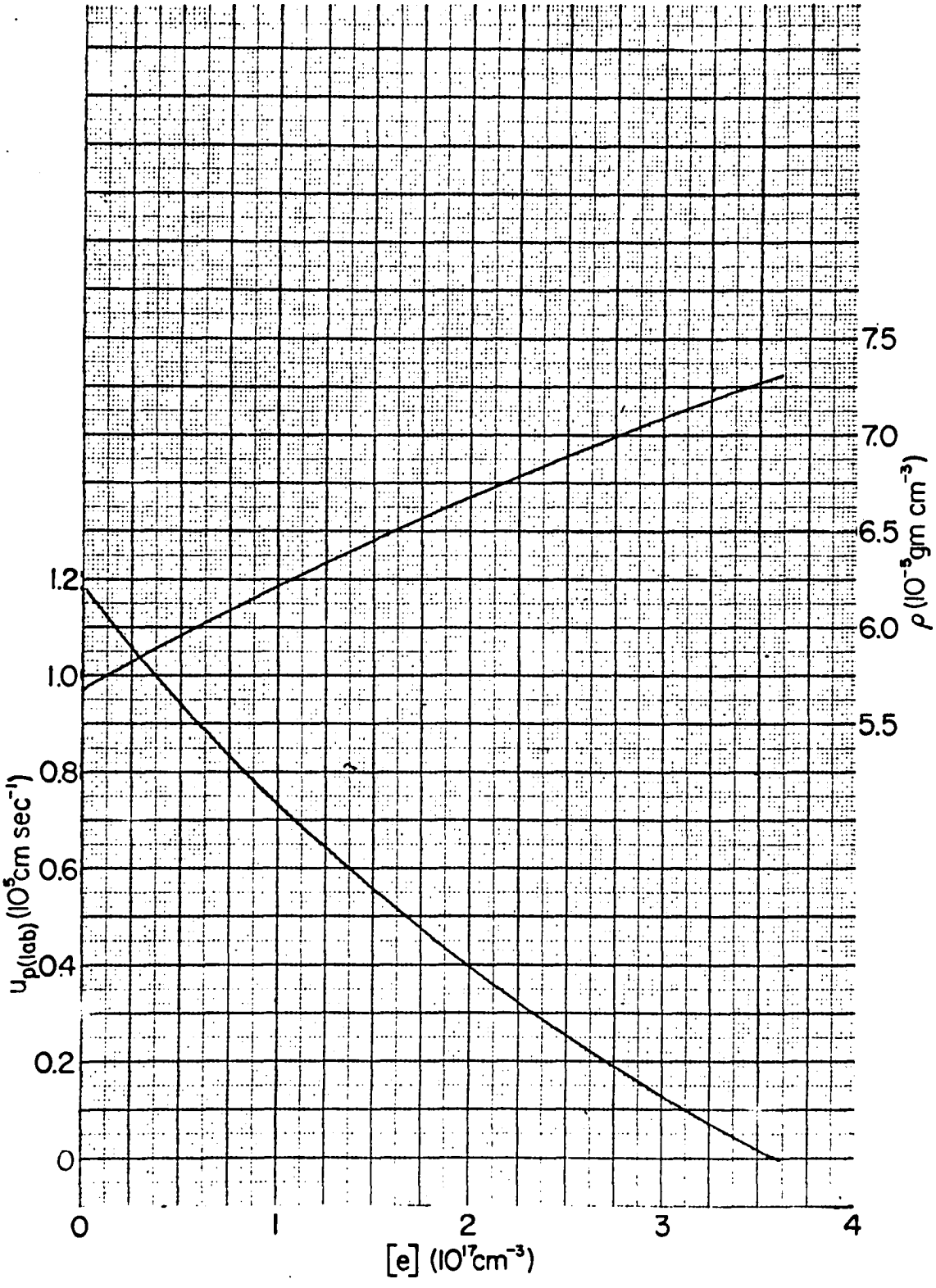

Fig. 39. State of Relaxation Zone, u_2 and ρ, P_o = 30 mm (TNT)

LASL-AEC-OFFICIAL